THE UNIVERSITY OF CHICAGO

COMPACT APPROXIMATION METHODS FOR NEUTRINO OSCILLATIONS IN MATTER

A DISSERTATION SUBMITTED TO
THE FACULTY OF THE DIVISION OF THE PHYSICAL SCIENCES
IN CANDIDACY FOR THE DEGREE OF
DOCTOR OF PHILOSOPHY

DEPARTMENT OF PHYSICS

BY
XINING ZHANG

CHICAGO, ILLINOIS
JUNE 2021

TABLE OF CONTENTS

LIST OF FIGURES

LIST OF TABLES

ACKNOWLEDGMENTS

I would like to express sincere gratitude to my advisor Dr. Stephen Parke for guiding, mentoring, and inspiring my PhD journey. I will never complete this dissertation without his supervision. I appreciate my department sponsor Prof. Carlos E. M. Wagner for his support, especially in the early stage of my graduate career in the University of Chicago. I also appreciate Prof. Kathryn Levin and Prof. David Schmitz for serving my thesis committee. I am honor to have Dr. Peter Denton as a valuable collaborator. Finally, I appreciate my colleagues and friends Dr. Yuxiao Wu, Xiaofeng Dong, Rong Nie, Dr. Yin Lin, and Yikun Wang for the nice and memorable years.

ABSTRACT

This dissertation presents a series of compact perturbative methods to calculate neutrino oscillations in matter with uniform density. In the method we implement multiple rotations to figure out zeroth order approximations. The rotations are able to resolve zeroth order degeneracy so the higher order corrections can converge for the complete matter potential versus baseline divided by neutrino energy plane. The rotations also diminish scales of perturbative terms of the Hamiltonian operator. The expansion parameter used in the method is not a constant. Its scale can be restricted to be smaller than ratio of the solar to the atmospheric Δm^2 globally. In vacuum the expansion parameter is strictly equal to zero, thus the zeroth order approximations return to the exact vacuum values. We use analytic derivations and numerical tests to prove the favorable properties. Moreover, the zeroth order eigenvalues of the Hamiltonian (differences of neutrino mass squares) can be inserted into a recently rediscovered identity which relates a Hermitian operator's eigenvalues to eigenvectors to give simple and symmetric expressions of the mixing angles and CP phase with extraordinary precision. Finally, the method can be extended from the standard three flavors neutrino scheme to a scheme with one more sterile neutrino, with its advantages inherited.

CHAPTER 1

INTRODUCTION

Neutrinos are elementary particles which have three possible flavors, ν_e, ν_μ, and ν_τ. A neutrino created with one specific flavor has a non-zero probability (which is called oscillation probability) to propagate into another flavor later. This phenomenon is called neutrino oscillation. Since in Schrodinger's equation the Hamiltonian operator generates the time evolution, neutrino oscillations prove a non-zero Hamiltonian operator of neutrinos. The Hamiltonian operator must have non-zero eigenvalues, thus the corresponding eigenstates are massive. This is an assuredly signal of physics beyond the Standard Model because in the Standard Model neutrinos are presumed to be massless. The discovery of neutrino oscillation has provoked plenty of interests and inspired and triggered theoretical and experimental researches in the past decades.

As the flavor eigenstates are not invariant in time evolution, they are not parallel to any eigenstates of the Hamiltonian. The basis formed by the Hamiltonian's eigenstates is called energy or mass basis, and the flavor eigenstates form the flavor basis. As a straightforward conclusion in linear algebra, the two basis can be related by a unitary transformation. The unitary matrix representing this transformation is defined as Pontecorvo-Maki-Nakagawa-Sakata (PMNS) matrix [47, 56]. For a Hilbert space spanned by the three flavor eigenstates (also by the energy basis), both the Hamiltonian and the PMNS matrix are 3×3 matrices. A 3×3 unitary matrix can be written as product of three complex rotations, each rotation is constraint in a 2-dimensional plane. Therefore in mathematics the PMNS matrix can be uniquely determined by at most three real rotation angles, which are defined to be mixing angles, and three complex phases. On the other hand, in physics if all the flavor (or energy) eigenstates multiply a same complex phase simultaneously, no observable will be changed hence we are free to eliminate two complex phases. The only surviving phase is called CP phase because it is related to neutrino CP violation. In modern theories, vacuum values of

the mixing angles and CP phase are fundamental parameters in nature. Values of the mixing angles and CP phase are not observables, thus cannot be measured directly by experiments. However, these values are closely related to the oscillation probabilities which are measurable.

Common solutions to measuring neutrino oscillation probabilities on the Earth are accelerator neutrino projects. Present projects include but are not limited to T2K [40], NOνA [14]. Projected ones include DUNE [8], T2HK [3], etc. Typical structure of such an experimental facility includes a source of neutrino beam, a near detector, and a far detector. The near detector is quite close to the source and measure flux of the initial neutrino beam (usually in a pure flavor). Then the neutrino beam propagates a significant distance to the far detector and flux of a selected flavor (can be same as or different from the initial flavor) is measured. In this way people can figure out a disappearance (same flavor) or appearance (different flavors) probability of the given setup. If the neutrino beam's energy is E, spatial distance between the near and the far detectors (baseline length) is L, and the near detector measures flavor α and the far detector measures flavor β, in theory the oscillation probability is given by

$$P_{\alpha\to\beta} = \left| \sum_j U^*_{\alpha\, j}\, U_{\beta\, j}\, e^{-i\,\frac{m_j^2\, L}{2E}} \right|^2, \tag{1.1}$$

where $U_{\alpha\, j}$ is the PMNS matrix's element in the αth row, jth column and m_j^2 is the Hamiltonian's jth eigenvalue (m_j is a value of neutrino mass). It is trivial to prove that the oscillation probabilities will not be changed if the Hamiltonian adds a multiple of identity matrix. Therefore the oscillations probabilities depend on gaps between the eigenvalues $\Delta m^2_{ij} = m_i^2 - m_j^2$ rather than the eigenvalues themselves. In vacuum, only absolute value of Δm^2_{32} can be determined but not its sign, we define $\Delta m^2_{32} > 0$ to be normal mass order (NO) and < 0 to be inverted mass order (IO). A neutrino beam propagates in straight line and L can be as long as hundreds of kilometers (e.g. 810km for NOνA, 1,300km for DUNE). Because of curvature of the Earth surface, before reaching the far detector, the beam must propagate through the Earth crust and interact with the crust materials by the Wolfenstein

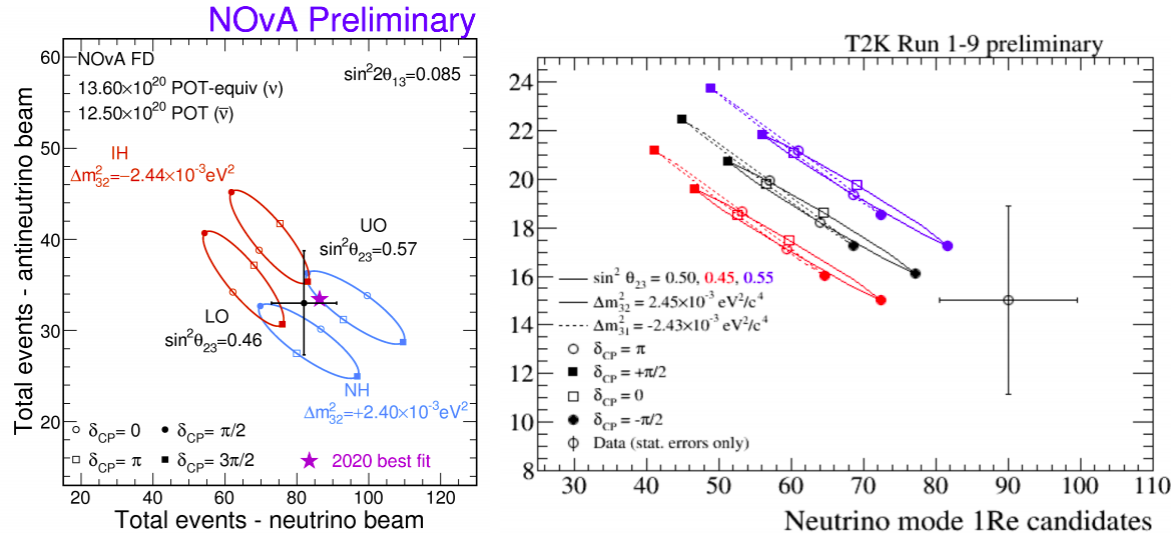

Figure 1.1: Bievents plots of NOνA (left) and T2K (right). In the left plot IH and NH mean inverted order and normal order, respectively. CP phase is the running parameter. Plots are taken from [15, 24]

matter effect [60]. Because of the matter effect, NH and IH will not give identical oscillation probabilities. Fig. 1.1 displays bievents plots of T2K and NOνA which can be used to distinguish mass hierarchies.

The matter effect adds a potential term into the Hamiltonian operator in vacuum and obviously the Hamiltonian' eigenvalues will be changed. The added potential term is diagonal in the flavor basis but not in the vacuum energy basis, which means that potential term does not commute with the vacuum Hamiltonian and the two matrices cannot be diagonalzied simultaneous. Therefore the PMNS matrix will also be changed. Density of shallow layer of the Earth crust is about a constant value. For the Wolfenstein matter effect with uniform matter density, exact analytic solutions for the standard three flavors scheme were calculated [17, 62]. However, because of the exact solutions' complex expressions which impede understanding of the structure of the neutrino oscillations, their usages have been seriously limited. Alternatively, approximated methods based on perturbative expansions have been developed for theoretical and computational approaches to neutrino oscillations. Possible options of expansion parameter which have been used include vacuum values of $\sin\theta_{13}$ (θ_{13} is rotation

angle of the 13 plane rotation of the PMNS matrix) and $\Delta m^2_{\odot}/\Delta m^2_{\text{atm}} = \Delta m^2_{21}/\Delta m^2_{32}$ [13, 20, 48]. For $\sin\theta_{13}$, based on recent measurements its vacuum value is around 0.13, which is not very small, therefore to achieve an acceptable level of precision one must go to higher order correction terms making lengthy expressions. Moreover, if we expand with $\sin\theta_{13}$, two 0th order eigenvalues (diagonal elements of the Hamiltonian) will cross near $E \simeq 10\text{GeV}$. Because of this degeneracy the higher order expansion terms will not converge. In vacuum $\Delta m^2_{21}/\Delta m^2_{32} \simeq 0.03$ which is smaller than $\sin\theta_{13}$. But a 0th order degeneracy problem still exists near $E \simeq 140\text{MeV}$. Because of the defects of the previous perturbation methods, we need to figure out new approximation approaches.

We develop and improve a series of new compact perturbative methods to calculate neutrino oscillations in matter. We use rotations to resolve any possible 0th order degeneracy and decrease scales of perturabtive terms. The expansion parameter will not be a constant but guaranteed to be smaller than $\Delta m^2_{21}/\Delta m^2_{32}$ and exactly zero in case of vacuum. The new method will be simple and with high precision. Considering the plenty of computing resources consumed in analysis process in neutrino experiments (for example, see [57] for NOνA), the methods of this dissertation have potential usage in future analysis of neutrino oscillations. In this dissertation a recently rediscovered identity in linear algebra called *eigenvector-eigenvalue identity* and its application in neutrino physics will also be introduced. Affects of this work in the high energy physics community and media can be found in [21, 59].

This dissertation is organized as follows. We first derive the new method of rotations for the standard three flavors neutrino scheme in details in Chapter 2 and demonstrate its desirable properties by analytic and numerical calculations. In Chapter 3 we compare the rotations with perturbative expansions and strictly analyze precision of the eigensystems given by the rotation method. In Chapter 4 we introduce the *eigenvector-eigenvalue identity* and its application in neutrino physics and discuss how the approximated results from the rotation method can be inserted into the identity. In Chapter 5 we extend the rotation

method from the standard three flavors scheme to a scheme with one more sterile neutrino. Conclusions are in Chapter 6. Some useful supplementary materials can be found in appendices.

Materials of this dissertation include methods and conclusions from five published papers [27, 54, 29, 26, 28] by the author. [27, 29, 28] are coauthored with Peter. B. Denton and Stephen Parke. [54] is coauthored with Stephen Parke. [26] is coauthored with Peter. B. Denton, Stephen Parke, and Terence Tao.

CHAPTER 2

COMPACT PERTURBATIVE EXPRESSIONS FROM ROTATIONS

We start from the standard three flavors neutrino scheme. The Schröger equation for neutrino oscillations in matter is:

$$i\frac{\partial}{\partial t}\left|\nu\right\rangle = H\left|\nu\right\rangle . \tag{2.1}$$

In the flavor basis $|\nu\rangle = |\nu_f\rangle = (\nu_e, \nu_\mu, \nu_\tau)^T$, the Hamiltonian represented in the same basis is

$$H = H_f = \frac{1}{2E}\left[U_{\rm PMNS}\,{\rm diag}(0, \Delta m^2_{21}, \Delta m^2_{31})\,U^\dagger_{\rm PMNS} + {\rm diag}(a(x), 0, 0)\right]. \tag{2.2}$$

The unitary PMNS matrix $U_{\rm PMNS}$ can be written as product of three complex rotations in 12, 13, and 23 planes as:

$$U_{\rm PMNS} = U_{23}(\theta_{23}, \delta)\,U_{13}(\theta_{13})\,U_{12}(\theta_{12}), \tag{2.3}$$

with

$$U_{23}(\theta_{23}, \delta) = \begin{pmatrix} 1 & & \\ & c_{23} & s_{23}\,e^{i\delta} \\ & -s_{23}\,e^{-i\delta} & c_{23} \end{pmatrix}, \quad U_{13}(\theta_{13}) = \begin{pmatrix} c_{13} & & s_{13} \\ & 1 & \\ -s_{13} & & c_{13} \end{pmatrix},$$
$$U_{12}(\theta_{12}) = \begin{pmatrix} c_{12} & s_{12} & \\ -s_{12} & c_{12} & \\ & & 1 \end{pmatrix} \tag{2.4}$$

In the above equations $s_{ij} \equiv \sin\theta_{ij}$, $c_{ij} \equiv \cos\theta_{ij}$, θ_{ij} represents the real rotation angle in the ij plane and δ is a complex phase. In neutrino physics θ_{ij} are called (vacuum) mixing angles and δ is called the CP-phase. For three complex rotations there should be three complex

angles but in Eq. 2.3 there is only one. The reason is that the whole flavor or energy basis are free to multiply a same complex phase and this does not change any physics observable. Therefore it is free to eliminate two complex phases. For a uniform matter density in Eq. 2.1 $a(x)/2E = a/2E$ is a constant, a is given by

$$a \equiv 2\sqrt{2}G_F\, N_e\, E \simeq 1.52 \times 10^{-4}\left(\frac{Y_e\rho}{\mathrm{g}\cdot\mathrm{cm}^{-3}}\right)\left(\frac{E}{\mathrm{GeV}}\right), \tag{2.5}$$

where Y_e is the number of electron per nucleon and ρ is the matter density.

2.1 Zeroth Order Approximation from Rotations

In this section we are going to review a process [25] of implementing a sequence of rotations to transform the Hamiltonian operator given in Eq. 2.2. The rotated Hamiltonian's diagonal elements will be zeroth order approximations of the eigenvalues with high precision and sizes of the off-diagonal elements will be controlled small. Moreover, the rotations can resolve crossings of the diagonal elements thus resolve possible zeroth order degeneracy and make perturbative expansions well-defined for arbitrary neutrino energy. The flavor neutrino basis will be rotated simultaneously and naturally induce zeroth order energy basis (eigenvectors of the Hamiltonian) in matter.

In the flavor basis, it is observed that the matter potential term is invariant under any 23 rotation and the Hamiltonian's complex phase, known as CP phase, is introduced by the complex rotation in 23 plane $U_{23}(\theta_{23}, \delta)$. If we implement its inverse rotation, the Hamiltonian will be real and the following calculation will be significantly simplified. Therefore we can first define

$$\tilde{H} \equiv U_{23}^{\dagger}(\tilde{\theta}_{23}, \tilde{\delta})\, H_f\, U_{23}(\tilde{\theta}_{23}, \tilde{\delta}), \quad \text{with} \quad \tilde{\theta}_{23} = \theta_{23},\, \tilde{\delta} = \delta. \tag{2.6}$$

In the above equation even $\tilde{\theta}_{23}$ and $\tilde{\delta}$ have the same values with the corresponding vacuum

parameters, they should not be replaced by θ_{23} and δ. The reason is that we are using a tilde symbol to indicate the zeroth order approximation of a parameter in matter. After calculating the matrices production it can be shown that

$$\tilde{H} = \frac{1}{2E}\begin{pmatrix} \lambda_a & & s_{13}c_{13}\Delta m^2_{ee} \\ & \lambda_b & \\ s_{13}c_{13}\Delta m^2_{ee} & & \lambda_c \end{pmatrix} + \epsilon s_{12}c_{12}\frac{\Delta m^2_{ee}}{2E}\begin{pmatrix} & c_{13} & \\ c_{13} & & -s_{13} \\ & -s_{13} & \end{pmatrix}. \tag{2.7}$$

In R.H.S. of Eq. 2.7, s_{ij} and c_{ij} represent $\sin\theta_{ij}$ and $\cos\theta_{ij}$ respectively and ϵ is a small parameter defined as

$$\epsilon \equiv \Delta m^2_{21}/\Delta m^2_{ee}, \tag{2.8}$$

with

$$\Delta m^2_{ee} \equiv \cos^2\theta_{12}\Delta m^2_{31} + \sin^2\theta_{12}\Delta m^2_{32} = \Delta m^2_{31} - \sin^2\theta_{12}\Delta m^2_{21}. \tag{2.9}$$

The three diagonal elements of $\tilde{H}$ are defined as

$$\begin{aligned} \lambda_a &\equiv a + (s^2_{13} + \epsilon s^2_{12})\Delta m^2_{ee}, \\ \lambda_b &\equiv \epsilon c^2_{12}\Delta m^2_{ee}, \\ \lambda_c &\equiv (c^2_{13} + \epsilon s^2_{12})\Delta m^2_{ee}. \end{aligned} \tag{2.10}$$

Observe the elements of $\tilde{H}$, it is evident that the 13 sector contributes the leading order off-diagonal entries. Moreover, in Eq. 2.3, the convention to write the PMNS matrix as rotations' product indicates that a rotation in 13 plane should be perform after the 23 rotation. Therefore it's reasonable to make $U_{13}(\tilde{\theta}_{13})$ diagonalize this sector. After this rotation

$$\hat{H} \equiv U^\dagger_{13}(\tilde{\theta}_{13})\tilde{H}U_{13}(\tilde{\theta}_{13})$$

$$= \frac{1}{2E}\begin{pmatrix} \lambda_- & & \\ & \lambda_0 & \\ & & \lambda_+ \end{pmatrix} + \epsilon c_{12}s_{12}\frac{\Delta m^2_{ee}}{2E}\begin{pmatrix} & c_{(\tilde{\theta}_{13}-\theta_{13})} & \\ c_{(\tilde{\theta}_{13}-\theta_{13})} & & s_{(\tilde{\theta}_{13}-\theta_{13})} \\ & s_{(\tilde{\theta}_{13}-\theta_{13})} & \end{pmatrix}, \quad (2.11)$$

where

$$\lambda_\pm = \frac{1}{2}\left[(\lambda_a+\lambda_c) \pm \text{sign}(\Delta m^2_{ee})\sqrt{(\lambda_a-\lambda_c)^2 + 4(s_{13}c_{13}\Delta m^2_{ee})^2}\right],$$
$$\lambda_0 = \epsilon c^2_{12}\Delta m^2_{ee}. \quad (2.12)$$

With the diagonal elements above, $\tilde{\theta}_{13}$ can be determined by

$$\sin^2\tilde{\theta}_{13} = \frac{\lambda_+ - \lambda_c}{\lambda_+ - \lambda_-}, \quad \tilde{\theta}_{13} \in [0, \pi/2]. \quad (2.13)$$

The next rotation will be in the 12 plane. It is not only because of the convention in Eq. 2.3. More importantly, it can be shown that after the first two rotations, the zeroth order degeneracy near the solar resonance still exists [49]. This degeneracy will be removed by a 12 rotation. Now $U_{12}(\tilde{\theta}_{12})$ is required to diagonalize the 12 sector of $\hat{H}$, and we define $\check{H}$ to be obtained after this rotation.

$$\check{H} \equiv U^\dagger_{12}(\tilde{\theta}_{12})\hat{H}U_{12}(\tilde{\theta}_{12})$$
$$= \frac{1}{2E}\begin{pmatrix} \lambda_1 & & \\ & \lambda_2 & \\ & & \lambda_3 \end{pmatrix} + \epsilon s_{(\tilde{\theta}_{13}-\theta_{13})}s_{12}c_{12}\frac{\Delta m^2_{ee}}{2E}\begin{pmatrix} & & -\tilde{s}_{12} \\ & & \tilde{c}_{12} \\ -\tilde{s}_{12} & \tilde{c}_{12} & \end{pmatrix}, \quad (2.14)$$

where

$$\lambda_{1,2} = \frac{1}{2}\left[(\lambda_0+\lambda_-) \mp \sqrt{(\lambda_0-\lambda_-)^2 + 4(\epsilon c_{(\tilde{\theta}_{13}-\theta_{13})}s_{12}c_{12}\Delta m^2_{ee})^2}\right],$$

$$\lambda_3 = \lambda_+, \tag{2.15}$$

and

$$\sin^2\tilde{\theta}_{12} = \frac{\lambda_2 - \lambda_0}{\lambda_2 - \lambda_1}, \quad \tilde{\theta}_{12} \in [0, \pi/2]. \tag{2.16}$$

We can define a new expansion parameter

$$\epsilon' \equiv \epsilon s_{(\tilde{\theta}_{13} - \theta_{13})} s_{12} c_{12}. \tag{2.17}$$

Then in the R.H.S. of Eq. 2.14 it is straightforward to find the zeroth order term $\check{H}_0$ and the perturbative term $\check{H}_1$:

$$\check{H} = \check{H}_0 + \check{H}_1, \tag{2.18}$$

with

$$\check{H}_0 = \frac{1}{2E}\begin{pmatrix} \lambda_1 & & \\ & \lambda_2 & \\ & & \lambda_3 \end{pmatrix}, \quad \check{H}_1 = \frac{\epsilon' \Delta m^2_{ee}}{2E}\begin{pmatrix} & & -\tilde{s}_{12} \\ & & \tilde{c}_{12} \\ -\tilde{s}_{12} & \tilde{c}_{12} & \end{pmatrix}. \tag{2.19}$$

λ_1, λ_2, and λ_3 are the three zeroth order eigenvalues. Plots in Fig. 2.1 show that their crossings have been resolved so the zeroth order degeneracy has been removed.

The three rotations also give zeroth order approximations of the energy eigenvectors. The zeroth order approximated energy eigenvectors are given by

$$|\check{\nu}\rangle^{(0)} = U^\dagger_{12}(\tilde{\theta}_{12})\, U^\dagger_{13}(\tilde{\theta}_{13})\, U^\dagger_{23}(\tilde{\theta}_{23}, \tilde{\delta})\ |\nu_f\rangle\,. \tag{2.20}$$

It is evident that in vacuum, i.e. when $a = 0$, we have $\tilde{\theta}_{13} = \theta_{13}$ and $\tilde{\theta}_{12} = \theta_{12}$ thus the perturbative Hamiltonian term will vanish so the zeroth order approximations will go back to the exact solutions.

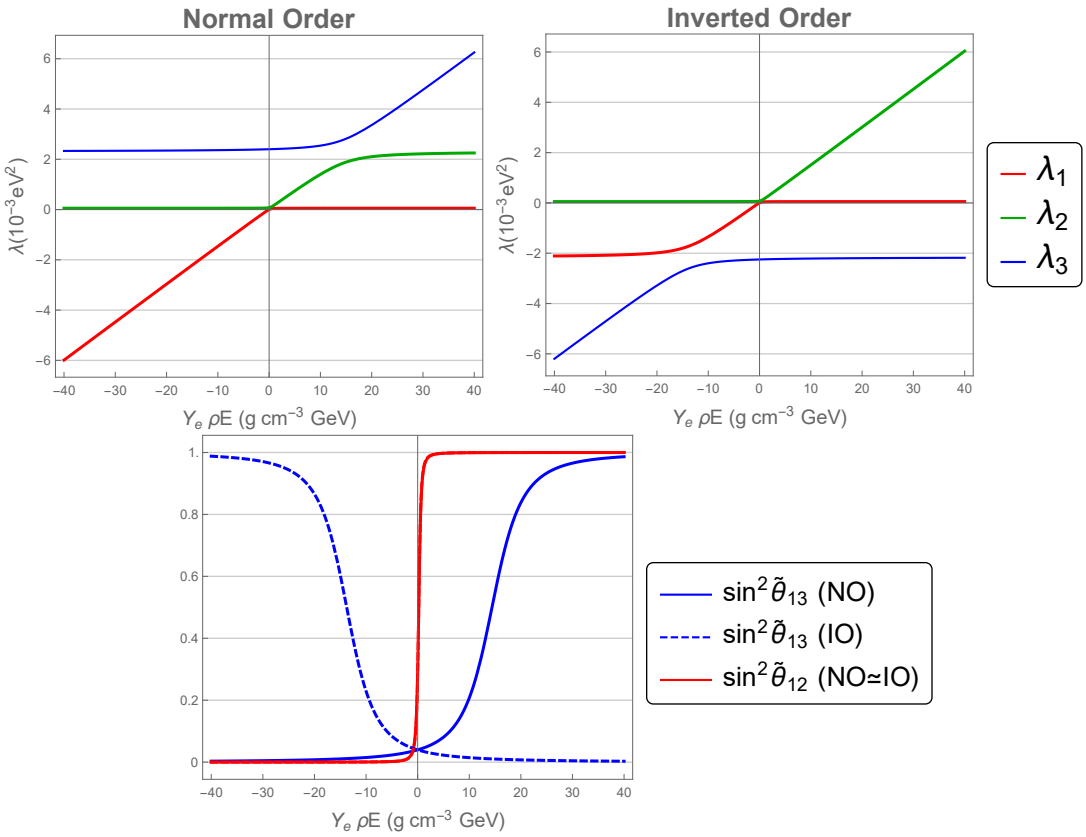

Figure 2.1: The upper two figures show the eigenvalues to zeroth order in matter as functions of the matter potential. The upper-left plot is for normal mass ordering and the upper-right plot is for inverted mass order. The lower plot shows the mixing angles $\sin^2\tilde{\theta}_{12}$, $\sin^2\tilde{\theta}_{13}$ to zeroth order in matter, and the solid (dashed) curves are for normal (inverted) mass ordering. For $\sin^2\tilde{\theta}_{12}$, the curves of both mass orders overlap but are not identical.

2.2 Perturbative Expansions

In this section we are going to go through the first two orders' corrections using perturbative expansion [25, 27]. Eq. 2.19 gives the zeroth order and the perturbative Hamiltonian. Zeroth order eigenvalues and (energy) eigenvectors are given in Eq. 2.15 and Eq. 2.20, respectively.

2.2.1 Eigenvalues

We firstly focus on the eigenvalues. The exact eigenvalues can be written as

$$\lambda_i^{\text{ex}} = \lambda_i + \lambda_i^{(1)} + \lambda_i^{(2)} + \dots . \tag{2.21}$$

It is noticed that all diagonal elements of the perturbative Hamiltonian are zero which means all the first order corrections to the eigenvalues vanish, i.e.

$$\lambda_i^{(1)} = 2E\,(\check{H}_1)_{ii} = 0. \tag{2.22}$$

Actually we can prove that for the perturbative Hamiltonian $\check{H}_1$, all the oddth (e.g. 1st, 3rd, 5th...) order corrections to the eigenvalues vanish, this will be discussed in details in Section 2.3. The second order corrections to the eigenvalues can be figured out by the equation below:

$$\lambda_i^{(2)} = \sum_{k\neq i} \frac{[2E(\check{H}_1)_{ik}]^2}{\lambda_i - \lambda_k}. \tag{2.23}$$

Second order eigenvalue corrections are:

$$\begin{aligned}
\lambda_1^{(2)} &= -(\epsilon'\,\Delta m^2_{ee})^2\,\frac{\tilde{s}^2_{12}}{\lambda_3 - \lambda_1} \\
\lambda_2^{(2)} &= -(\epsilon'\,\Delta m^2_{ee})^2\,\frac{\tilde{c}^2_{12}}{\lambda_3 - \lambda_2} \\
\lambda_3^{(2)} &= -\big(\,\lambda_1^{(2)} + \lambda_2^{(2)}\,\big).
\end{aligned} \tag{2.24}$$

2.2.2 Eigenvectors

The exact (energy) eigenvectors $|\check{\nu}\rangle^{\text{ex}}$ and their zeroth order approximations are related by an equation:

$$|\check{\nu}\rangle^{\text{ex}} = W\ |\check{\nu}\rangle^{(0)}\,, \quad \text{with} \quad W = \left(\mathbb{1} + W^{(1)} + W^{(2)} + \dots\right) \tag{2.25}$$

In the above equation $W^{(i)}$ is an ith order 3×3 matrix. The first order correction is given by

$$\left(W^{(1)}\right)_{ij} = (\delta_{ij} - 1)\,\frac{2E\,(\check{H}_1)_{ij}}{\lambda_i - \lambda_j}. \tag{2.26}$$

If we substitute $\check{H}_1$'s elements into the above equation, it is straightforward to have

$$W^{(1)} = \epsilon' \Delta m^2_{ee} \begin{pmatrix} & & -\frac{\tilde{s}_{12}}{\lambda_3 - \lambda_1} \\ & & \frac{\tilde{c}_{12}}{\lambda_3 - \lambda_2} \\ \frac{\tilde{s}_{12}}{\lambda_3 - \lambda_1} & -\frac{\tilde{c}_{12}}{\lambda_3 - \lambda_2} & \end{pmatrix}. \tag{2.27}$$

The second order correction matrix $W^{(2)}$ can be calculated by

$$(W^{(2)})_{ij} = \begin{cases} -\frac{1}{2} \sum\limits_{k \neq i} \frac{|2E(\check{H}_1)_{ik}|^2}{(\lambda_i - \lambda_k)^2} & i = j \\ \frac{1}{\lambda_i - \lambda_j} \sum\limits_{k \neq i, k \neq j} \frac{2E(\check{H}_1)_{ik} 2E(\check{H}_1)_{kj}}{\lambda_k - \lambda_j} & i \neq j \end{cases}. \tag{2.28}$$

We can figure out all $W^{(2)}$'s elements:

$$W^{(2)} = -\frac{(\epsilon' \Delta m^2_{ee})^2}{2} \begin{pmatrix} \left(\frac{\tilde{s}_{12}}{\lambda_3 - \lambda_1}\right)^2 & -\frac{2\tilde{s}_{12}\tilde{c}_{12}}{(\lambda_3 - \lambda_2)(\lambda_2 - \lambda_1)} & 0 \\ \frac{2\tilde{s}_{12}\tilde{c}_{12}}{(\lambda_3 - \lambda_1)(\lambda_2 - \lambda_1)} & \left(\frac{\tilde{c}_{12}}{\lambda_3 - \lambda_2}\right)^2 & 0 \\ 0 & 0 & \left(\frac{\tilde{s}_{12}}{\lambda_3 - \lambda_1}\right)^2 + \left(\frac{\tilde{c}_{12}}{\lambda_3 - \lambda_2}\right)^2 \end{pmatrix}. \tag{2.29}$$

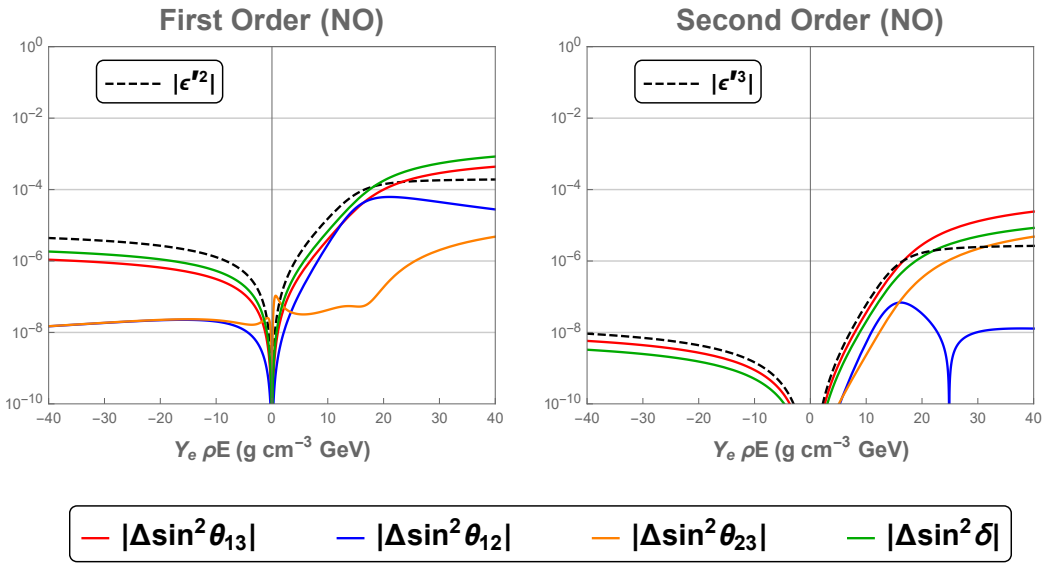

Figure 2.2: The absolute accuracy of the approximations of the mixing angles and CP phase in matter in this chapter to first order (left) and second order (right) for the normal mass ordering. The black dashed curves in the left and right plots are $|\epsilon'^2|$ and $|\epsilon'^3|$, respectively. It is evident that the error of $\sin^2$ of each mixing angle and phase at first (second) order is about ϵ'^2 (ϵ'^3).

2.2.3 Mixing angles and CP phase

We can also figure out correction terms to the mixing angles and the CP phase. Let's assume that the exact PMNS matrix with the given a is

$$\begin{aligned} U_{\rm PMNS}^{\rm ex} &= e^{iA}\, U_{23}(\tilde{\theta}_{23}^{\rm ex}, \tilde{\delta}^{\,\rm ex})\, U_{13}(\tilde{\theta}_{13}^{\rm ex})\, U_{12}(\tilde{\theta}_{12}^{\rm ex})\, e^{iB} \\ &= U_{23}(\tilde{\theta}_{23}, \tilde{\delta}) U_{13}(\tilde{\theta}_{13}) U_{12}(\tilde{\theta}_{12}) W, \end{aligned} \tag{2.30}$$

In the above equation $\tilde{\theta}_{ij}^{\rm ex}$ and $\tilde{\delta}^{\,\rm ex}$ are the exact mixing angles and CP phase in matter and both A and B are some real numbers. Eq. 2.30 can be solved orders by order (in ϵ'). We present the first two order of correction terms below [27]. Numerical tests of the precision are presented in Fig. 2.2.

The first order corrections are:

$$\begin{aligned}
\tilde{\theta}_{13}^{(1)} &= \epsilon' \Delta m_{ee}^2 \tilde{s}_{12}\tilde{c}_{12}\left(\frac{1}{\lambda_3-\lambda_2}-\frac{1}{\lambda_3-\lambda_1}\right),\\
\tilde{\theta}_{12}^{(1)} &= -\epsilon' \Delta m_{ee}^2 \frac{\tilde{s}_{13}}{\tilde{c}_{13}}\left(\frac{\tilde{s}_{12}^2}{\lambda_3-\lambda_1}+\frac{\tilde{c}_{12}^2}{\lambda_3-\lambda_2}\right),\\
\tilde{\theta}_{23}^{(1)} &= \epsilon' \Delta m_{ee}^2 \frac{\tilde{c}_{\delta}}{\tilde{c}_{13}}\left(\frac{\tilde{s}_{12}^2}{\lambda_3-\lambda_1}+\frac{\tilde{c}_{12}^2}{\lambda_3-\lambda_2}\right),\\
\tilde{\delta}^{(1)} &= -\epsilon' \Delta m_{ee}^2 \frac{2c_{2\tilde{\theta}_{23}}\tilde{s}_{\delta}}{s_{2\tilde{\theta}_{23}}\tilde{c}_{13}}\left(\frac{\tilde{s}_{12}^2}{\lambda_3-\lambda_1}+\frac{\tilde{c}_{12}^2}{\lambda_3-\lambda_2}\right).
\end{aligned} \tag{2.31}$$

The second order corrections are:

$$\begin{aligned}
\tilde{\theta}_{13}^{(2)} &= -\frac{\tilde{s}_{13}}{2\tilde{c}_{13}}\left[(W_1')_{23}\right]^2,\\
\tilde{\theta}_{12}^{(2)} &= (W_2')_{12}-\frac{\tilde{s}_{13}^2}{\tilde{c}_{13}^2}(W_1')_{13}(W_1')_{23},\\
\tilde{\theta}_{23}^{(2)} &= \frac{\tilde{c}_{\delta}\tilde{s}_{13}}{\tilde{c}_{13}^2}(W_1')_{13}(W_1')_{23}+\frac{c_{2\tilde{\theta}_{23}}\tilde{s}_{\delta}^2}{s_{2\tilde{\theta}_{23}}\tilde{c}_{13}^2}\left[(W_1')_{23}\right]^2,\\
\tilde{\delta}^{(2)} &= -\frac{2c_{2\tilde{\theta}_{23}}\tilde{s}_{\delta}\tilde{s}_{13}}{s_{2\tilde{\theta}_{23}}\tilde{c}_{13}^2}(W_1')_{13}(W_1')_{23}+\frac{2(1+c_{2\tilde{\theta}_{23}}^2)\tilde{s}_{\delta}\tilde{c}_{\delta}}{\tilde{c}_{13}^2 s_{2\tilde{\theta}_{23}}^2}[(W_1')_{23}]^2,
\end{aligned} \tag{2.32}$$

where W_1' and W_2' are 3×3 matrices. W_1' is in first order (of ϵ') and W_2' is in second order. In the above equations $(W_1')_{13}$, $(W_1')_{23}$, and $(W_2')_{12}$ are

$$(W_1')_{13} = \epsilon' \Delta m_{ee}^2 \tilde{s}_{12}\tilde{c}_{12}\left(\frac{1}{\lambda_3-\lambda_2}-\frac{1}{\lambda_3-\lambda_1}\right), \tag{2.33}$$

$$\begin{aligned}
(W_1')_{23} &= \epsilon' \Delta m_{ee}^2\left(\frac{\tilde{s}_{12}^2}{\lambda_3-\lambda_1}+\frac{\tilde{c}_{12}^2}{\lambda_3-\lambda_2}\right),\\
(W_2')_{12} &= (\epsilon' \Delta m_{ee}^2)^2 \tilde{s}_{12}\tilde{c}_{12}\left\{\frac{\tilde{c}_{12}^2}{(\lambda_3-\lambda_2)(\lambda_2-\lambda_1)}\right.\\
&\quad \left.+\frac{\tilde{s}_{12}^2}{(\lambda_3-\lambda_1)(\lambda_2-\lambda_1)}-\frac{1}{2}\left[\frac{\tilde{c}_{12}^2}{(\lambda_3-\lambda_2)^2}-\frac{\tilde{s}_{12}^2}{(\lambda_3-\lambda_1)^2}\right]\right\}.
\end{aligned} \tag{2.34}$$

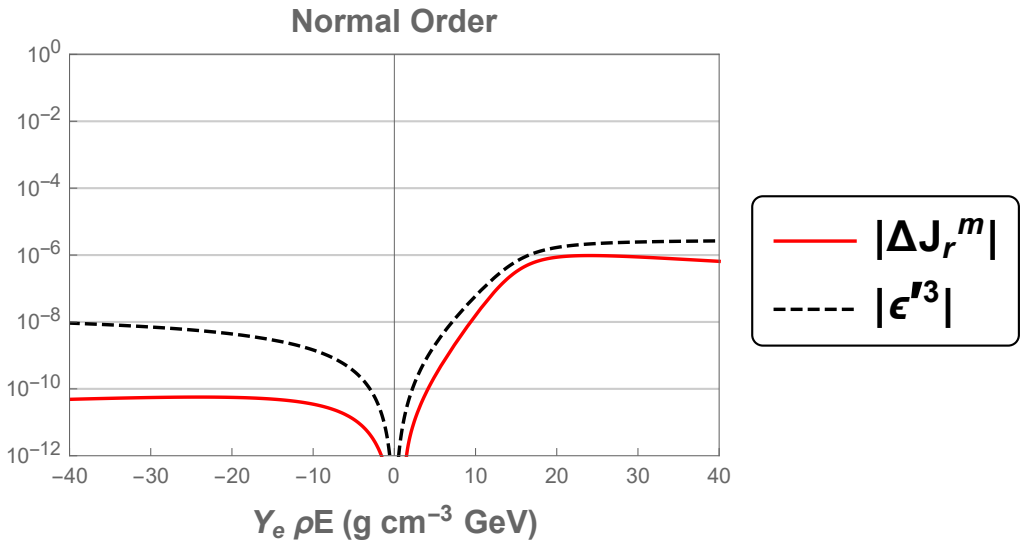

Figure 2.3: This figure shows ΔJ_r^m defined in Eq. 2.40 through second order (red curve) for the normal mass ordering. The black dashed line is ϵ'^3.

2.2.4 Some identities

In general all the mixing angles, CP phase and eigenvalues will be altered by the matter effect. However, there are still some quantities which are invariant in matter, thus give some identities.

One of such identities is the Naumov-Harrison-Scott identity [50, 39]. It is written as

$$s_{12}c_{12}s_{13}c_{13}^2s_{23}c_{23}s_\delta \prod_{i>j}\Delta m_{ij}^2 = \tilde{s}_{12}^{\rm ex}\,\tilde{c}_{12}^{\rm ex}\,\tilde{s}_{13}^{\rm ex}\,\tilde{c}_{13}^{\rm ex\,2}\,\tilde{s}_{23}^{\rm ex}\,\tilde{c}_{23}^{\rm ex}\,\tilde{s}_\delta^{\rm ex}\prod_{i>j}(\lambda_i^{\rm ex}-\lambda_j^{\rm ex}). \tag{2.35}$$

As in Eq. 2.30, the *ex* superscript means the exact values in matter. A simpler identity known as the Toshev identity [58] is written as

$$s_{2\theta_{23}}s_\delta = s_{2\tilde{\theta}_{23}}^{\rm ex}\tilde{s}_\delta^{\rm ex}. \tag{2.36}$$

Combining the above two identities a third identity can be derived [43]

$$s_{12}c_{12}s_{13}c_{13}^2\frac{\prod_{i>j}\Delta m_{ij}^2}{\prod_{i>j}(\lambda_i^{\rm ex}-\lambda_j^{\rm ex})} = \tilde{s}_{12}^{\rm ex}\,\tilde{c}_{12}^{\rm ex}\,\tilde{s}_{13}^{\rm ex}\,\tilde{c}_{13}^{\rm ex\,2}. \tag{2.37}$$

If we define

$$\begin{aligned} J_r &\equiv s_{12}c_{12}s_{13}c_{13}^2, \\ J_r^m &\equiv \tilde{s}_{12}^{\rm ex}\,\tilde{c}_{12}^{\rm ex}\,\tilde{s}_{13}^{\rm ex}\,\tilde{c}_{13}^{\rm ex\,2}, \end{aligned} \tag{2.38}$$

where J_r is a reduced Jarlskog factor [41] and similarly for the matter values, the third identity can be rewritten as

$$J_r\frac{\prod_{i>j}\Delta m_{ij}^2}{\prod_{i>j}(\lambda_i^{\rm ex}-\lambda_j^{\rm ex})} = J_r^m. \tag{2.39}$$

For the third identity shown in Eq. 2.39, analytic verification is complicated. An alternative numerical test is provided. We define an error function as

$$\Delta J_r^m \equiv J_r^m - J_r\frac{\prod_{i>j}\Delta m_{ij}^2}{\prod_{i>j}(\lambda_i^{\rm ex}-\lambda_j^{\rm ex})} \tag{2.40}$$

With the exact solutions in matter the error function ΔJ_r^m should always be zero. However, if we use our second order approximations to replace the exact values $\tilde{s}_{ij}^{\rm ex}$, $\tilde{c}_{ij}^{\rm ex}$, $\lambda_i^{\rm ex}$, then the expected error function should be in $\mathcal{O}(\epsilon'^3)$ or smaller. We have shown the scale of it (as a function of energy) in Fig. 2.3, in which we can see that the third identity holds to third order of ϵ' or better.

2.3 Arbitrary oddth order corrections to the eigenvalues

In Section 2.2 we have noticed that first order corrections to all of the eigenvalues vanish. Actually this fact is a special case of a more general result that give $\check{H}_1$ in Eq. 2.19, arbitrary oddth order corrections to the eigenvalues vanish.

2.3.1 A formal proof in mathematics

We define that H_0 is the zeroth order Hamiltonian and V is a first order perturbative term, both of them are Hermitian. $|n^{(0)}\rangle$ and $E_n^{(0)}$ are the zeroth order eigenvectors and eigenvalues respectively. With the perturbative Hamiltonian, the eigensystem will be modified as

$$\begin{aligned} |n\rangle &= \sum_i \sum_k a_{nk}^{(i)} |k^{(0)}\rangle , \\ E_n &= \sum_i E_n^{(i)}, \end{aligned} \tag{2.41}$$

where the index i indicates the ith order values. The modified eigensystem must satisfy the following equation

$$(H_0 + V) |n\rangle = E_n |n\rangle , \tag{2.42}$$

i.e.

$$(H_0 + V) \sum_i \sum_k a_{nk}^{(i)} |k^{(0)}\rangle = \Big(\sum_j E_n^{(j)} \Big) \sum_i \sum_k a_{nk}^{(i)} |k^{(0)}\rangle . \tag{2.43}$$

Definition 1. *For p, q, $N \in \mathbf{N}$, an Nth order p-q path c_{pq}^N is a product of N matrix elements of V and can be written in the form of*

$$c_{pq}^N = V_{pk_1} \Big(\prod_{i=1}^{N-2} V_{k_i k_{i+1}} \Big) V_{k_{N-1} q}, \tag{2.44}$$

where $V_{ij} \equiv \langle^{(0)} i| V |j^{(0)}\rangle$. The set of c_{pq}^N is represented by $\mathcal{C}_{pq}^N$.

Definition 2. *For n, p, q, $N \in \mathbf{N}$, an Nth order closed n-path c_n^N is an Nth order p-q path with $p = q = n$, i.e.*

$$c_n^N \equiv c_{nn}^N. \tag{2.45}$$

We name set of all c_n^N to be $\mathcal{C}_n^N$.

Definition 3. *A simple Nth order m-path is an Nth order m-path such that in Eq. 2.44 $k_i \neq n$ for $1 \leq i \leq N-1$.*

Proposition 1. *The product of an Nth order p-q path and an Mth order q-r path is an $(N+M)$th order p-r path; the product of an Nth order closed m-path and an Mth order closed m-path is an $(N+M)$th order closed m-path. (trivial to prove.)*

Proposition 2. *The complex conjugate of an Nth order p-q path is an Nth order q-p path.*

Proof of Proposition 2 Because V is Hermitian, $V_{ij}^* = V_{ji}$, so

$$\begin{aligned} c_{pq}^{*N} &= V_{pk_1}^* \Big(\prod_{i=1}^{N-2} V_{k_i k_{i+1}}^* \Big) V_{k_{N-1} q}^* \\ &= V_{k_1 p} \Big(\prod_{i=1}^{N-2} V_{k_{i+1} k_i} \Big) V_{q k_{N-1}} \\ &= c_{qp}^N. \end{aligned} \tag{2.46}$$

□

Proposition 3. *To the ith order corrections, $E_n^{(i)}$ is the sum of monomials proportional to ith order closed n-paths. $a_{nk}^{(i)}$ is the sum of monomials proportional to ith order k-n paths.*

Before giving the proof of Proposition 3, we would like to give some examples to make its expression more concrete. To first order

$$E_n^{(1)} = V_{nn}, \quad a_{nk}^{(1)} = \frac{V_{kn}}{E_n^{(0)} - E_k^{(0)}} \text{ for } k \neq n. \tag{2.47}$$

In the above equations V_{nn} is a 1st order closed n-path, and V_{kn} is a 1st order k-n path. To second order

$$E_n^{(2)} = \sum_{k\neq n} \frac{V_{nk}V_{kn}}{E_n^{(0)} - E_k^{(0)}},$$
$$a_{nk}^{(2)} = \sum_{l\neq n} \frac{V_{kl}V_{ln}}{(E_n^{(0)} - E_k^{(0)})(E_n^{(0)} - E_l^{(0)})} - \frac{V_{kn}V_{nn}}{(E_n^{(0)} - E_k^{(0)})^2} \text{ for } k \neq n. \tag{2.48}$$

In the above equations $V_{nk}V_{kn}$ is a 2nd order closed n-path; $V_{kl}V_{ln}$ and $V_{kn}V_{nn}$ are 2nd order k-n paths. With the above examples we are ready to give the proof of lemma 3.

Proof of Proposition 3 We are going to use the induction to give the proof. Obviously the proposition is correct for the several low order corrections. Let's assume that the proposition is true until the $(i-1)$th order corrections.

By Eq. 2.43 we have

$$\langle^{(0)} n| \left(H_0 + V\right) \sum_i \sum_k a_{nk}^{(i)} |k^{(0)}\rangle = \langle^{(0)} n| \left(\sum_j E_n^{(j)}\right) \sum_i \sum_k a_{nk}^{(i)} |k^{(0)}\rangle . \tag{2.49}$$

If we just extract the ith order equivalence

$$E_n^{(0)} a_{nn}^{(i)} + \sum_k V_{nk} a_{nk}^{(i-1)} = \sum_{j=0}^{i} E_n^{(j)} a_{nn}^{(i-j)}. \tag{2.50}$$

Since $a_{ij}^{(0)} = \delta_{ij}$, the above equation gives

$$E_n^{(i)} = \sum_k V_{nk} a_{nk}^{(i-1)} - \sum_{j=1}^{i-1} E_n^{(j)} a_{nn}^{(i-j)}. \tag{2.51}$$

Let's look at the first summation on the R.H.S.. By the assumption that $a_{nk}^{(i-1)}$ consists

of terms proportional to $(i-1)$th order k-n paths, V_{nk} is a 1st order n-k path, to apply Proposition 1 their product consists of terms proportional to ith order n-n paths, i.e. ith order closed n-paths. In the second summation, by the assumption $E_n^{(j)}$ consists of terms proportional to jth order closed n-paths, $a_{nn}^{(i-j)}$ consists of terms proportional to $(i-j)$th order closed n-paths, by applying Proposition 1 again, their product also consists of terms proportional to ith order closed n-paths.

Now let's focus on the proposition related to $a_{nk}^{(i)}$ in Proposition 3. The Eq. 2.43 also leads to

$$\langle^{(0)}k|\,(H_0+V)\sum_i\sum_m a_{nm}^{(i)}\,|m^{(0)}\rangle = \langle^{(0)}k|\,\Big(\sum_j E_n^{(j)}\Big)\sum_i\sum_m a_{nm}^{(i)}\,|m^{(0)}\rangle \quad \text{for } k\neq n. \tag{2.52}$$

Again we can extract the ith order equivalence

$$E_k^{(0)}a_{nk}^{(i)} + \sum_j V_{kj}a_{nj}^{(i-1)} = \sum_{m=0}^{i} E_n^{(m)}a_{nk}^{(i-m)}. \tag{2.53}$$

We can solve $a_{nk}^{(i)}$ from the above equation

$$a_{nk}^{(i)} = \frac{1}{E_k^{(0)}-E_n^{(0)}}\Big(\sum_{m=1}^{i} E_n^{(m)}a_{nk}^{(i-m)} - \sum_j V_{kj}a_{nj}^{(i-1)}\Big) \tag{2.54}$$

On the right hand side, in the first summation in the bracket, $E_n^{(m)}$ consists of terms proportional to mth order closed n-paths, $a_{nk}^{(i-m)}$ consists of terms proportional to $(i-m)$th order k-n paths so their product consists of terms proportional to ith order k-n paths. In the second summation V_{kj} is a first order k-j path and $a_{nj}^{(i-1)}$ consists of terms proportional to $(i-1)$th order j-n paths, their product consists of terms proportional to ith order k-n path.

Finally we require the corrected eigenvectors to be normalized, i.e.

$$\langle n|n\rangle = 1. \tag{2.55}$$

Substitute Eq. 2.44 into the above equation we get

$$\sum_p \sum_q \langle^{(0)} p| \sum_i a_{np}^{*(i)} \sum_j a_{nq}^{(j)} \, |q^{(0)}\rangle = 1. \tag{2.56}$$

Because $a_{ij}^{(0)} = \delta_{ij}$, the ith order equivalence is

$$\sum_p \sum_q \left(a_{np}^{*(0)} a_{nq}^{(i)} + a_{np}^{*(i)} a_{nq}^{(0)} + \sum_{j=1}^{i-1} a_{np}^{*(j)} a_{nq}^{(i-j)} \right) \delta_{pq} = 0. \tag{2.57}$$

This gives

$$a_{nn}^{*(i)} + a_{nn}^{(i)} = -\sum_p \sum_{j=1}^{i-1} a_{np}^{*(j)} a_{np}^{(i-j)}. \tag{2.58}$$

Since each eigenstate multiplies a pure complex phase is still an eigenstate, we are free to set all the $a_{nn}^{(i)}$ to be real, i.e.

$$a_{nn}^{(i)} = -\frac{1}{2} \sum_p \sum_{j=1}^{i-1} a_{np}^{*(j)} a_{np}^{(i-j)}. \tag{2.59}$$

Because of Proposition 2 and the initial assumption $a_{np}^{*(j)}$ must be proportional to a jth order n-p path, $a_{np}^{*(j)} a_{np}^{(i-j)}$ must be proportional to a closed ith order n-path.

The above derivations complete the inductive step. □

Proposition 4. *If i is an odd number, an ith order closed n-path c_n^i is not simple, there must exist at least one odd number j and a simple jth order closed n-path c_n^j such that $c_n^{(i)} = c_n^{(i-j)} \, c_n^j$.*

Proof of Proposition 4 This proof is also trivial. Obviously a non-simple ith order closed n-path can be written as the product of two or more lower order simple closed n-paths. If all of these lower order paths are in even orders, the product must be also in even order. This contradicts the precondition that i is odd. □

Proposition 5. *With $V = \check{H}_1$ in Eq. 2.19, an oddth order simple closed n-path vanishes.*

Proof of Proposition 5 Now we have

$$V \propto \begin{pmatrix} & & -\tilde{s}_{12} \\ & & \tilde{c}_{12} \\ -\tilde{s}_{12} & \tilde{c}_{12} & \end{pmatrix}. \tag{2.60}$$

A first order closed n-path is just the nth diagonal element of V which is obviously zero. A simple 3rd order closed n-path is $V_{nk_1}V_{k_1k_2}V_{k_2n}$. Neither k_1 nor k_2 can be n otherwise it breaks the simple condition. If $k_1 = k_2$, $V_{k_1k_2}$ vanishes, if $k_1 \neq k_2$, the pairs nk_1, k_1k_2 and k_2n traversing all the off-diagonal indices and V_{12} (or V_{21}) kills the whole path. For $i \geq 5$, let's consider $V_{nk_1}V_{k_1k_2}\cdots V_{k_jk_{j+1}}\cdots V_{k_{i-1}n}$. Again any same neighboring index will produce an diagonal element of V and kills the whole chain. The only possible non-vanishing choice is $k_j = k_{j+2}$. However, because i is odd, $k_{i-1} = k_2 \neq k_1$, then nk_1, k_1k_2 and $k_{i-1}n$ traversing all the off-diagonal indices again. Thus the whole path must be zero. □

Proposition 6. *This is the main result. If the perturbative Hamiltonian $V = \check{H}_1$ defined in Eq. 2.19, $E_n^{(i)} = 0$ for i is odd.*

Proof of Proposition 6 Apply Proposition 4 to Proposition 5, we see that all the oddth order closed m-paths vanish. Then apply this conclusion to Proposition 3, we prove the main result. □

2.3.2 An extension to more general cases

The proof in the last subsection can apply to a more general perturbative Hamiltonian. Now we consider an $n \times n$ Hamiltonian and a perturbative term which has a form of

$$V_{n\times n} = \begin{pmatrix} 0_{r\times r} & V_{r\times(n-r)} \\ V_{(n-r)\times r} & 0_{(n-r)\times(n-r)} \end{pmatrix}, \tag{2.61}$$

with $0 \leq r \leq n$. The Propositions 1-4 still hold because their proofs do not rely on dimension of the Hamiltonian. Therefore we only need to prove Proposition 5. We consider a 3rd order non-zero closed k_1-path $V_{k_1k_2}V_{k_2k_3}V_{k_3k_1}$. If $k_1 \leq r$, then we have $k_2 > r$ otherwise $V_{k_1k_2}$ vanishes, then we must also have $k_3 \leq r$ otherwise $V_{k_2k_3}$ vanishes, finally we see $V_{k_3k_1}$ is in the $0_{r\times r}$ block thus the closed path is zero. Therefore we see a non-zero 3rd order closed k_1-path with $k_1 \leq r$ does not exist. We can do a similar reasoning if $k_1 > r$. In this way we can prove Proposition 5. Because the main result Proposition 6 is just applying Proposition 4 to Proposition 5, we prove that for an arbitrary perturbative Hamiltonian with the form of Eq. 2.61, all oddth order corrections to the eigenvalues vanish. $\check{H}_1$ in Eq. 2.19 is a special case of $n = 3$ and $r = 2$.

CHAPTER 3

ROTATIONS VERSUS PERTURBATION THEORY

In Chapter 2, starting from the Hamiltonian in the flavor basis, we implemented three rotations to figure out the zeroth order approximations then performed perturbative expansions to calculate higher order corrections. The three rotations resolved zeroth order degeneracy and diminished scales of the perturbative terms (off-diagonal elements). In principle, we can perform more rotations to further decrease scales of the off-diagonal elements of the Hamiltonian thus improve the zeroth order. This idea is initialized in [53] and studied in details in [27]. In this Chapter, we will analyze relations between the additional rotations and perturbation theory.

3.1 Detailed calculation to second order

In Section 2.2 we derived detailed second order approximations from perturbation theory. In this section we are going to demonstrate that second order precision can alternatively be achieved by three more rotations.

3.1.1 Neutrino case

For neutrinos, $Y_e\rho E$ is positive and from [25] we have $|\tilde{s}_{12}| \gtrsim |\tilde{c}_{12}|$ in this case. Thus in Eq. 2.19 the 13 sector has the largest (absolute value) off-diagonal elements. We will implement a rotation to diagonalize this sector. We define α_{13} to be the rotation angle. The Hamiltonian after this rotation is defined to be

$$\check{H}' \equiv U_{13}^{\dagger}(\alpha_{13})\check{H}U_{13}(\alpha_{13}). \tag{3.1}$$

Elements of $\check{H}'$ can be found in Appendix A. It can be solved that

$$\alpha_{13} = -\frac{1}{2}\arctan\frac{2\epsilon'\Delta m^2_{ee}\tilde{s}_{12}}{\lambda_3-\lambda_1} = -\frac{\epsilon'\Delta m^2_{ee}\tilde{s}_{12}}{\lambda_3-\lambda_1} + \mathcal{O}(\epsilon'^3). \tag{3.2}$$

Because $\lambda_3 - \lambda_1 \gtrsim \Delta m^2_{ee}$, α_{13} is in order of ϵ' or smaller. We define λ'_i to be the new zeroth order eigenvalues (diagonal elements), they are

$$\begin{aligned}
\lambda'_1 &= c^2_{\alpha_{13}}\lambda_1 + s^2_{\alpha_{13}}\lambda_3 + 2s_{\alpha_{13}}c_{\alpha_{13}}\tilde{s}_{12}\epsilon'\Delta m^2_{ee} = \lambda_1 - (\epsilon'\Delta m^2_{ee})^2\frac{\tilde{s}^2_{12}}{\lambda_3-\lambda_1} + \mathcal{O}(\epsilon'^4),\\
\lambda'_2 &= \lambda_2,\\
\lambda'_3 &= s^2_{\alpha_{13}}\lambda_1 + c^2_{\alpha_{13}}\lambda_3 - 2s_{\alpha_{13}}c_{\alpha_{13}}\tilde{s}_{12}\epsilon'\Delta m^2_{ee} = \lambda_3 + (\epsilon'\Delta m^2_{ee})^2\frac{\tilde{s}^2_{12}}{\lambda_3-\lambda_1} + \mathcal{O}(\epsilon'^4).
\end{aligned} \tag{3.3}$$

From the above equations it is not hard to notice that the $U_{13}(\alpha_{13})$ rotation only gives second order corrections to the zeroth order eigenvalues. On the other hand, Eq. 2.22 shows that all first order corrections to the eigenvalues vanish. This equivalence indicates an intrinsic relation between the additional rotations and the perturbation theory which will be discussed in Section 3.1.4.

Since α_{13} is small, the leading order off-diagonal elements of $\check{H}'$ are proportional to $\tilde{c}_{12}c_{\alpha_{13}}$ so the next rotation should diagonalize the 23 sector with a new angle α_{23}. The rotated Hamiltonian is

$$\check{H}'' \equiv U^\dagger_{23}(\alpha_{23})U^\dagger_{13}(\alpha_{13})\check{H}U_{13}(\alpha_{13})U_{23}(\alpha_{23}), \tag{3.4}$$

details of $\check{H}''$ can be found in Appendix A. The rotation angle is

$$\alpha_{23} = \frac{1}{2}\arctan\frac{2\epsilon'\Delta m^2_{ee}c_{\alpha_{13}}\tilde{c}_{12}}{\lambda'_3-\lambda'_2} = \frac{\epsilon'\Delta m^2_{ee}\tilde{c}_{12}}{\lambda_3-\lambda_2} + \mathcal{O}(\epsilon'^3). \tag{3.5}$$

α_{23} is also at least first order in ϵ' since $\lambda_3 - \lambda_2 \gtrsim \Delta m^2_{ee}$. The new eigenvalues are

$$\begin{aligned}
\lambda''_1 &= \lambda'_1 = \lambda_1 - (\epsilon' \Delta m^2_{ee})^2 \frac{\tilde{s}^2_{12}}{\lambda_3 - \lambda_1} + \mathcal{O}(\epsilon'^4), \\
\lambda''_2 &= c^2_{\alpha_{23}} \lambda'_2 + s^2_{\alpha_{23}} \lambda'_3 - 2 s_{\alpha_{23}} c_{\alpha_{23}} c_{\alpha_{13}} \tilde{c}_{12} \epsilon' \Delta m^2_{ee} \\
&= \lambda_2 - (\epsilon' \Delta m^2_{ee})^2 \frac{\tilde{c}^2_{12}}{\lambda_3 - \lambda_2} + \mathcal{O}(\epsilon'^4), \\
\lambda''_3 &= s^2_{\alpha_{23}} \lambda'_2 + c^2_{\alpha_{23}} \lambda'_3 + 2 s_{\alpha_{23}} c_{\alpha_{23}} c_{\alpha_{13}} \tilde{c}_{12} \epsilon' \Delta m^2_{ee} \\
&= \lambda_3 + (\epsilon' \Delta m^2_{ee})^2 \left(\frac{\tilde{s}^2_{12}}{\lambda_3 - \lambda_1} + \frac{\tilde{c}^2_{12}}{\lambda_3 - \lambda_1} \right) + \mathcal{O}(\epsilon'^4).
\end{aligned} \tag{3.6}$$

Compare the above results with Eq. 2.24, it is evident that eigenvalue corrections from the two additional rotations are equivalent to ones from a second order perturbation theory.

α_{23} is a small angle (in scale of ϵ' or smaller). After the $U_{23}(\alpha_{23})$ rotation the leading order off-diagonal elements are in the 12 sector. We assume that $U_{12}(\alpha_{12})$ can diagonalize the sector and after this rotation the Hamiltonian becomes

$$\check{H}''' \equiv U^\dagger_{12}(\alpha_{12}) U^\dagger_{23}(\alpha_{23}) U^\dagger_{13}(\alpha_{13}) \check{H} U_{13}(\alpha_{13}) U_{23}(\alpha_{23}) U_{12}(\alpha_{12}). \tag{3.7}$$

Elements of $\check{H}'''$ can be found in Appendix A. Value of α_{12} can be figured out by

$$\alpha_{12} = -\frac{1}{2} \arctan \frac{2\epsilon' \Delta m^2_{ee} c_{\alpha_{23}} s_{\alpha_{13}} \tilde{c}_{12}}{\lambda''_2 - \lambda''_1} = \frac{(\epsilon' \Delta m^2_{ee})^2 \tilde{s}_{12} \tilde{c}_{12}}{(\lambda_2 - \lambda_1)(\lambda_3 - \lambda_1)} + \mathcal{O}(\epsilon'^4). \tag{3.8}$$

The zeroth order eigenvalues become

$$\begin{aligned}
\lambda'''_1 &= c^2_{\alpha_{12}} \lambda''_1 + s^2_{\alpha_{12}} \lambda''_2 + 2 s_{\alpha_{12}} c_{\alpha_{12}} c_{\alpha_{23}} s_{\alpha_{13}} \tilde{c}_{12} \epsilon' \Delta m^2_{ee} \\
&= \lambda_1 - (\epsilon' \Delta m^2_{ee})^2 \frac{\tilde{s}^2_{12}}{\lambda_3 - \lambda_1} + \mathcal{O}(\epsilon'^4), \\
\lambda'''_2 &= s^2_{\alpha_{12}} \lambda''_1 + c^2_{\alpha_{12}} \lambda''_2 - 2 s_{\alpha_{12}} c_{\alpha_{12}} c_{\alpha_{23}} s_{\alpha_{13}} \tilde{c}_{12} \epsilon' \Delta m^2_{ee}
\end{aligned}$$

$$= \lambda_2 - (\epsilon' \Delta m^2_{ee})^2 \frac{\tilde{c}^2_{12}}{\lambda_3 - \lambda_2} + \mathcal{O}(\epsilon'^4),$$

$$\lambda'''_3 = \lambda''_3 = \lambda_3 + (\epsilon' \Delta m^2_{ee})^2 \left(\frac{\tilde{s}^2_{12}}{\lambda_3 - \lambda_1} + \frac{\tilde{c}^2_{12}}{\lambda_3 - \lambda_2} \right) + \mathcal{O}(\epsilon'^4). \tag{3.9}$$

It is noteworthy that λ'''_i and λ''_i are at least identical to second order. To understand this observation, we need to study the perturbative Hamiltonian after each rotation. It is known that in a perturbative expansion, leading order corrections to the eigenvalues are the diagonal elements of the perturbative Hamiltonian. In Appendix A, we shall demonstrate that after the first two additional rotations, the perturbative Hamiltonian whose diagonal entries are all zero, is in second order; thus errors of λ''_i are already controlled to fourth order. And after the third $U_{12}(\alpha_{12})$ rotation, the perturbative Hamiltonian (still with vanishing diagonal entries) is in third order; thus errors of λ'''_i are further diminished to sixth order. Therefore, it is not unexpected that λ''_i and λ'''_i are identical to second order.

Terms of order ϵ'^3 are no larger than 3×10^{-6}. In principle, we can continue performing rotations to control the off-diagonal elements to arbitrary precision. Considering the precision of the experimental uncertainties $\sim 1\%$ [7, 55, 2, 4, 42], stopping at $U_{12}(\alpha_{12})$ is more than enough. In Section 3.1.3 we will show that it is equal to second order (in ϵ') perturbation theory when considering eigenvectors.

3.1.2 Anti-neutrino case

For anti-neutrinos, $Y_e \rho E$ is negative and from [25] we have $|\tilde{c}_{12}| \gtrsim |\tilde{s}_{12}|$ in this case. The following calculation process will be similar to the case of neutrinos. In Eq. 2.19 the 23 sector has the largest (absolute value) off-diagonal elements. We will firstly implement a rotation to diagonalize this sector. We define $\bar{\alpha}_{23}$ to be the rotation angle and it is solved as

$$\bar{\alpha}_{23} = \frac{1}{2} \arctan \frac{2\epsilon' \Delta m^2_{ee} \tilde{c}_{12}}{\lambda_3 - \lambda_2} = \frac{\epsilon' \Delta m^2_{ee} \tilde{c}_{12}}{\lambda_3 - \lambda_2} + \mathcal{O}(\epsilon'^3). \tag{3.10}$$

After this rotation the zeroth order eigenvalues are

$$
\begin{aligned}
&\bar{\lambda}'_1 = \lambda_1, \\
&\bar{\lambda}'_2 = c^2_{\bar{\alpha}_{23}}\lambda_2 + s^2_{\bar{\alpha}_{23}}\lambda_3 - 2s_{\bar{\alpha}_{23}}c_{\bar{\alpha}_{23}}\tilde{c}_{12}\epsilon'\Delta m^2_{ee} = \lambda_2 - (\epsilon'\Delta m^2_{ee})^2\frac{\tilde{c}^2_{12}}{\lambda_3-\lambda_2} + \mathcal{O}(\epsilon'^4), \\
&\bar{\lambda}'_3 = s^2_{\bar{\alpha}_{23}}\lambda_2 + c^2_{\bar{\alpha}_{23}}\lambda_3 + 2s_{\bar{\alpha}_{23}}c_{\bar{\alpha}_{23}}\tilde{c}_{12}\epsilon'\Delta m^2_{ee} = \lambda_3 + (\epsilon'\Delta m^2_{ee})^2\frac{\tilde{c}^2_{12}}{\lambda_3-\lambda_2} + \mathcal{O}(\epsilon'^4). \quad (3.11)
\end{aligned}
$$

Before performing the next additional rotation in 13 sector, there are some comments on the above U_{23} rotation. In some former works, e.g. [19], a similar approach was followed with a rotation in the 23 sector as above, although there the rotation was used for both neutrinos and anti-neutrinos. In Section 3.1.4, we shall discuss the fact that one additional rotation does not improve the accuracy of the approximated eigenvectors. More specifically, if $|\check{\nu}\rangle^{\rm ex}$ are the exact eigenvectors in matter, errors of the initial zeroth order eigenvectors are estimated as $|\check{\nu}\rangle^{\rm ex} - |\check{\nu}\rangle^{(0)} \simeq \mathcal{O}(\epsilon')$. After the U_{23} rotation, the eigenvectors are corrected to be $U^\dagger_{23}|\check{\nu}\rangle^{(0)}$, which still have first order errors, i.e. $|\check{\nu}\rangle^{\rm ex} - U^\dagger_{23}|\check{\nu}\rangle^{(0)} \simeq \mathcal{O}(\epsilon')$ still holds. This indicates that to achieve better accuracy, we must perform an additional rotation.

After the $U_{23}(\bar{\alpha}_{23})$ rotation, the following rotation should be in the 13 sector and the rotation angel is $\bar{\alpha}_{13}$ given by

$$
\bar{\alpha}_{13} = -\frac{1}{2}\arctan\frac{2\epsilon'\Delta m^2_{ee}c_{\bar{\alpha}_{23}}\tilde{s}_{12}}{\bar{\lambda}'_3 - \bar{\lambda}'_1} = -\frac{\epsilon'\Delta m^2_{ee}\tilde{s}_{12}}{\lambda_3-\lambda_1} + \mathcal{O}(\epsilon'^3). \quad (3.12)
$$

The zeroth order eigenvalues after this rotation are

$$
\begin{aligned}
\bar{\lambda}''_1 &= c^2_{\bar{\alpha}_{13}}\bar{\lambda}'_1 + s^2_{\bar{\alpha}_{13}}\bar{\lambda}'_3 + 2s_{\bar{\alpha}_{13}}c_{\bar{\alpha}_{13}}c_{\bar{\alpha}_{23}}\tilde{s}_{12}\epsilon'\Delta m^2_{ee} \\
&= \lambda_1 - (\epsilon'\Delta m^2_{ee})^2\frac{\tilde{s}^2_{12}}{\lambda_3-\lambda_1} + \mathcal{O}(\epsilon'^3), \\
\bar{\lambda}''_2 &= \bar{\lambda}'_2 = \lambda_2 - (\epsilon'\Delta m^2_{ee})^2\frac{\tilde{c}^2_{12}}{\lambda_3-\lambda_2} + \mathcal{O}(\epsilon'^3),
\end{aligned}
$$

$$\begin{aligned}\bar{\lambda}_3'' &= s^2_{\bar{\alpha}_{13}}\bar{\lambda}_1' + c^2_{\bar{\alpha}_{13}}\bar{\lambda}_3' - 2s_{\bar{\alpha}_{13}}c_{\bar{\alpha}_{13}}c_{\bar{\alpha}_{23}}\tilde{s}_{12}\epsilon'\Delta m^2_{ee} \\ &= \lambda_3 + (\epsilon'\Delta m^2_{ee})^2\left(\frac{\tilde{s}^2_{12}}{\lambda_3-\lambda_1} + \frac{\tilde{c}^2_{12}}{\lambda_3-\lambda_2}\right) + \mathcal{O}(\epsilon'^3). \end{aligned} \tag{3.13}$$

Then we will perform a rotation $U_{12}(\bar{\alpha}_{12})$ to diagonalize the 12 sector. The rotation angle is

$$\bar{\alpha}_{12} = \frac{1}{2}\arctan\frac{2\epsilon'\Delta m^2_{ee}s_{\bar{\alpha}_{23}}c_{\bar{\alpha}_{13}}\tilde{s}_{12}}{\bar{\lambda}_2'' - \bar{\lambda}_1''} = \frac{(\epsilon'\Delta m^2_{ee})^2\tilde{s}_{12}\tilde{c}_{12}}{(\lambda_2-\lambda_1)(\lambda_3-\lambda_2)} + \mathcal{O}(\epsilon'^4). \tag{3.14}$$

The rotated zeroth order eigenvalues are

$$\begin{aligned}\bar{\lambda}_1''' &= c^2_{\bar{\alpha}_{12}}\bar{\lambda}_1'' + s^2_{\bar{\alpha}_{12}}\bar{\lambda}_2'' - 2s_{\bar{\alpha}_{12}}c_{\bar{\alpha}_{12}}c_{\bar{\alpha}_{13}}s_{\bar{\alpha}_{23}}\tilde{s}_{12}\epsilon'\Delta m^2_{ee} \\ &= \lambda_1 - (\epsilon'\Delta m^2_{ee})^2\frac{\tilde{s}^2_{12}}{\lambda_3-\lambda_1} + \mathcal{O}(\epsilon'^3), \\ \bar{\lambda}_2''' &= s^2_{\bar{\alpha}_{12}}\bar{\lambda}_1'' + c^2_{\bar{\alpha}_{12}}\bar{\lambda}_2'' + 2s_{\bar{\alpha}_{12}}c_{\bar{\alpha}_{12}}c_{\bar{\alpha}_{13}}s_{\bar{\alpha}_{23}}\tilde{s}_{12}\epsilon'\Delta m^2_{ee} \\ &= \lambda_2 - (\epsilon'\Delta m^2_{ee})^2\frac{\tilde{c}^2_{12}}{\lambda_3-\lambda_2} + \mathcal{O}(\epsilon'^3), \\ \bar{\lambda}_3''' &= \bar{\lambda}_3'' = \lambda_3 + (\epsilon'\Delta m^2_{ee})^2\left(\frac{\tilde{s}^2_{12}}{\lambda_3-\lambda_1} + \frac{\tilde{c}^2_{12}}{\lambda_3-\lambda_2}\right) + \mathcal{O}(\epsilon'^3). \end{aligned} \tag{3.15}$$

3.1.3 Rotated eigenvectors

Now let's consider the zeroth order eigenvectors after the additional rotations. We first define

$$W^R \equiv \begin{cases} U_{13}(\alpha_{13})U_{23}(\alpha_{23})U_{12}(\alpha_{12}) & \text{for neutrinos} \\ U_{23}(\bar{\alpha}_{23})U_{13}(\bar{\alpha}_{13})U_{12}(\bar{\alpha}_{12}) & \text{for anti-neutrinos} \end{cases}, \tag{3.16}$$

Then after the addition rotations the zeroth order eigenvectors become

$$|\check{\nu}\rangle_{W^R} = W^{R\dagger}\,|\check{\nu}\rangle^{(0)}\,, \tag{3.17}$$

We firstly consider the case of neutrinos. Substitute the values from Eq. 3.2, Eq. 3.5, and Eq. 3.8 into W^R, it can be verified that

$$
\begin{aligned}
W^R &= U_{13}(\alpha_{13})U_{23}(\alpha_{23})U_{12}(\alpha_{12}) \\
&= \mathbb{1} + \epsilon' \Delta m^2_{ee} \begin{pmatrix} & & -\frac{\tilde{s}_{12}}{\lambda_3-\lambda_1} \\ & & \frac{\tilde{c}_{12}}{\lambda_3-\lambda_2} \\ \frac{\tilde{s}_{12}}{\lambda_3-\lambda_1} & -\frac{\tilde{c}_{12}}{\lambda_3-\lambda_2} & \end{pmatrix} \\
&\quad - \frac{(\epsilon' \Delta m^2_{ee})^2}{2} \begin{pmatrix} \left(\frac{\tilde{s}_{12}}{\lambda_3-\lambda_1}\right)^2 & -\frac{2\tilde{s}_{12}\tilde{c}_{12}}{(\lambda_3-\lambda_2)(\lambda_2-\lambda_1)} & 0 \\ \frac{2\tilde{s}_{12}\tilde{c}_{12}}{(\lambda_3-\lambda_1)(\lambda_2-\lambda_1)} & \left(\frac{\tilde{c}_{12}}{\lambda_3-\lambda_2}\right)^2 & 0 \\ 0 & 0 & \left(\frac{\tilde{s}_{12}}{\lambda_3-\lambda_1}\right)^2 + \left(\frac{\tilde{c}_{12}}{\lambda_3-\lambda_2}\right)^2 \end{pmatrix} \\
&\quad + \mathcal{O}(\epsilon'^3).
\end{aligned} \tag{3.18}
$$

Compare with Eq. 2.27 and Eq. 2.29 we find that

$$W^R = \mathbb{1} + W^{(1)} + W^{(2)} + \mathcal{O}(\epsilon'^3) \tag{3.19}$$

It can also be verified that the above equation holds for the anti-neutrino case. Therefore, we demonstrate that for the eigenvectors implementing the three additional rotations is equivalent to perturbation theory to second order.

Several remarkable observations in Eq. 3.18 are listed below.

- Both $U_{13}(\alpha_{13})$ and $U_{23}(\alpha_{23})$ contribute to the first order term $W^{(1)}$. For example, if $\alpha_{13} = 0$, $(W^{(1)})_{13}$ and $(W^{(1)})_{31}$ equal zero; and if $\alpha_{23} = 0$, $(W^{(1)})_{23}$ and $(W^{(1)})_{32}$ vanish.

- Since α_{12} contributes only at second order, if we just perform the first two additional rotations, i.e. $\alpha_{12} = 0$, the first order $W^{(1)}$ will not be affected.

- $U_{12}(\alpha_{12})$ does contribute to the second order term $W^{(2)}$. For example, $(W^{(2)})_{21} = 0$

if $\alpha_{12} = 0$. That is, although the eigenvalues after two and three additional rotations, i.e. λ_i'' and λ_i''' are identical to second order, the eigenvectors are not.

These observations are necessary to the discussions in the next section about the relations between the additional rotations and perturbation theory.

3.1.4 Discussion and summary

From Eq. 3.18 and observations at the end of last subsection, we can draw following conclusions about the eigenvectors.

- After performing one additional rotation ($U_{13}(\alpha_{13})$ for neutrinos and $U_{23}(\bar{\alpha}_{23})$ for anti-neutrinos), the accuracy of the rotated eigenstates is not improved compared with the initial zeroth order $|\check{\nu}\rangle^{(0)}$, i.e. errors of the eigenstates are still in $\mathcal{O}(\epsilon')$.

- For neutrinos (anti-neutrinos), after performing two additional rotations in 13 and then 23 sectors (23 and then 13 sectors), errors of the rotated eigenstates are diminished to $\mathcal{O}(\epsilon'^2)$. Thus the eigenstates are equivalent to the ones of a first order perturbation theory through $\mathcal{O}(\epsilon')$ terms.

- Errors of the eigenstates will be further diminished to $\mathcal{O}(\epsilon'^3)$ by performing just one more rotation in 12 sector. Now the eigenstates have the same accuracy as the ones from a second order perturbation theory.

From Eq. 3.6 and Eq. 3.9 (and the corresponding equations for the anti-neutrino cases), we can make following conclusions about the eigenvalues.

- Errors of the eigenvalues after the first two additional rotations are already lower than $\mathcal{O}(\epsilon'^3)$ (that is, the eigenvalues are correct through $\mathcal{O}(\epsilon'^2)$). To reconcile with the conclusions of the eigenstates, we say that the eigenvalues after the first two additional rotations have at least the accuracy of the first order perturbation theory.

- Errors of the eigenvalues after the three additional rotations are even smaller, so of course lower than $\mathcal{O}(\epsilon'^3)$. Again to reconcile with the the conclusions of the eigenstates, we say that their accuracy is at least equivalent to the ones' corrected by a second order perturbation theory.

If we combine the conclusions about the eigenvectors and the eigenvalues together, we can figure out some equivalences between performing the additional rotations and perturbation theory.

- By performing two additional rotations in 13 and 23 sector (the order is exchanged for anti-neutrinos), we can improve the eigenvectors and eigenvalues to be as precise as the ones from first order perturbation theory.

- By performing three additional rotations, we can improve the eigenvectors and eigenvalues to be as precise as the ones from a second order perturbation theory.

3.2 Fibonacci fast convergence of the rotations

In the last section we have shown that a second order perturbation theory can be replaced by three additional rotations. In this section , we are going to provide an analytic approach to study improvement of precision by the rotations [28].

For an arbitrary $n \times n$ Hermitian matrix $\mathcal{H}$, we choose two diagonal elements $\mathcal{H}_{pp}$ and $\mathcal{H}_{qq}$ and the two corresponding off-diagonal element $\mathcal{H}_{pq}$ and $\mathcal{H}_{qp}$. The selected four elements form a 2×2 Hermitian submatrix h,

$$\mathrm{h} = \begin{pmatrix} \mathcal{H}_{pp} & \mathcal{H}_{pq} \\ \mathcal{H}_{qp} & \mathcal{H}_{qq} \end{pmatrix} . \tag{3.20}$$

It can be diagonalized by a single 2×2 complex rotation

$$\mathrm{u} = \begin{pmatrix} \cos\gamma & e^{i\beta}\sin\gamma \\ -e^{-i\beta}\sin\gamma & \cos\gamma \end{pmatrix}, \tag{3.21}$$

namely

$$\mathrm{u}^\dagger \, \mathrm{h} \, \mathrm{u} = \mathrm{diag}(\lambda_u, \, \lambda_v) \, , \tag{3.22}$$

where

$$\gamma = \frac{1}{2} \arctan \frac{|\mathcal{H}_{pq}|}{\mathcal{H}_{qq} - \mathcal{H}_{pp}} \, , \quad \beta = \mathrm{Arg}[\mathcal{H}_{pq}] \, , \tag{3.23}$$

and the new diagonal elements are

$$\lambda_{u,v} = \frac{1}{2} \left[\mathcal{H}_{pp} + \mathcal{H}_{qq} \mp \sqrt{(\mathcal{H}_{pp} - \mathcal{H}_{qq})^2 + 4|\mathcal{H}_{pq}|^2} \right] . \tag{3.24}$$

From Eq. 3.24 we see that the gap between $\lambda_{u,v}$ is at least $2|\mathcal{H}_{pq}|$ so any level crossings of the chosen diagonal elements will be resolved. Since the rotation will not increase the scales of any other elements, if the chosen $\mathcal{H}_{pq}$ is the largest in absolute value among all the off-diagonal elements of the full matrix, the leading scale of perturbative terms (off-diagonal elements) has been reduced. The above process can be repeated. By implementing a series of rotations one can eliminate all the crossings of the eigenvalues and squeeze the off-diagonal elements as much as desired.

This procedure, selecting the largest off-diagonal element (LODE), maximizes the precision of the entire matrix. If however, only certain elements of the matrix are necessary for a given calculation, different techniques may be more optimal. In the context of neutrino oscillations, our goal is to provide as unified of a framework as possible to apply equally to all channels. There is also an alternative approach to select the rotated sector. We can select the sector which requires the largest rotation angle (LROT) to diagonalize it. However, the LDOE strategy is superior in precision so we do not adopt the LROT. We will discuss the

LROT strategy in details in Appendix B.

3.2.1 Fibonacci recursive

For simplicity we focus on a 3×3 Hamiltonian, although our results are generally valid. After the preliminary rotations, the Hamiltonian is

$$H = H_0 + H_1 \,, \tag{3.25}$$

where H_0 is a diagonal zeroth order Hamiltonian and H_1 is the perturbative part where all diagonal elements vanish. That is,

$$H_0 = \begin{pmatrix} \lambda_u & & \\ & \lambda_v & \\ & & \lambda_w \end{pmatrix} \tag{3.26}$$

and WLOG H_1 has a form

$$H_1 = \begin{pmatrix} & & \epsilon^a\, x \\ & & \epsilon^b\, y \\ \epsilon^a\, x^* & \epsilon^b\, y^* & \end{pmatrix} \,, \tag{3.27}$$

where $0 < \epsilon \ll 1$ is a small scale, a, b are some positive numbers, and $|x|$, $|y| \sim \mathcal{O}(1)$. Please note that in this example $(H_1)_{12}$ is zero since for neutrino oscillations the final rotation to remove the level crossings is the 12 rotation. Depending on the initial Hamiltonian before the preliminary rotations, the pair of vanishing off-diagonal elements of H_1 may be different, it will not affect the following derivation.

Again WLOG, we assume that $b \geq a > 0$, thus $\epsilon^a\, x$ is the leading order off-diagonal element now so we should implement a rotation in the 13 sector. Substitute H_1 into Eq. 3.23

we get

$$\gamma_{13} = \frac{1}{2} \arctan \frac{\epsilon^a |x|}{\lambda_w - \lambda_u}, \quad \beta_{13} = \mathrm{Arg}[x]. \tag{3.28}$$

After this rotation the perturbative Hamiltonian in the new basis becomes

$$H_1' = \epsilon^b \begin{pmatrix} & -y^* \sin\gamma_{13}\, e^{i\beta_{13}} & \\ y \sin\gamma_{13}\, e^{-i\beta_{13}} & & y\cos\gamma_{13} \\ & y^* \cos\gamma_{13} & \end{pmatrix}. \tag{3.29}$$

By Eq. 3.28 we see that $\sin\gamma_{13} \sim \mathcal{O}(\epsilon^a)$, therefore the orders the H_1''s elements are $(H_1')_{23} \sim \mathcal{O}(\epsilon^b)$ and $(H_1')_{12} \sim \mathcal{O}(\epsilon^{a+b})$. Then H_1' can take the place of H_1 and one more rotation in the (2-3) sector will extinguish the element $(H_1')_{23}$.

For the sake of simplicity we define H_1 to have the order of (a, b) and H_1' have the order of $(b, a+b)$ where in this definition the first number is smaller (corresponding to the order of the largest off diagonal term). It is easy to see that the rotation angle which can extinguish $(H_1')_{23}$ must be in order of $\mathcal{O}(\epsilon^b)$ and after that the rotated perturbative Hamiltonian must have order of $(a+b, a+b+b)$. This is the famous Fibonacci sequence; that is, the order of the size of the largest off-diagonal element is the sum of the order after each of the previous two rotations. The order of the smallness parameter in the perturbative part of the Hamiltonian will increases exponentially in the number of rotations since the Fibonacci sequence grows exponentially. This means that the diagonal part of the Hamiltonian will converge on the true expression very rapidly. Starting from $H_1 \propto \epsilon$, to achieve precision at the ϵ^n level, the rotation method takes just $\mathcal{O}(\log n)$ rotations.

A useful special case of H_1 is $a = b = 1$. We define $H_1^{(N)}$ to be the perturbative Hamiltonian after N rotations (not including the preliminary rotations). Then, we have

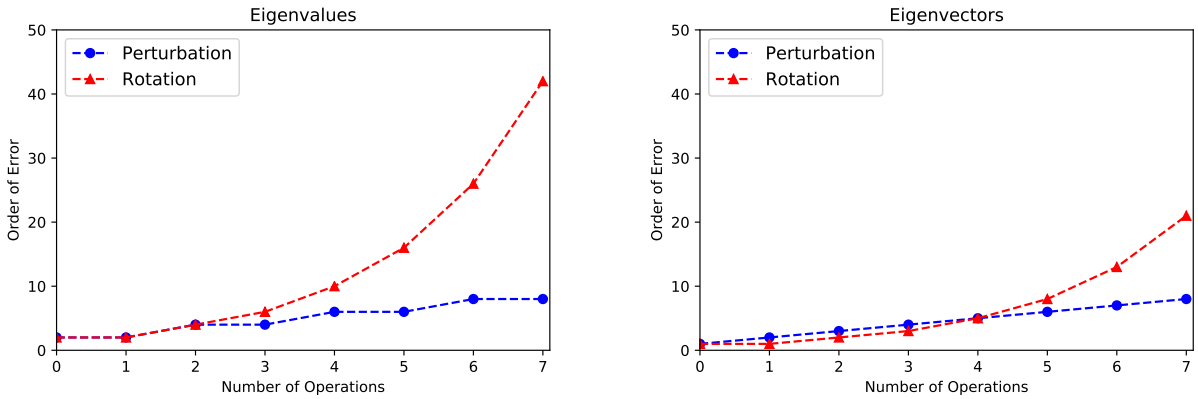

Figure 3.1: Here we show the relative growth in precision by using rotations or following perturbation theory. The horizontal axis is the number of operations: either the number of rotations of the order in perturbation theory. The vertical axis shows the power m of the size of the error, ϵ^m. **Left:** The order of the error of the eigenvalues scales like $n+2$ using perturbation theory and $2F_{n+1}$ using rotations where F_n is the n^{th} Fibonacci number. **Right:** The order of the error of the eigenvectors scales like $n+1$ using perturbation theory and F_{n+1} using rotations.

that the size of the Hamiltonian shrinks exponentially as described by

$$\log_\epsilon H_1^{(N)} \sim \frac{1}{\sqrt{5}} \left(\frac{1+\sqrt{5}}{2} \right)^N . \tag{3.30}$$

Moreover, we notice that all the perturbative Hamiltonian's diagonal elements are zero. Since the first order corrections to the eigenvalues are the diagonal elements of the perturbative Hamiltonian, therefore the order of errors of the eigenvalues will be double of the order of the perturbative Hamiltonian [29].

For $a = b = 1$, we compare orders of errors of the eigenvalues and eigenvectors given by perturbation expansions and the rotation method in Fig. 3.1. The order of the size of the error in the eigenvalues (eigenvectors) grows like $2F_{n+1}$ (F_{n+1}) where F_n is the Fibonacci sequence defined as $F_0 \equiv 0$, $F_1 \equiv 1$, and $F_n = F_{n-1} + F_{n-2}$ for $n > 1$.

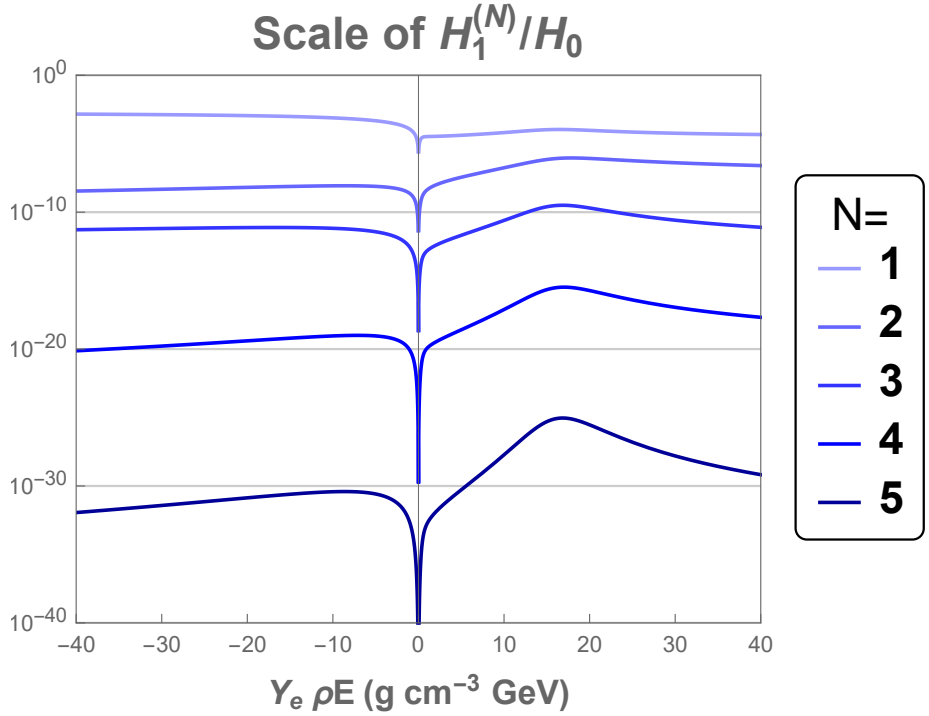

Figure 3.2: Ratio scales of the perturbative Hamiltonian to the zeroth order Hamiltonian. N is the total number of rotations implemented (not counting the three zeroth order rotations). The scale of H_0 is typically of the order of $\Delta m^2_{ee}/2E$, E is the neutrino beam's energy. The scale of each $H_1^{(N)}$ is represented by its leading order element. The vacuum parameters used are $\sin^2\theta_{12} = 0.31$, $\sin^2\theta_{13} = 0.022$, $\sin^2\theta_{23} = 0.58$, $\delta = 215°$, $\Delta m^2_{21} = 7.4 \times 10^{-5}$ eV^2, and $\Delta m^2_{31} = 2.5 \times 10^{-3}$ eV^2 [32].

3.2.2 Numerical test

Now we illustrate this procedure. We set

$$H_0 = \check{H}_0,$$
$$H_1 = \check{H}_1, \tag{3.31}$$

where $\check{H}_0$ and $\check{H}_1$ are defined in Eq. 2.19. In Fig. 3.2 we display the ratio of the perturbative Hamiltonian after N rotations (not counting the preliminary rotations) to the zeroth order Hamiltonian. As expected, it is shown that the order spans of each rotation increase with the total number of rotations.

CHAPTER 4

EIGENVECTOR-EIGENVALUE IDENTITY IN NEUTRINO PHYSICS

The most essential motivation of the work of this dissertation (and all other approximation methods for calculating neutrino oscillations in matter) is the complexity of the exact analytic solutions. For 3νSM, the first full exact solution was published by Zaglauer and Schwarzer (ZS) in 1988 [62]. The process to derive the exact solution encounters a cubic equation and the final expressions of the eigenvalues include puzzling $\cos(\frac{1}{3}\arccos(\dots))$ terms. Besides developments of approximation methods, multiple works of rewriting and simplifying the exact solution have also been published, see [61, 43, 12, 34, 37, 51].

We also develop a new expression of the exact solution based on a recently rediscovered and extensively surveyed fundamental identity in linear algebra: *eigenvector-eigenvalue identity* [29, 26]. The new approach provides simple, clear, and symmetric formulas of the mixing angles. Moreover, the simple zeroth order eigenvalues derived from the rotation method in Chapter 2 can be easily inserted into the new expressions to achieve even simpler results with second order precision.

4.1 A formal description and proof of the identity

A is an $n \times n$ Hermitian matrix. The n real eigenvalues of A are $\lambda_1(A)$, ..., $\lambda_n(A)$. The corresponding n eigenvectors of A are v_1, ..., v_n. We can get an $(n-1) \times (n-1)$ minor M_j by deleting the jth row and column of A. Obviously M_j is an $(n-1) \times (n-1)$ Hermitian matrix. We define M_j's real eigenvalues to be $\lambda_1(M_j)$, ..., $\lambda_{n-1}(M_j)$. Then for an arbitrary v_i, its ith component $v_{i,j}$ is related to eigenvalues of A and M_j by the following equation.

Theorem 1.

$$|v_{i,j}|^2 \prod_{k=1;k\neq i}^{n} (\lambda_i(A) - \lambda_k(A)) = \prod_{k=1}^{n-1} (\lambda_i(A) - \lambda_k(M_j)) \tag{4.1}$$

Proof of Theorem 1 There are multiple proofs of the identity, a comprehensive survey of it can be found in [26]. We only present one proof here. If we see v_i as a column vectors, it is trivial to see that

$$A = \sum_{i=1}^{n} \lambda_i(A)\, v_i\, v_i^{\dagger}. \tag{4.2}$$

$\mathrm{adj}(A)$ is the adjugate matrix of A and

$$\mathrm{adj}(A)\, A = A\, \mathrm{adj}(A) = det(A)\, \mathbb{1}_{n\times n}. \tag{4.3}$$

$\mathrm{adj}(A)$ and A can be diagonalzied simultaneously, it can be written as

$$\mathrm{adj}(A) = \sum_{i=1}^{n} (\prod_{k=1;k\neq i} \lambda_k(A))\, v_i\, v_i^{\dagger}. \tag{4.4}$$

In the above equation if we replace A by $\lambda_i(A)\mathbb{1}_{n\times n} - A$, we can immediately have

$$\mathrm{adj}(\lambda_i(A)\mathbb{1}_{n\times n} - A) = \prod_{k=1;k\neq i} (\lambda_i(A) - \lambda_k(A))\, v_i\, v_i^{\dagger}. \tag{4.5}$$

If we only consider jth diagonal element of the above equation, by the definition of adjugate matrix we get

$$det\big(\lambda_i(A)\mathbb{1}_{(n-1)\times(n-1)} - M_j\big) = \prod_{k=1;k\neq i} (\lambda_i(A) - \lambda_k(A))\, |v_{i,j}|^2. \tag{4.6}$$

Because

$$det\big(\lambda_i(A)\mathbb{1}_{(n-1)\times(n-1)} - M_j\big) = \prod_{k=1}^{n-1} (\lambda_i(A) - \lambda_k(M_j)), \tag{4.7}$$

we complete the proof. □

4.2 Mixing angles and CP phase

Now we are ready to apply the identity to neutrino oscillations. The Hamiltonian of 3νSM is a 3×3 Hermitian matrix which can be diagonalized by its PMNS matrix. Thus each column vector of the PMNS matrix is a normalized eigenvector of the Hamiltinian. Norm square of an element of the PMNS matrix in matter is

$$|\tilde{U}_{\alpha i}|^2 = \frac{(\tilde{\lambda}_i - \xi_\alpha)(\tilde{\lambda}_i - \chi_\alpha)}{(\tilde{\lambda}_i - \tilde{\lambda}_j)(\tilde{\lambda}_i - \tilde{\lambda}_k)}. \tag{4.8}$$

In the above equation, $\tilde{\lambda}_i$ is an eigenvalue of $(2E)H$ and ξ_α, χ_α are the two eigenvalues of the minor formed by deleting αth row and column with $\alpha \in \{e, \nu, \tau\}$, they can be figured out by solving quadratic equations. (i, j, k) is a permutation of $(1, 2, 3)$. Analytic solutions of the eigenvalues $\tilde{\lambda}_{1,2,3}$ from ZS are listed in Appendix C. Details of calculations of ξ_α and χ_α in the standard three flavors scheme can be found in Appendix D.

The mixing angles and elements of the PMNS matrix are related by

$$\begin{aligned}
\tilde{s}^2_{12}\tilde{c}^2_{13} = |\tilde{U}_{e2}|^2 &= \frac{(\tilde{\lambda}_2 - \xi_e)(\tilde{\lambda}_2 - \chi_e)}{(\tilde{\lambda}_2 - \tilde{\lambda}_1)(\tilde{\lambda}_2 - \tilde{\lambda}_3)}, \\
\tilde{s}^2_{13} = |\tilde{U}_{e3}|^2 &= \frac{(\tilde{\lambda}_3 - \xi_e)(\tilde{\lambda}_3 - \chi_e)}{(\tilde{\lambda}_3 - \tilde{\lambda}_1)(\tilde{\lambda}_3 - \tilde{\lambda}_2)}, \\
\tilde{s}^2_{23}\tilde{c}^2_{13} = |\tilde{U}_{\mu3}|^2 &= \frac{(\tilde{\lambda}_3 - \xi_\mu)(\tilde{\lambda}_3 - \chi_\mu)}{(\tilde{\lambda}_3 - \tilde{\lambda}_1)(\tilde{\lambda}_3 - \tilde{\lambda}_2)}.
\end{aligned} \tag{4.9}$$

Here we need a short clarification of the symbols and notations. In Chapter 2 and Chapter 3, the tilde superscripts have been used for the zeroth order values of the mixing angles and CP phase in matter. However, in this chapter the tilde superscript is generally used for values in matter, no specific precision is indicated by it. Precision of the mixing angles and CP phase will be determined by the eigenvalues' precision.

Eqs. 4.9 do not give information of the CP phase. We can derive the CP phase from the

Naumov-Harrison-Scott (NHS) identity [50, 39] as mentioned in Section 2.2.4, i.e.

$$\tilde{J} = \frac{\Delta m^2_{21}\,\Delta m^2_{31}\,\Delta m^2_{32}}{(\tilde{\lambda}_2 - \tilde{\lambda}_1)(\tilde{\lambda}_3 - \tilde{\lambda}_1)(\tilde{\lambda}_3 - \tilde{\lambda}_2)}\, J, \tag{4.10}$$

with

$$J = s_{23}\, c_{23}\, s_{13}\, c^2_{13}\, s_{12}\, c_{12}\, \sin\delta. \tag{4.11}$$

If we know the mixing angles and the eigenvalues in matter, the NHS identity can give the value of $\sin\delta$ in matter.

A simpler way to calculate the CP phase in matter is using the Toshev identity [58] which shows that $\sin 2\theta_{23}\,\sin\delta$ is invariant under the matter effect. Therefore we have

$$\sin\tilde{\delta} = \frac{\sin 2\theta_{23}\,\sin\delta}{\sin 2\tilde{\theta}_{23}} \tag{4.12}$$

4.3 Combine the rotation method

In Eqs. 4.9, we still need to figure out the eigenvalues in matter. As mentioned in the first paragraph of this chapter, the exact analytic solutions from ZS are complicated and puzzling. An alternative approach is using the zeroth order eigenvalues given by the rotations in Eqs. 2.15. Section 2.2 has shown that all the first order corrections to those eigenvalues vanish, thus we would obtain simple expressions of the mixing angles and the CP phase in matter with second order precision.

CHAPTER 5

ROTATION METHOD FOR MODEL WITH ONE MORE STERILE NEUTRINO

The phenomenon of neutrino oscillations can not be reconciled with the Standard Model since in the Standard Model neutrinos are massless particles. To reveal the origin of the neutrino masses, many studies of neutrino scenarios beyond the three flavors Standard Model (3νSM) have been conducted. One promising solution is a theoretical scheme with additional sterile neutrinos. In such a scheme, neutrino oscillations will be modified because of the additional mixing with sterile neutrinos. In matter, calculations of neutrino propagation will be significantly more complicated since the sterile neutrinos also change the Wolfenstein matter effect term [60] in the Hamiltonian. There have been some analytic derivations of the matter effect in a 3+1 scenario [46], i.e., one sterile neutrino in addition to the three active ones. However, just as the case of 3νSM, the exact analytic solutions are intricate and impenetrable. Consequently, alternative perturbation approaches should be considered. We will extend the rotation method from the standard three flavors scheme to a scheme with one more sterile neutrinos (3+1). Materials of this chapter follow [54].

5.1 The 3+1 model and its PMNS matrix

If there are $3+n$ neutrino mass eigenstates, the leptonic charged current is written as [38]

$$\mathcal{L} = -\frac{g}{\sqrt{2}} \left(\bar{e}_L,\, \bar{\nu}_L,\, \bar{\tau}_L\right) \gamma^\mu \, U \left(\nu_1,\, \nu_2,\, \nu_3,\, \ldots,\, \nu_{3+n}\right)^T W_\mu^+ + \text{h.c.}. \tag{5.1}$$

Obviously in the above equation U is no longer a square matrix as in the standard 3ν scheme but has dimensions $3 \times (3+n)$. Since we see the flavor basis as an orthonormal basis, U must satisfy

$$U\, U^\dagger = \mathbb{1}_{3\times 3} \tag{5.2}$$

Then it is trivial to demonstrate that by the Gram-Schmidt process we can find at least one $(3+n)\times(3+n)$ unitary matrix such that U is just the top three rows of the unitary matrix. Arbitrary $(3+n)\times(3+n)$ unitary matrix can be written as product of $(n+3)(n+2)/2$ complex rotations.

For a scheme with one more sterile neutrino (3+1), there are at most six complex rotations to determine the unitary matrix. Compared with a scheme of $n=0$, there are three more mixing angles and three more complex phases. However, the flavor eigenstates do not contain a fourth vector thus we can free one more complex phase. In summary for the 3+1 scheme there will be three more mixing angles and two more CP phases (compared with the standard three flavors scheme).

In the flavor basis, the Hamiltonian is given by

$$\begin{aligned}\mathbf{H}_{3+1} =&\frac{1}{2E}\Big[\mathbf{U}_{\rm PMNS}\,{\rm diag}(0,\,\Delta m^2_{21},\,\Delta m^2_{31},\,\Delta m^2_{41})\,\mathbf{U}^\dagger_{\rm PMNS}\\ &+{\rm diag}(a,\,0,\,0,\,b)\Big].\end{aligned}\tag{5.3}$$

Now the PMNS matrix $\mathbf{U}_{\rm PMNS}$ is a 4×4 unitary matrix. Besides a given by Eq. 2.5, we have one more potential term

$$b=\sqrt{2}G_F N_n E,\tag{5.4}$$

where N_n is the number density of neutrons. For the Earth crust $N_n\simeq N_e$ so we have $b\simeq a/2$.

To write the PMNS matrix as a product of a series of (complex) rotations [47, 56], in the standard three flavors case, the convention is chosen to be $\mathbf{U}^{3\nu}_{\rm PMNS}\equiv\mathbf{U}_{23}\,\mathbf{U}_{13}\,\mathbf{U}_{12}$. In a $3+N$ scheme, there will be extra rotations mixing with sterile neutrinos. It is natural to require that the convention is equivalent to that of the standard three flavors scheme if all the extra rotations are trivial. Therefore, we will keep the relative positions of the three rotation matrices in the active sector when defining the PMNS matrix with sterile neutrinos.

Also, it is observed that both the second and the third rows vanish in the matter potential term in Eq. 5.3; thus, we will keep $\mathbf{U}_{23}$ as the first rotation in the PMNS matrix so the rhs of Eq. 5.3 will be independent of the 23 mixing parameters if we perform the $\mathbf{U}_{23}$ rotation. The last step to determine the convention of the PMNS matrix is finding places after the $\mathbf{U}_{23}$ for the rotations mixing with the sterile neutrinos. By trying different choices to simplify the calculation processes, we adopt the following convention of the PMNS matrix,

$$\mathbf{U}_{\rm PMNS} \equiv \mathbf{U}_{23}(\theta_{23}, \delta_{23})\, \mathbf{U}_{\rm sterile}\, \mathbf{U}_{13}(\theta_{13})\, \mathbf{U}_{12}(\theta_{12}), \tag{5.5}$$

where $\mathbf{U}_{\rm sterile}$ is the product of all the rotations mixing with sterile neutrinos. This choice leads to significant reductions in the complexity of the calculations and the resulting expressions. Physics, of course, is independent of this choice.

In the following sections, we develop details of the expressions for the scheme with one sterile neutrino. In particular, we choose [1]

$$\mathbf{U}^{3+1}_{\rm sterile} \equiv \mathbf{U}_{34}(\theta_{34}, \delta_{34})\, \mathbf{U}_{24}(\theta_{24}, \delta_{24})\, \mathbf{U}_{14}(\theta_{14}). \tag{5.6}$$

Current global fits [23, 30, 31] suggest $|U_{i4}| \sim 0.1$, so in this chapter, we assume that $\mathbf{U}_{\rm sterile} \simeq \mathbb{1} + \mathcal{O}(\sqrt{\epsilon})$, which means that $s_{i4} \sim \mathcal{O}(\sqrt{\epsilon})$ for $i = 1, 2, 3$. The small parameter ϵ is defined in Eq. 2.8.

The convention in Eq. 5.5 is different from the usual one used by many papers in which $\mathbf{U}_{\rm sterile}$ comes before (i.e. on the left side of) all the three rotations in the active sector (see, e.g., Ref. [18]). We will derive the relations of the mixing angles and phases connecting both conventions in Appendix E.1.

1. Convention of the CP phases is chosen to simplify the calculation process. Different conventions can be related by pure phase transformations.

5.2 Zeroth order from rotations

We first define a rotated basis $|\tilde{\nu}\rangle$ by

$$\begin{aligned}|\tilde{\nu}\rangle \equiv & \mathbf{U}^{\dagger}_{\text{sterile}}\,\mathbf{U}^{\dagger}_{23}\,|\nu_f\rangle \\ =&\mathbf{U}^{\dagger}_{14}(\theta_{14})\mathbf{U}^{\dagger}_{24}(\theta_{24},\delta_{24})\mathbf{U}^{\dagger}_{34}(\theta_{34},\delta_{34})\mathbf{U}^{\dagger}_{23}(\theta_{23},\delta_{23})\,|\nu_f\rangle\,,\end{aligned} \tag{5.7}$$

After the rotations, the Hamiltonian becomes

$$\tilde{\mathbf{H}} \equiv \mathbf{U}^{\dagger}_{\text{sterile}}\,\mathbf{U}^{\dagger}_{23}(\theta_{23},\delta_{23})\,\mathbf{H}\,\mathbf{U}_{23}(\theta_{23},\delta_{23})\,\mathbf{U}_{\text{sterile}}$$

$$= \begin{pmatrix} \tilde{H} & & \\ & & \\ & & \frac{M^2}{2E} \end{pmatrix} + \tilde{\mathbf{H}}_M. \tag{5.8}$$

In the above equation $M^2(b) \equiv \Delta m^2_{41} + b\,c^2_{14}c^2_{24}c^2_{34}$, $\tilde{H}$ is a 3×3 submatrix in the active sector and in $\tilde{\mathbf{H}}_M$ all the elements not in the fourth column or row vanish.

Based on the scales, we can distribute the elements of $\tilde{H}$ into two parts, i.e.,

$$\tilde{H} = \tilde{H}_0 + \tilde{H}_1. \tag{5.9}$$

The leading order term is

$$\tilde{H}_0 = \frac{1}{2E}\begin{pmatrix} \lambda_a & & s_{13}c_{13}\Delta m^2_{ee} + \epsilon\, b k_{13}c_{24}c_{34}e^{-i\delta_{34}} \\ & \lambda_b & \\ s_{13}c_{13}\Delta m^2_{ee} + \epsilon\, b k_{13}c_{24}c_{34}e^{i\delta_{34}} & & \lambda_c \end{pmatrix}, \tag{5.10}$$

where

$$k_{ij} \equiv \frac{s_{i4}s_{j4}}{\epsilon} \sim \mathcal{O}(1), \quad i,j \in \{1,2,3\} \tag{5.11}$$

and the diagonal elements, which can be approximations to the eigenvalues are

$$\begin{aligned}
\lambda_a &= (s_{13}^2 + \epsilon\, s_{12}^2)\, \Delta m_{ee}^2 + a\, c_{14}^2 + \epsilon\, b\, k_{11}\, c_{24}^2 c_{34}^2, \\
\lambda_b &= \epsilon\, (c_{12}^2\, \Delta m_{ee}^2 + b\, k_{22}\, c_{34}^2), \\
\lambda_c &= (\, c_{13}^2 + \epsilon\, s_{12}^2\,)\, \Delta m_{ee}^2 + \epsilon\, b\, k_{33}.
\end{aligned} \tag{5.12}$$

In the first order term $\tilde{H}_1$, all the diagonal elements vanish, and the off-diagonal elements are

$$\begin{aligned}
(\tilde{H}_1)_{12} &= \frac{\epsilon}{2E} \Big(c_{12} s_{12} c_{13}\, \Delta m_{ee}^2 + b\, k_{12}\, c_{24} c_{34}^2\, e^{-i\delta_{34}} \Big), \\
(\tilde{H}_1)_{23} &= \frac{\epsilon}{2E} \Big[- c_{12} s_{12} s_{13}\, \Delta m_{ee}^2 + b\, k_{23}\, c_{34}\, e^{i(\delta_{24} - \delta_{34})} \Big], \\
(\tilde{H}_1)_{13} &= 0.
\end{aligned} \tag{5.13}$$

Nonzero elements of $\tilde{\mathbf{H}}_M$ are listed below (the Hamiltonian is a Hermitian matrix)

$$\begin{aligned}
(\tilde{\mathbf{H}}_M)_{14} &= -\frac{1}{2E} \left(a + b\, c_{24}^2 c_{34}^2 \right) c_{14} s_{14}, \\
(\tilde{\mathbf{H}}_M)_{24} &= -\frac{b}{2E}\, c_{14} c_{24} s_{24} c_{34}^2\, e^{i\delta_{24}}, \\
(\tilde{\mathbf{H}}_M)_{34} &= -\frac{b}{2E}\, c_{14} c_{24} c_{34} s_{34}\, e^{i\delta_{34}}. \\
(\tilde{\mathbf{H}}_M)_{44} &= 0.
\end{aligned} \tag{5.14}$$

Since $s_{i4} \sim \mathcal{O}(\sqrt{\epsilon})$, it is easy to see that $\tilde{\mathbf{H}}_M \sim \mathcal{O}(\sqrt{\epsilon})$. Although $\tilde{\mathbf{H}}_M$ is not as small as $\mathcal{O}(\epsilon)$, it will be a part of the perturbative Hamiltonian. However, this does not mean that the first order corrections must be as large as $\mathcal{O}(\sqrt{\epsilon})$. The mass of the heavy sterile neutrino will be an alternative parameter which controls scales of the correction terms. More specifically, in a perturbative expression, all nonzero elements of $\tilde{\mathbf{H}}_M$ are divided by M^2. For large M^2, the quotient gives a small term in the perturbation expansion. Another condition that is

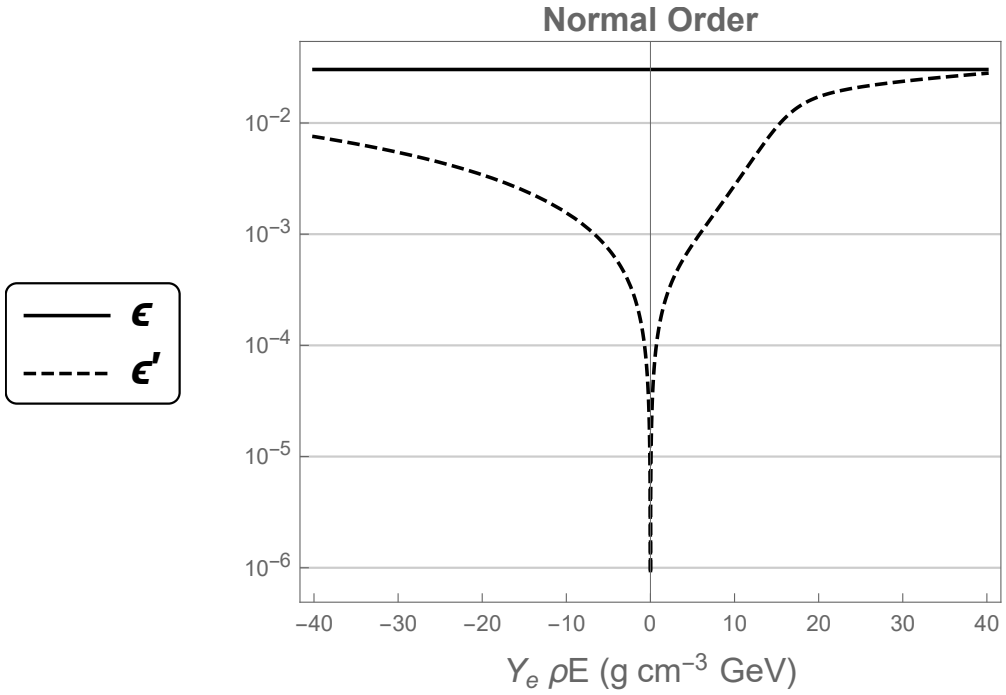

Figure 5.1: The perturbing parameter ϵ' as function of $Y_e\,\rho E$ with $b = a/2$. In the region where a is comparable to Δm^2_{ee}, $\epsilon' \leq \epsilon$. The parameters used are in Table 5.1.

necessary for $\tilde{\mathbf{H}}_M$ being a perturbative Hamiltonian is that it consists of terms proportional to a and b, which means that it vanishes in vacuum. This is crucial because we require the perturbative expressions to be exact in vacuum.

Now, the dominating off-diagonal term (except the ones in $\tilde{\mathbf{H}}_M$) comes from the 13 sector of $\tilde{H}_0$. Because of the complex phase δ_{34}, the rotation will not be real. Let us assume that the rotation is $\mathbf{U}_{13}(\tilde{\theta}_{13}, \alpha_{13})$, where $\tilde{\theta}_{13}$ is a real rotation angle and ${\alpha_{13}}^2$ is a complex phase. After this rotation, the neutrino states becomes

$$\begin{aligned} |\hat{\nu}\rangle &\equiv \mathbf{U}^\dagger_{13}(\tilde{\theta}_{13}, \alpha_{13})\,|\tilde{\nu}\rangle \\ &= \mathbf{U}^\dagger_{13}(\tilde{\theta}_{13}, \alpha_{13})\mathbf{U}^\dagger_{\text{sterile}}\mathbf{U}^\dagger_{23}(\theta_{23}, \delta_{23})\,|\nu_f\rangle\,, \end{aligned} \tag{5.15}$$

2. Here, we are not using the usual phase symbol δ since α_{13} is not an effective physical phase in matter. In Appendix E.2 it can be eliminated by implementing a pure phase transformation of the neutrino basis.

where $\mathbf{U}^{\dagger}_{\text{sterile}} = \mathbf{U}^{\dagger}_{14}(\theta_{14})\mathbf{U}^{\dagger}_{24}(\theta_{24},\delta_{24})\mathbf{U}^{\dagger}_{34}(\theta_{34},\delta_{34})$. The Hamiltonian becomes

$$\hat{\mathbf{H}} \equiv \mathbf{U}^{\dagger}_{13}(\tilde{\theta}_{13},\, \alpha_{13})\, \tilde{\mathbf{H}}\, \mathbf{U}_{13}(\tilde{\theta}_{13}, \alpha_{13}). \tag{5.16}$$

Since the fourth index is not engaged in the rotation, we can just focus on the first three indices and define a 3×3 submatrix U_{13} to be the active sectors of $\mathbf{U}_{13}$, i.e.,

$$\mathbf{U}_{13} = \begin{pmatrix} U_{13} & & \\ & & \\ & & 1 \end{pmatrix}. \tag{5.17}$$

After the rotation, the sub-Hamiltonian in the active sector $\tilde{H}$ becomes

$$\hat{H} \equiv U^{\dagger}_{13}(\tilde{\theta}_{13}, \alpha_{13})\, \tilde{H}\, U_{13}(\tilde{\theta}_{13}, \alpha_{13}). \tag{5.18}$$

We require the 13 sector of $\tilde{H}$ to be diagonalized by $U_{13}(\tilde{\theta}_{13}, \alpha_{13})$. Since the 13 sector of $\tilde{H}_1$ vanishes, it is equivalent to diagonalizing this sector of $\tilde{H}_0$, i.e.,

$$\begin{aligned} \hat{H}_0 &\equiv U^{\dagger}_{13}(\tilde{\theta}_{13}, \alpha_{13})\, \tilde{H}_0\, U_{13}(\tilde{\theta}_{13}, \alpha_{13}) \\ &= \frac{1}{2E} \begin{pmatrix} \lambda_- & & \\ & \lambda_0 & \\ & & \lambda_+ \end{pmatrix}, \end{aligned} \tag{5.19}$$

with $\lambda_{\pm}$ and λ_0 to be determined. Simultaneously, $\tilde{H}_1$ becomes

$$\hat{H}_1 \equiv U^{\dagger}_{13}(\tilde{\theta}_{13}, \alpha_{13})\, \tilde{H}_1\, U_{13}(\tilde{\theta}_{13}, \alpha_{13}). \tag{5.20}$$

It can be shown that

$$\lambda_{\mp} = \frac{1}{2}\Big[(\lambda_a + \lambda_c) \mp \mathrm{sign}(\Delta m^2_{ee}) \sqrt{(\lambda_c - \lambda_a)^2 + 4 \left| s_{13} c_{13}\, \Delta m^2_{ee} + \epsilon\, b\, k_{13}\, c_{24} c_{34}\, e^{-i\delta_{34}} \right|^2} \Big],$$
$$\lambda_0 = \lambda_b = \epsilon\, c^2_{12}\, \Delta m^2_{ee} + \epsilon\, b\, k_{22}\, c^2_{34}. \tag{5.21}$$

The real rotation angle and the complex phase can be determined by

$$\cos 2\tilde{\theta}_{13} = \frac{\lambda_c - \lambda_a}{\lambda_+ - \lambda_-},$$
$$\alpha_{13} = \mathrm{Arg}\big[s_{13} c_{13}\, \Delta m^2_{ee} + \epsilon\, b\, k_{13}\, c_{24} c_{34}\, e^{-i\delta_{34}} \big]. \tag{5.22}$$

The elements of $\hat{H}_1$ are

$$(\hat{H}_1)_{12} = \frac{\epsilon}{2E}$$
$$\times \Big\{ c_{12} s_{12}\, (\, c_{13}\tilde{c}_{13} + s_{13}\tilde{s}_{13}\, e^{-i\,\alpha_{13}}\,)\, \Delta m^2_{ee}$$
$$+ b \Big[\, k_{12}\, c_{24} c^2_{34} \tilde{c}_{13} - k_{23}\, c_{34} \tilde{s}_{13}\, e^{i(\delta_{34} + \alpha_{13})} \,\Big]\, e^{-i\delta_{24}} \Big\},$$
$$(\hat{H}_1)_{23} = \frac{\epsilon}{2E}$$
$$\times \Big\{ c_{12} s_{12}\, (\, -s_{13}\tilde{c}_{13} + c_{13}\tilde{s}_{13}\, e^{i\,\alpha_{13}}\,)\, \Delta m^2_{ee}$$
$$+ b \Big(\, k_{12}\, c_{24} c^2_{34} \tilde{s}_{13}\, e^{i\,\alpha_{13}} + k_{23}\, c_{34} \tilde{c}_{13}\, e^{-i\delta_{34}} \,\Big)\, e^{i\delta_{24}} \Big\},$$
$$(\hat{H}_1)_{13} = 0. \tag{5.23}$$

The Hamiltonian in the sterile sector becomes

$$\hat{\mathbf{H}}_M \equiv \mathbf{U}^{\dagger}_{13}(\tilde{\theta}_{13}, \alpha_{13})\, \tilde{\mathbf{H}}_M\, \mathbf{U}_{13}(\tilde{\theta}_{13}, \alpha_{13}). \tag{5.24}$$

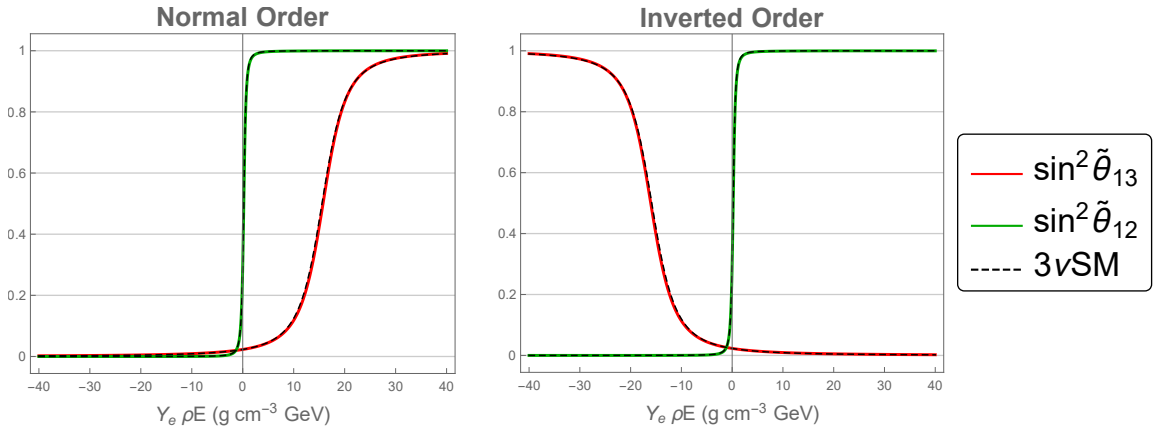

Figure 5.2: Values of $\sin^2\tilde{\theta}_{13}$ and $\sin^2\tilde{\theta}_{12}$. The solid lines are values in the 3+1 scheme; as a comparison the dashed lines are the values in $3\nu SM$. The differences are small but non-negligible. The parameters used are in Table 5.1.

We define a real parameter ϵ' and a phase α_ϵ,

$$\epsilon' \equiv \left|\frac{2E}{\Delta m^2_{ee}}(\hat{H}_1)_{23}\right|,$$
$$\alpha_\epsilon \equiv \mathrm{Arg}\Big[\frac{2E}{\Delta m^2_{ee}}(\hat{H}_1)_{23}\Big]. \tag{5.25}$$

Obviously, $\epsilon' \sim \epsilon$ and $(\hat{H}_1)_{23} = e^{i\alpha_\epsilon}\epsilon'\Delta m^2_{ee}/2E$. It is not hard to see that in the standard three flavors scheme $\epsilon' = |\epsilon \sin(\tilde{\theta}_{13} - \theta_{13})\, s_{12}c_{12}|$, which reconciles with the one defined in Chapter 2. The two new defined parameters will frequently emerge in the following calculations. Since in vacuum a, $b = 0$, $\tilde{\theta}_{13} = \theta_{13}$, and $\alpha_{13} = 0$, ϵ' must be zero then, as shown in Fig. 5.1. This guarantees that the perturbative expressions will be exact in vacuum.

As pointed out in Ref. [25] and Chapter 2, to resolve the λ_1 and λ_0 crossing at the solar resonance, one more rotation that diagonalizes the 12 sector is necessary. Again, since $(\hat{H}_1)_{12}$ is complex, the rotation cannot be real in general. We assume that the rotation in the 12 sector is $\mathbf{U}_{12}(\tilde{\theta}_{12}, \alpha_{12})$, and after this rotation, the neutrino states becomes

$$|\check{\nu}\rangle \equiv \mathbf{U}^\dagger_{12}(\tilde{\theta}_{12}, \alpha_{12})\,|\hat{\nu}\rangle$$

$$= \mathbf{U}_{12}^{\dagger}(\tilde{\theta}_{12}, \alpha_{12}) \mathbf{U}_{13}^{\dagger}(\tilde{\theta}_{13}, \alpha_{13}) \mathbf{U}_{\text{sterile}}^{\dagger} \mathbf{U}_{23}^{\dagger}(\theta_{23}, \delta_{23}) \left|\nu_f\right\rangle , \tag{5.26}$$

where $\mathbf{U}_{\text{sterile}} = \mathbf{U}_{14}^{\dagger}(\theta_{14}) \mathbf{U}_{24}^{\dagger}(\theta_{24}, \delta_{24}) \mathbf{U}_{34}^{\dagger}(\theta_{34}, \delta_{34})$ The Hamiltonian becomes

$$\check{\mathbf{H}} \equiv \mathbf{U}_{12}^{\dagger}(\tilde{\theta}_{12}, \alpha_{12}) \, \hat{\mathbf{H}} \, \mathbf{U}_{12}(\tilde{\theta}_{12}, \alpha_{12}). \tag{5.27}$$

Similar to the case of the 13 rotation, we can again define a 3×3 submatrix U_{12} by

$$\mathbf{U}_{12} = \begin{pmatrix} U_{12} & & \\ & & \\ & & 1 \end{pmatrix}. \tag{5.28}$$

Now we require the $U_{12}(\tilde{\theta}_{12}, \alpha_{12})$ to diagonalize the 12 sector of $\hat{H}$. After the rotation the sub-Hamiltonian is

$$\begin{aligned} \check{H} &\equiv U_{12}^{\dagger}(\tilde{\theta}_{12}, \alpha_{12}) \, \hat{H} \, U_{12}(\tilde{\theta}_{12}, \alpha_{12}) \\ &= \check{H}_0 + \check{H}_1, \end{aligned} \tag{5.29}$$

where $\check{H}_0$ and $\check{H}_1$ are in zeroth and first orders, respectively, i.e.,

$$\begin{aligned} \check{H}_0 &= \frac{1}{2E} \begin{pmatrix} \lambda_1 & & \\ & \lambda_2 & \\ & & \lambda_3 \end{pmatrix}, \\ \check{H}_1 &= \frac{\epsilon' \Delta m_{ee}^2}{2E} \\ &\times \begin{pmatrix} & & -\tilde{s}_{12} \, e^{i(\alpha_{12}+\alpha_\epsilon)} \\ & & \tilde{c}_{12} \, e^{i\alpha_\epsilon} \\ -\tilde{s}_{12} \, e^{-i(\alpha_{12}+\alpha_\epsilon)} & \tilde{c}_{12} \, e^{-i\alpha_\epsilon} & \end{pmatrix}. \end{aligned} \tag{5.30}$$

The diagonal elements of $\check{H}_0$ are

$$\lambda_{1,2} = \frac{1}{2}\Big[(\lambda_- + \lambda_0) \mp \sqrt{(\lambda_- - \lambda_0)^2 + 4|(\hat{H}_1)_{12}|^2} \Big],$$
$$\lambda_3 = \lambda_+. \tag{5.31}$$

The real rotation angle and the complex phase can be determined by

$$\cos 2\tilde{\theta}_{12} = \frac{\lambda_0 - \lambda_-}{\lambda_2 - \lambda_1},$$
$$\alpha_{12} = \mathrm{Arg}\big[(\hat{H}_1)_{12}\big]. \tag{5.32}$$

Values of $\sin^2\tilde{\theta}_{13}$ and $\sin^2\tilde{\theta}_{12}$ are plotted in Fig. 5.2. After this 12 rotation, crossings of the first two diagonal elements $\lambda_{1,2}$ have been resolved, as shown in the top panels of Fig. 5.3. They will be the zeroth order eigenvalues in the following perturbation expansions in the next section. The difference between 3+1 and 3νSM is small in both panels of Fig. 5.2 and the bottom panels of Fig. 5.3 but is not insignificant.

The Hamiltonian in the sterile sector now is

$$\check{\mathbf{H}}_M \equiv \mathbf{U}_{12}^\dagger(\tilde{\theta}_{12}, \alpha_{12})\, \hat{\mathbf{H}}_M\, \mathbf{U}_{12}(\tilde{\theta}_{12}, \alpha_{12}). \tag{5.33}$$

From $\tilde{\mathbf{H}}_M$ to $\check{\mathbf{H}}_M$, we implemented two rotations in the 13 and 12 sectors. Because the active and sterile sectors are not mixed by the two rotations, the elements are still a combinations of the terms proportional to $s_{i4} \sim \mathcal{O}(\sqrt{\epsilon})$. Elements of $\check{\mathbf{H}}_M$ can be found in Appendix E.3.

In principle, there are still some possible crossings of the diagonal elements, namely the crossings to the fourth diagonal element. Since both the 13 and the 12 rotations are in the active space (first three rows and columns), the fourth element is still

$$M^2(b) \equiv \Delta m^2_{41} + b\, c^2_{14} c^2_{24} c^2_{34}. \tag{5.34}$$

Since Δm^2_{41} is much larger than the active eigenvalues in vacuum, the crossings to M^2 can only happen with very high neutrino energy, as shown in the top panels of Fig. 5.3. From the figure, we can see that if $Y_e\rho = 1.4\,\mathrm{g}\cdot\mathrm{cm}^{-3}$, for the Earth's crust, the neutrino energy must be $\mathcal{O}(1)\,\mathrm{TeV}$. Considering the energy scales of the current and future accelerator based oscillation experiments, we are therefore not considering the energy region of these additional crossings, so they will not affect our result. For much higher energy experiments these additional level crossings would have to be dealt with using matter additional rotations.

Now, $\check{H}_0$'s diagonal elements, $\lambda_{1,2,3}$, do not cross (crossings to M^2 will not happen in the energy region of interest). All the off-diagonal elements in the active sectors are of the scale ϵ'. We will distribute all the diagonal elements to the zeroth order Hamiltonian and all the off-diagonal elements to the perturbative Hamiltonian, i.e.

$$\check{\mathbf{H}}_0 = \begin{pmatrix} \check{H}_0 & & \\ & & \\ & & \frac{M^2}{2E} \end{pmatrix}, \quad \check{\mathbf{H}}_1 = \begin{pmatrix} \check{H}_1 & & \\ & & \\ & & 0 \end{pmatrix} + \check{\mathbf{H}}_M. \tag{5.35}$$

The zeroth order effective PMNS matrix in matter is

$$\begin{aligned} &\mathbf{U}^m_{\mathrm{PMNS}} \\ =&\mathbf{U}_{23}(\theta_{23},\delta_{23})\mathbf{U}_{34}(\theta_{34},\delta_{34})\mathbf{U}_{24}(\theta_{24},\delta_{24})\mathbf{U}_{14}(\theta_{14}) \\ &\times \mathbf{U}_{13}(\tilde{\theta}_{13},\alpha_{13})\mathbf{U}_{12}(\tilde{\theta}_{12},\alpha_{12}). \end{aligned} \tag{5.36}$$

Since all possible degeneracies have been removed in the energy scale in which we are interested, we are free to implement a perturbation expansion to achieve even better accuracy. The process of reducing errors by performing rotations and perturbative expansions is summarized in Fig. 5.4.

5.3 Perturbative expressions

Since all the crossings of the zeroth order eigenvalues have been resolved (except for the crossings with M^2, which are not in the energy region of interest) by the rotations and all the off-diagonal elements are small, we can now calculate the higher order corrections to the eigenvalues and eigenvectors by perturbation methods.

5.3.1 Derive the perturbative terms

We define $\mathbf{V}$ to be the exact PMNS matrix in matter. It can be related to the zeroth order $\mathbf{U}^m_{\rm PMNS}$ by

$$\mathbf{V} = \mathbf{U}^m_{\rm PMNS}(\mathbb{1} + \mathbf{W}_1 + \mathbf{W}_2 + \cdots), \tag{5.37}$$

where $\mathbf{W}_n$ is an nth order correction (here $\mathbf{W}_n$ is similar to $W^{(n)}$ in Eq. 2.25. The exact eigenvalues are

$$\lambda_i^{(ex)} = \lambda_i + \lambda_i^{(1)} + \lambda_i^{(2)} + \cdots, \quad i = 1, 2, 3, 4 \ , \tag{5.38}$$

where $\lambda_{1,2,3}$ are defined in Eq. 2.15 and $\lambda_4 = M^2$, $\lambda_i^{(n)}$ is the nth order correction.

First order corrections to the eigenvalues are

$$\lambda_i^{(1)} = 2E(\check{\mathbf{H}}_1)_{ii} = 0. \tag{5.39}$$

First order corrections to the eigenstates are determined by $\mathbf{W}_1$ defined in Eq. 5.37, which are

$$(\mathbf{W}_1)_{ij} = \begin{cases} 0 & i = j \\ -\frac{2E(\check{\mathbf{H}}_1)_{ij}}{\lambda_i - \lambda_j} & i \neq j \end{cases}. \tag{5.40}$$

The detailed first and second order formulas of the perturbation expansions can be found in Appendix E.4. In general, with crossings of the zeroth order eigenvalues ruled out, perturbative expansions can go to arbitrary precision. However, numerical tests will suggest that

it is sufficient to terminate the approach at second order.

5.3.2 Numerical tests

We now test the accuracy of our perturbative expressions. We choose the $\nu_\mu \to \nu_e$ channel and 1300 km baseline of DUNE to do the numerical test. The density of the earth crust is chosen to be $Y_e\rho = 1.4\,\mathrm{g{\cdot}cm^{-3}}$, $b = a/2$, and all the mixing parameters are listed in Table 5.1. The exact oscillation probabilities can be figured out by Ref. [46] or given by a computer algebra system[3]. The results are shown in Fig. 5.5. The error in the zeroth order expression is expected to be no more than $\epsilon \sim 10^{-2}$, which is confirmed by the red curve in the plot; the green curve depicts the error of the first order perturbative expansion, which is under $\epsilon^2 \sim 10^{-4}$; to second order, the error further declines to $\epsilon^3 \sim 10^{-6}$, which also coincides with the prediction. In Fig. 5.5, the expectation values are obtained by averaging over the fast oscillation terms, i.e., the terms with angular velocities proportional to $(\lambda_4 - \lambda_i)$. More specifically,

$$\left\langle \sin / \cos \frac{(\lambda_4 - \lambda_i)L}{2E} \right\rangle = 0, \ \left\langle \sin^2 \frac{(\lambda_4 - \lambda_i)L}{4E} \right\rangle = \frac{1}{2}. \tag{5.41}$$

Based on the numerical results, we confirm that at least the second order perturbative expansion is significantly more accurate than any experimental results [7, 55, 2, 4, 42].

5.4 Oscillation probabilities and detecting sterile neutrinos

In this section, we will discuss a possible application of the perturbative expressions above for detecting sterile neutrinos. The principle of the approach is that one can calculate the theoretical predictions of the oscillation probabilities in different schemes and compare them with the experimental results. Usually, for a given baseline and neutrino energy, the predictions from different schemes are close; therefore, it is essential to figure out sufficiently

3. Only considering the 3+1 scheme, an analytical solution is still possible since one just need solve a quartic equation; but it is not the case for schemes with more sterile neutrinos

$U_{\rm PMNS} \equiv$	s^2_{12}	s^2_{13}	s^2_{23}	δ_{23}/π	s^2_{14}	s^2_{24}	δ_{24}/π	s^2_{34}	δ_{34}/π
$U_{\rm sterile}\, U_{23}\, U_{13}\, U_{12}$	0.3	0.02	0.44	-0.40	0.02	0.01	0.10	0.1	0
$U_{23}\, U_{\rm sterile}\, U_{13}\, U_{12}$			0.49	-0.39		0.02	0.50	0.09	0.08

Table 5.1: Mixing parameters and vacuum eigenvalues used for the numerical calculations [33, 45, 22, 1]. In different conventions to define the PMNS matrix (orders of U_{23} and $U_{\rm sterile}$, where $U_{\rm sterile} = U_{34}\, U_{24}\, U_{14}$, see Eq. 5.6), some of the parameters are different, and formulas to relate the parameters in both conventions are in Appendix E. In both conventions, the energy eigenvalues in vacuum are $\Delta m^2_{21} = 7.5 \times 10^{-5}\,{\rm eV}^2$, $\Delta m^2_{31} = 2.5 \times 10^{-3}\,{\rm eV}^2$, and $\Delta m^2_{41} = 0.1\,{\rm eV}^2$.

accurate expressions for the oscillation probabilities. A similar discussion can be found in Ref. [36].

In a scheme with N sterile neutrinos, the neutrino oscillation probabilities for $\nu_\alpha \to \nu_\beta$ ($\alpha, \beta \in \{e, \mu, \tau\}$) are

$$P_{\alpha\beta} = \left| \sum_{i=1}^{3+N} \mathbf{V}^*_{\alpha i} \mathbf{V}_{\beta i}\, e^{-i \frac{\lambda_i^{(ex)}}{2E} L} \right|^2, \tag{5.42}$$

where $\lambda_i^{(ex)}$ are exact eigenvalues. We can chose the zeroth order results as an approximation; i.e., we adopt

$$\mathbf{V} \simeq \mathbf{U}^m_{\rm PMNS}, \tag{5.43}$$

where $U^m_{\rm PMNS}$ is defined in Eq. 5.36 and

$$\lambda_i^{(ex)} \simeq \lambda_i, \quad i = 1, 2, 3, 4, \tag{5.44}$$

where $\lambda_{1,2,3}$ are defined in Eq. 2.15 and $\lambda_4 = M^2(b)$. For the mass of the sterile neutrino, since it is significantly larger than the active ones, the oscillations related to it will be averaged out.

Former and running experimental facilities have provided parameter fitting results of neutrino oscillations for different schemes, With these parameters, for future baselines, one can

predict the probabilities in different schemes and this is a potential approach to determining the existence of sterile neutrinos [36]. We present the probabilities given by the 3+1 scheme and the differences of the probabilities $|\langle P_{3+1}\rangle - P_{3\nu\mathrm{SM}}|$, in different channels, in Figs. 5.6, 5.7, and 5.8. The probabilities in the Standard Model are given by Refs. [62, 17]; the 3+1 scheme is calculated by the zeroth order rotation method developed in this chapter. All the parameters are given in Table 5.1.

In the figures, we can identify several regions in which the differences are significantly larger than errors of the perturbation expansions. For example, in the $\nu_\mu \to \nu_e$ channel, around the band of $L/E \simeq 700\,(\mathrm{km/GeV})$, $|\langle P_{3+1}\rangle - P_{3\nu\mathrm{SM}}|$ may be larger than 0.02, and the differences will be even larger than 0.05 if $L/E \gtrsim 1500\,\mathrm{km/GeV}$ and the baseline is longer than 500 km. In this channel, baselines of T2K/HyperK, NOVA and DUNE (estimated) are marked [5, 9, 52]. For the channel of $\nu_\mu \to \nu_\mu$, shifts from the 3νSM will be more than 0.05 with $L/E \simeq 1000(\mathrm{km/GeV})$ and the baseline is longer than 1000 km. For the $\nu_\mu \to \nu_\tau$ channel, the scale of the greatest difference is larger than 0.16 if $L/E \simeq 500(\mathrm{km/GeV})$ or $\simeq 1500(\mathrm{km/GeV})$. Future experiments may measure the oscillation probabilities with baselines and neutrino energies in the region of interest predicted above and compare the results with the numerical outcomes.

5.5 Compare to existing approximation formulas

Approximation methods to calculate neutrino oscillations in matter in the 3+1 scheme have been studied by many researchers; for example, see Refs. [44, 11, 10, 35, 36]. All these works chose to ignore the Hamiltonian's fourth row/column (except for the fourth diagonal element) in the zeroth order approximations; thus, the problem was reduced to the 3×3 case. However, solving a three-dimensional eigensystem is still not simple. Fong *et al.* (FMN) adopted the exact three-dimensional solutions [36], which was complicated; see Refs. [62, 43]. Klop and Palazzo (KP) used one more approximation method for the 3×3 submatrix [44],

which introduced extra errors. Figure. 5.9 compares fractional errors of the rotations method developed in this chapter (referred as PZ) with 0th order FMN and KP, assuming baselines of T2K/Hyper-K (T2K/HK), NOVA, HyperK-Korea (T2HKK), and DUNE. Compared with KP, just to zeroth order PZ is significantly more precise for almost all baselines and energy ranges. Based on Fig. 5.9, FMN's precision is similar to PZ's for most baselines and energy regions; however, we can still identify PZ's advantage for T2K's baseline or low energy (less than or similar to 1GeV) regions.

Method	$PZ^{(0)}$	$PZ^{(1)}$	$FMN^{(0)}$	KP	Analytic solution	Numerical method
Time Units	1.0	1.8	2.1	0.16	2.2	5.7

Table 5.2: Computation time consumed by different methods. Since a real time will depend on a specific computer's performance, zeroth order PZ's (rotation method developed in this chapter) time is set to be one unit time. FMN is from Fong, *et al.* [36]; KP is from Klop and Palazzo [44]; the analytical solution is given by Ref. [46]; and the numerical method is referred to Eigen 3.3.7.

We compare the computing time of the different methods in Table 5.2. Since any specific computing time heavily depends on performance of the computer, we provide a list of relative computing time, i.e., zeroth order PZ's computing time is set to be one unit time. The speed of a numerical method (using Eigen 3.3.7, http://eigen.tuxfamily.org/http://eigen.tuxfamily.org) is also included in the comparison. A similar comparison of the methods for the $3\nu SM$ scheme can be found in Ref. [16]. Table 5.2 shows that, compared with the rotation method developed in this chapter (PZ), only the KP method is faster; however, its advantage in speed will be offset by the relatively poor precision. The FMN method is comparable in time consumed to the exact analytical solution. For experimentalists, the speed of a numerical method for evaluating the oscillation probability is relevant because it affects the time and computing resources consumed by large multidimensional parameter scans.

Besides simplicity and better precision, the rotation method of this chapter also gives explicit expressions of zeroth order eigenvalues and mixing angles and CP phases with high precision which are not covered by any former references.

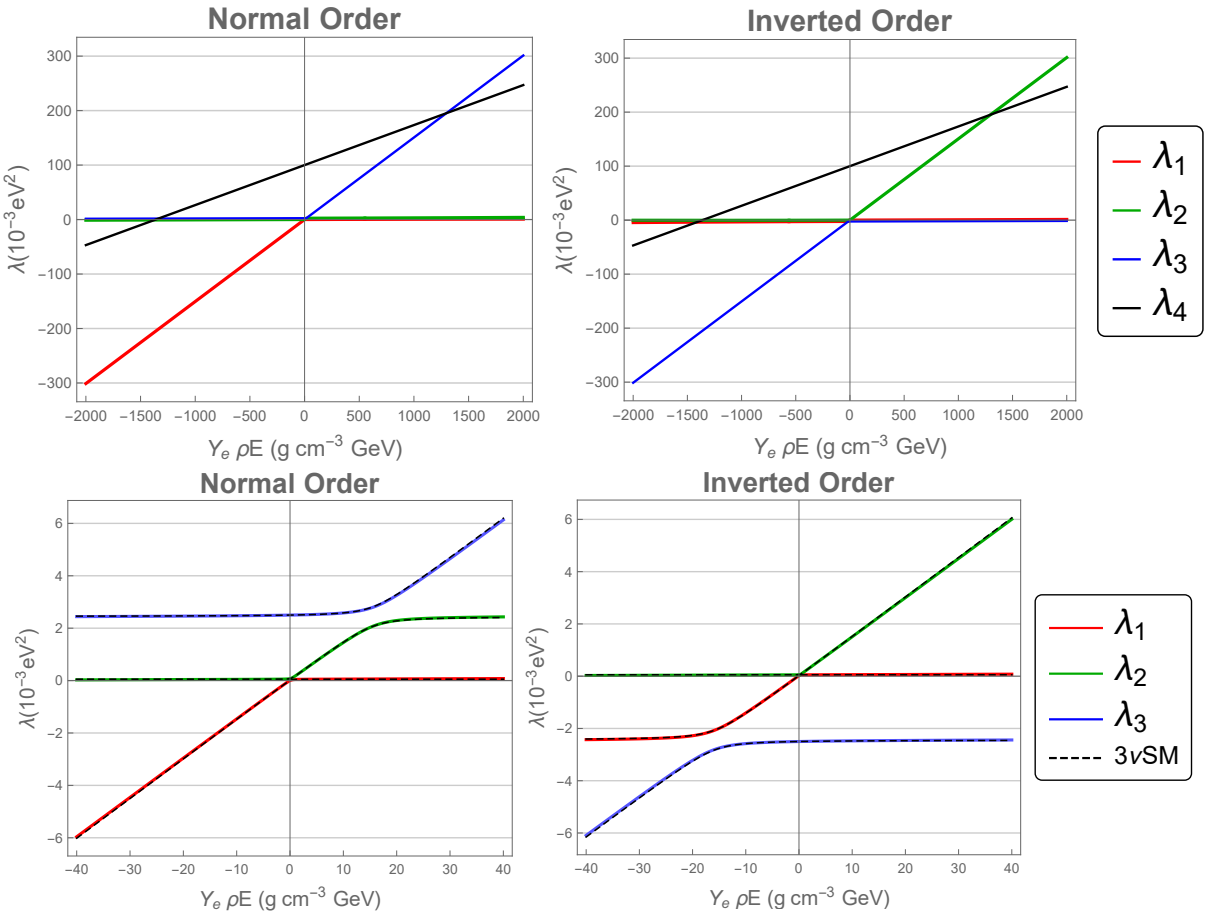

Figure 5.3: The top two panels give the crossing of the fourth eigenvalue (black), using $\Delta m^2_{41} = 0.1\,\mathrm{eV}^2$, with the active eigenvalues (red, green and blue). The active eigenvalues, $\lambda_{1,2,3}$ can cross $\lambda_4 = M^2(b)$ only if the neutrino energy is very large ($\mathcal{O}(1)$ TeV for earth densities). The bottom two panels are zoomed in to the region of primary interest; they show the zeroth order active eigenvalues in normal and inverted order; also for comparison, the dashed lines are the values in $3\nu SM$. Again the differences are small but non-negligible. The parameters used are in Table 5.1.

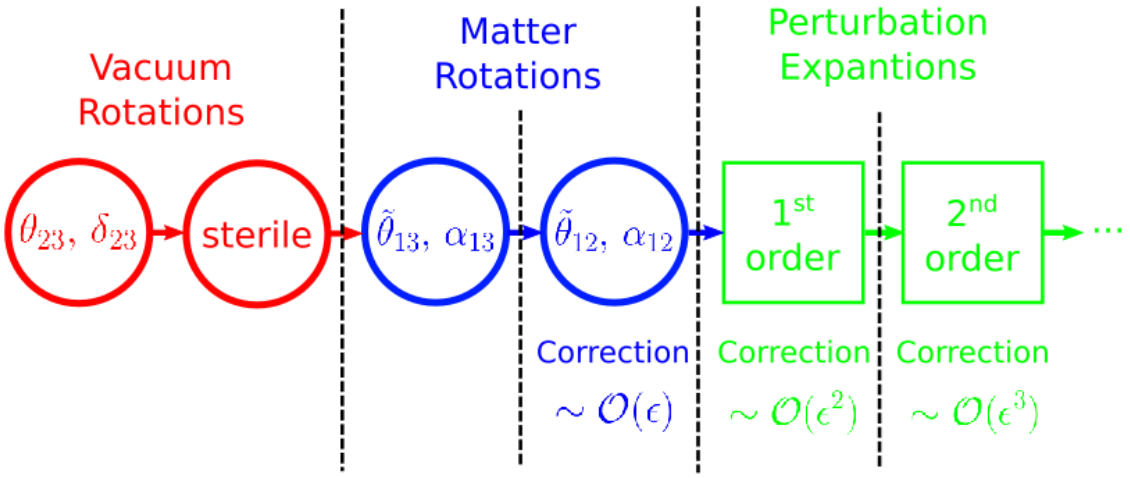

Figure 5.4: Summary of the rotations and the following perturbative expansions. We first implemented vacuum rotations in the (2-3) and sterile sectors. The red circle with text *sterile* inside indicates the rotations in sterile rotations, i.e., the rotations represented by $U_{\text{sterile}} = U_{34}\, U_{24}\, U_{14}$; see Eq. 5.6. Then, two matter rotations in the 13 and 12 sectors were performed. After the series of rotations, the zeroth order approximations of the eigenvalues and eigenvectors achieved $\mathcal{O}(\epsilon)$ accuracy. Perturbative expansions will be used to further improve the precision.

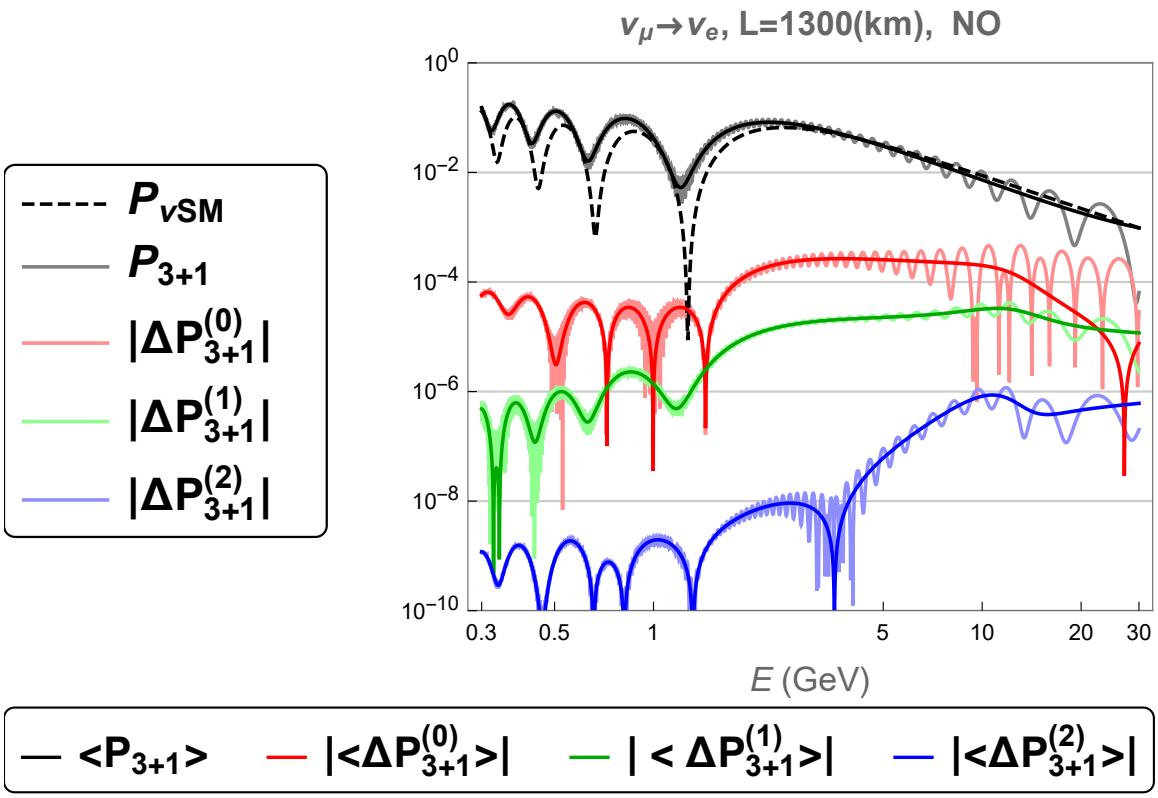

Figure 5.5: In the 3+1 scheme, errors of the zeroth, first, and second order approximations are presented by red, green, and blue curves, respectively. The light colors (which look like bold shadows in the low energy region) are representing true corrections; the darker ones are showing the expectation values. The exact probability (expectation value) in the 3+1 scheme, which is plotted by the gray solid (black solid) curve, can be calculated by Ref. [46]. As a contrast, the dashed black line is showing the probabilities in the Standard Model, with $Y_e\rho = 1.4\,\mathrm{g}\cdot\mathrm{cm}^{-3}$.

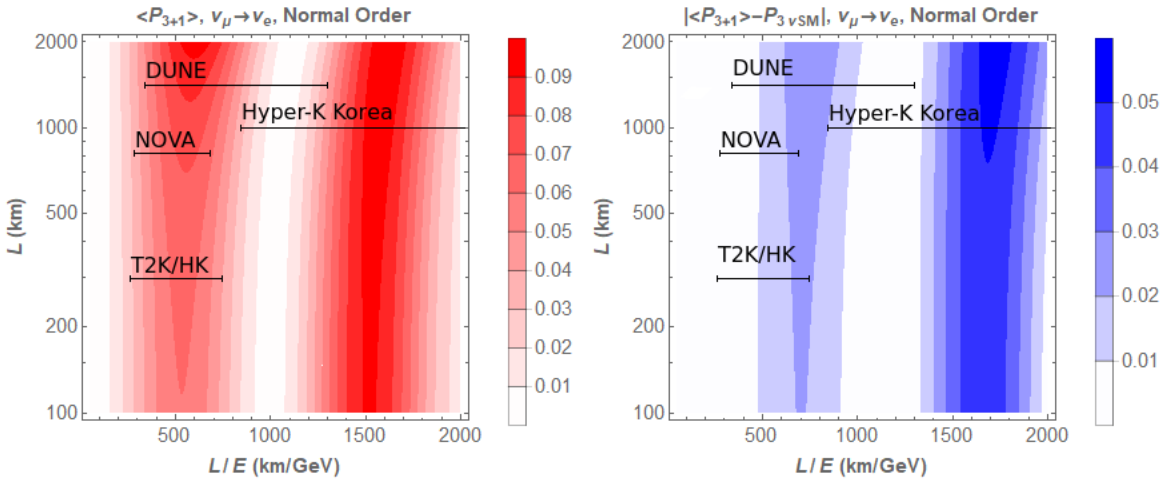

Figure 5.6: For the $\nu_\mu \to \nu_e$ channel, the left plot is showing the probabilities predicted by the 3+1 scheme; differences of the probabilities (expectation values, with fast oscillations averaged out) predicted by the standard three-flavor scheme and the 3+1 scheme are presented in the right plot. P_{3+1} in both figures is computed by the zeroth order rotation method developed in this chapter. Parameters used are given in Table 5.1. Neutrino flux energies used are $0.4 - 1.2\,\text{GeV}$ for T2K/HyperK (295 km), $1.2 - 3.0\,\text{GeV}$ for NOVA (810 km), $0.4 - 1.5\,\text{GeV}$ for T2HKK (1100 km), and $1.0 - 4.0\,\text{GeV}$ for DUNE (1300 km), see Refs. [5, 9, 52, 6].

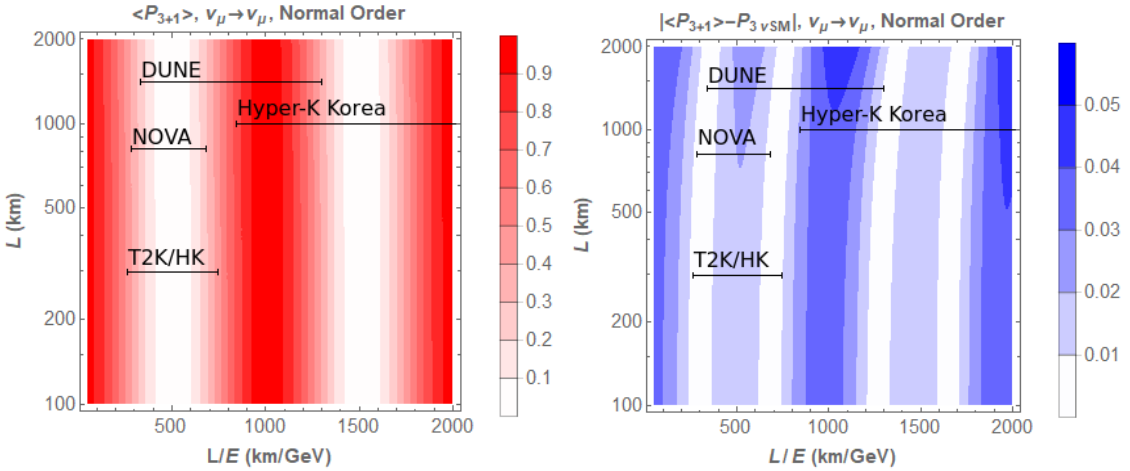

Figure 5.7: For the $\nu_\mu \to \nu_\mu$ channel, the left plot is showing the probabilities (expectation values, with fast oscillations averaged out) predicted by the 3+1 scheme; differences of the probabilities predicted by the standard three-flavor scheme and the 3+1 scheme are presented in the right plot. P_{3+1} in both figures is computed by the zeroth order rotation method developed in this chapter. Parameters used are given in Table 5.1. See Fig. 5.6 for neutrino flux energies of the listed facilities.

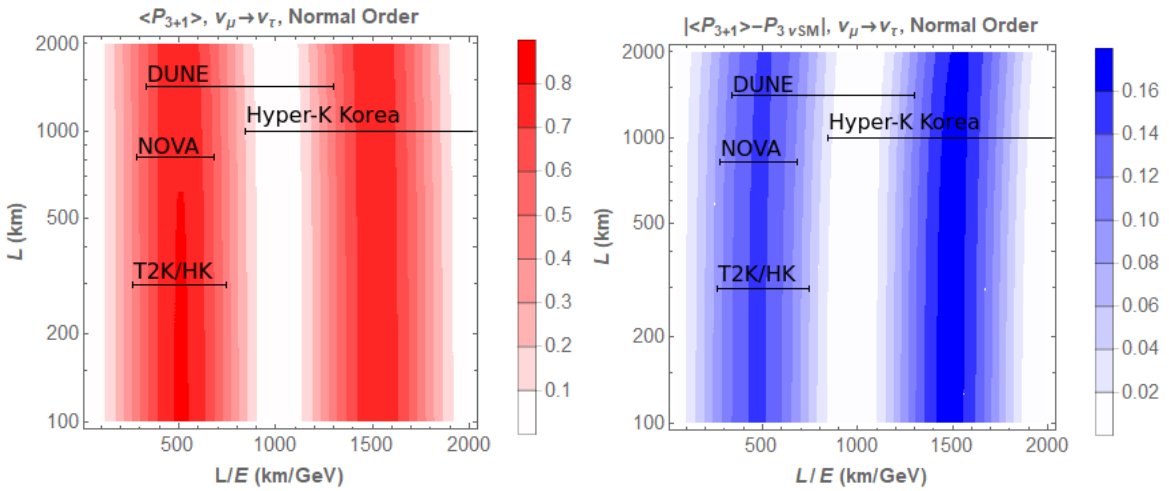

Figure 5.8: For the $\nu_\mu \to \nu_\tau$ channel, the left plot is showing the probabilities (expectation values, with fast oscillations averaged out) predicted by the 3+1 scheme; differences of the probabilities predicted by the standard three-flavor scheme and the 3+1 scheme are presented in the right plot. P_{3+1} in both figures is computed by the zeroth order rotation method developed in this chapter. Parameters used are given in Table 5.1. See Fig. 5.6 for neutrino flux energies of the listed facilities.

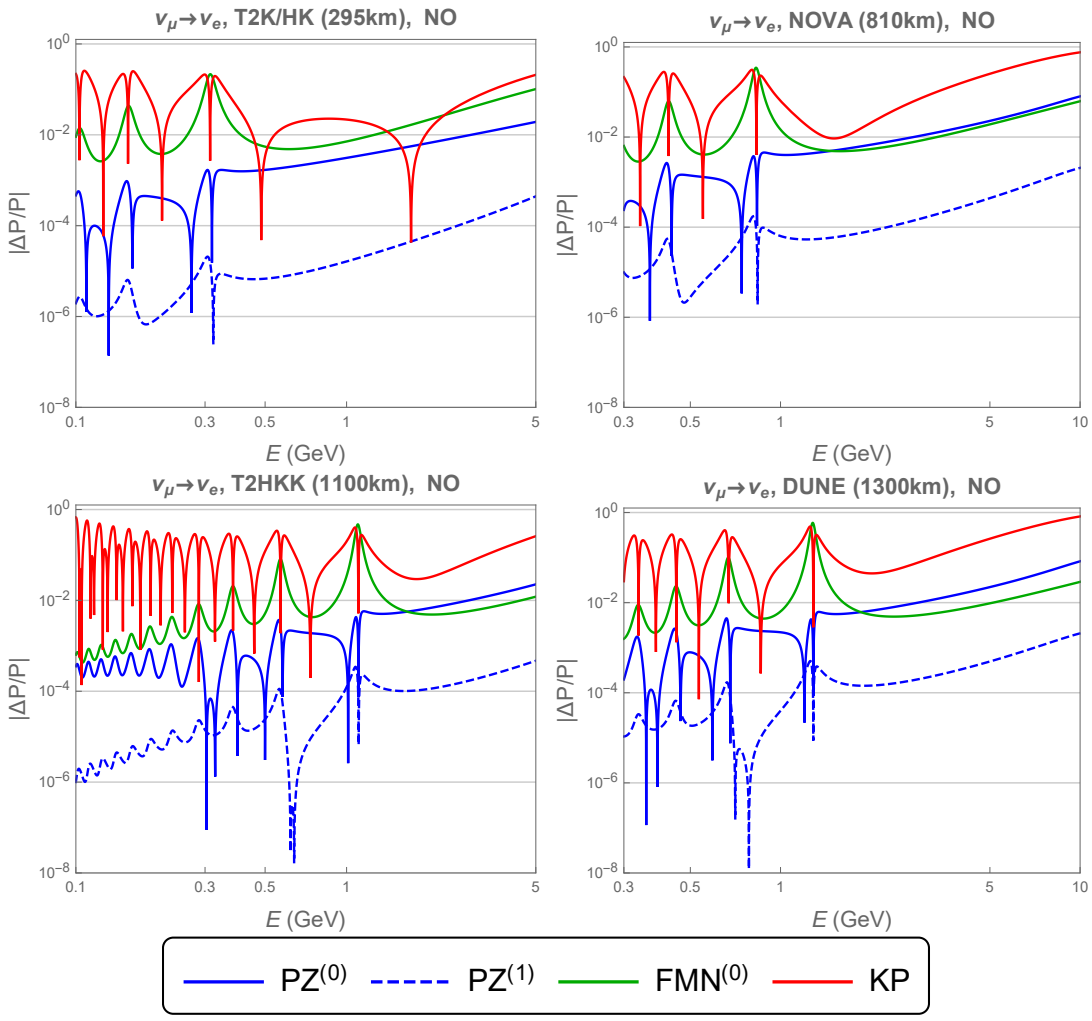

Figure 5.9: Fractional errors of oscillation probabilities (fast oscillations averaged out) given by different methods. The solid blue curve (PZ) indicates the zeroth order rotation method of this chapter, and the dashed blue line is the first order result; the green curve (FMN) is from Fong, *et al.* [36]; and the red curve (KP) is from Klop and Palazzo [44]. Parameters used for this sample calculation are listed in Table 5.1. The relative speed of the methods can be found in Table 5.2.

CHAPTER 6

CONCLUSION AND SUMMARY

Based on the standard three flavors scheme, we have developed a new simple and compact approximation method to calculate neutrino oscillations modified by the Wolfenstein matter effect with uniform density by implementing rotations. In this method, level crossings of zeroth order eigenvalues can be resolved by the rotations thus degeneracy near solar and atmospheric resonances can be eliminated and the method is applied to the whole range of L/E and matter potential. The expansion parameter used in the method is ϵ' which is not larger than $s_{12}c_{12}\Delta m^2_{21}/\Delta m^2_{ee} \simeq 0.014$. Moreover, when the matter potential a goes to zero ϵ' will also go to zero, the approximated results will converge to the vacuum values when $a = 0$.

After performing the rotations which produce zeroth order results, we can use perturbation theory to derive higher order correction terms. However, we can also implement some additional rotations to replace the perturbative expansions to obtain equivalent precision. We strictly prove that two more additional rotations can improve precision to be as good as a first order perturbation theory; after three (one more after the two) additional rotations precision can be improved to second order. Moreover, by analytic and numerical approaches, we prove that implementing additional rotations can increase order of errors in a Fibonacci recursive process, thus in exponential of number of rotations.

Besides the approximated method, we introduce a recently rediscovered identity in linear algebra into neutrino physics and use it to derive simple, clear, and symmetric formulas to calculate mixing angles and CP phase in matter. The identity relates norm squares of elements of the PMNS matrix with eigenvalues of the Hamiltonian operator and its principal minors. The new formulas can also be combined with the approximated results from the rotation method. Because all the first order corrections to the eigenvalues vanish, we can insert the zeroth order eigenvalues into the formulas to get concise approximated expressions

of mixing angles and CP phase with a second order precision.

Finally, we extend the rotation method from the standard three flavors scheme to a scheme with one more sterile neutrino. To simplify derivation and calculation process, we adopt a new convention to define the PMNS matrix as product of several real or complex rotation matrices. In our convention, U_{23} is the last rotation from the energy basis to the flavor basis. The extended method inherits good properties of the initial one. By numerical tests, we also compare the rotation method's precision and computing speed with other approximated methods previously developed for schemes with sterile schemes and show supremacy of the approach of this dissertation.

APPENDIX A

HAMILTONIANS AFTER THE ADDITIONAL ROTATIONS

In the case of neutrinos, after the $U_{13}(\alpha_{13})$ rotation, in Eq. 3.1 the Hamiltonian is $\check{H}' = \check{H}'_0 + \check{H}'_1$ where

$$\begin{aligned}
2E(\check{H}'_0)_{11} &= c^2_{\alpha_{13}}\lambda_1 + s^2_{\alpha_{13}}\lambda_3 + 2s_{\alpha_{13}}c_{\alpha_{13}}\,\tilde{s}_{12}\epsilon'\Delta m^2_{ee},\\
2E(\check{H}'_0)_{12} &= 0,\\
2E(\check{H}'_0)_{13} &= -\,s_{\alpha_{13}}c_{\alpha_{13}}\Delta\lambda_{31} + (s^2_{\alpha_{13}} - c^2_{\alpha_{13}})\,\tilde{s}_{12}\epsilon'\Delta m^2_{ee},\\
2E(\check{H}'_0)_{22} &= \lambda_2,\\
2E(\check{H}'_0)_{23} &= 0,\\
2E(\check{H}'_0)_{33} &= s^2_{\alpha_{13}}\lambda_1 + c^2_{\alpha_{13}}\lambda_3 - 2s_{\alpha_{13}}c_{\alpha_{13}}\,\tilde{s}_{12}\epsilon'\Delta m^2_{ee},
\end{aligned} \tag{A.1}$$

and $(\check{H}'_0)_{ij} = (\check{H}'_0)_{ji}$, and

$$\check{H}'_1 = \frac{\epsilon'\Delta m^2_{ee}\tilde{c}_{12}}{2E}\begin{pmatrix} & -s_{\alpha_{13}} & \\ -s_{\alpha_{13}} & & c_{\alpha_{13}} \\ & c_{\alpha_{13}} & \end{pmatrix} \tag{A.2}$$

We require the 13 sector to be diagonalized, i.e α_{13} must satisfy an equation:

$$-s_{\alpha_{13}}c_{\alpha_{13}}\Delta\lambda_{31} + (s^2_{\alpha_{13}} - c^2_{\alpha_{13}})\,\tilde{s}_{12}\epsilon'\Delta m^2_{ee} = 0. \tag{A.3}$$

The solution is Eq. 3.2.

After the $U_{23}(\alpha_{23})$ rotation, in Eq. 3.4 the Hamiltonian is $\check{H}'' = \check{H}''_0 + \check{H}''_1$, where

$$\begin{aligned}
2E(\check{H}''_0)_{11} &= \lambda'_1,\\
2E(\check{H}''_0)_{12} &= 0,
\end{aligned}$$

Neutrinos

Angles	$2E\,H_0$	$2E\,(H_1)_{13}/\mathcal{N}$	$2E\,(H_1)_{12}/\mathcal{N}$	$2E\,(H_1)_{23}/\mathcal{N}$	$\mathcal{N}$
	$(\lambda_a,\,\lambda_b,\,\lambda_c)$	$s_{13}c_{13}$	$c_{13}\,s_{12}c_{12}\epsilon$	$s_{13}\,s_{12}c_{12}\epsilon$	Δm^2_{ee}
$\tilde{\theta}_{13}$	$(\lambda_-,\,\lambda_0,\,\lambda_+)$	0	$c_{(\tilde{\theta}_{13}-\theta_{13})}$	$s_{(\tilde{\theta}_{13}-\theta_{13})}$	$\times\, s_{12}c_{12}\,\epsilon$
$\tilde{\theta}_{12}$	$(\lambda_1,\,\lambda_2,\,\lambda_3)$	$-\tilde{s}_{12}$	0	$\tilde{c}_{12}$	$\times\, s_{(\tilde{\theta}_{13}-\theta_{13})}$
α_{13}	$(\lambda'_1,\,\lambda'_2,\,\lambda'_3)$	0	$-s_{\alpha_{13}}$	$c_{\alpha_{13}}$	$\times\, \tilde{c}_{12}$
α_{23}	$(\lambda''_1,\,\lambda''_2,\,\lambda''_3)$	$s_{\alpha_{23}}$	$c_{\alpha_{23}}$	0	$\times\,(-s_{\alpha_{13}})$
α_{12}	$(\lambda'''_1,\,\lambda'''_2,\,\lambda'''_3)$	$c_{\alpha_{12}}$	0	$s_{\alpha_{12}}$	$\times\, s_{\alpha_{23}}$

Anti-Neutrinos

Angles	$2E\,H_0$	$2E\,(H_1)_{13}/\mathcal{N}$	$2E\,(H_1)_{12}/\mathcal{N}$	$2E\,(H_1)_{23}/\mathcal{N}$	$\mathcal{N}$
	$(\lambda_a,\,\lambda_b,\,\lambda_c)$	$s_{13}c_{13}$	$c_{13}\,s_{12}c_{12}\epsilon$	$s_{13}\,s_{12}c_{12}\epsilon$	Δm^2_{ee}
$\tilde{\theta}_{13}$	$(\lambda_-,\,\lambda_0,\,\lambda_+)$	0	$c_{(\tilde{\theta}_{13}-\theta_{13})}$	$s_{(\tilde{\theta}_{13}-\theta_{13})}$	$\times\, s_{12}c_{12}\,\epsilon$
$\tilde{\theta}_{12}$	$(\lambda_1,\,\lambda_2,\,\lambda_3)$	$-\tilde{s}_{12}$	0	$\tilde{c}_{12}$	$\times\, s_{(\tilde{\theta}_{13}-\theta_{13})}$
$\bar{\alpha}_{23}$	$(\bar{\lambda}'_1,\,\bar{\lambda}'_2,\,\bar{\lambda}'_3)$	$c_{\bar{\alpha}_{23}}$	$-s_{\bar{\alpha}_{23}}$	0	$\times\,(-\tilde{s}_{12})$
$\bar{\alpha}_{13}$	$(\bar{\lambda}''_1,\,\bar{\lambda}''_2,\,\bar{\lambda}''_3)$	0	$c_{\bar{\alpha}_{13}}$	$s_{\bar{\alpha}_{13}}$	$\times\,(-s_{\bar{\alpha}_{23}})$
$\bar{\alpha}_{12}$	$(\bar{\lambda}'''_1,\,\bar{\lambda}'''_2,\,\bar{\lambda}'''_3)$	$-s_{\bar{\alpha}_{12}}$	0	$c_{\bar{\alpha}_{12}}$	$\times\, s_{\bar{\alpha}_{13}}$

Table A.1: Entries of the Hamiltonian after each rotation for neutrinos and anti-neutrinos are presented. $\mathcal{N}$ in the last column is a normalization factor. For each row, $\mathcal{N}$ is equal to the product of all elements on and above this line. The first three rows are identical for neutrinos and anti-neutrinos.

$$
\begin{aligned}
2E(\check{H}''_0)_{13} &= 0,\\
2E(\check{H}''_0)_{22} &= c^2_{\alpha_{23}}\lambda'_2 + s^2_{\alpha_{23}}\lambda'_3\\
&\quad - 2s_{\alpha_{23}}c_{\alpha_{23}}\,c_{\alpha_{13}}\tilde{c}_{12}\epsilon'\Delta m^2_{ee},\\
2E(\check{H}''_0)_{23} &= -\,s_{\alpha_{23}}c_{\alpha_{23}}\Delta\lambda'_{32}\\
&\quad - (s^2_{\alpha_{23}} - c^2_{\alpha_{23}})\,c_{\alpha_{13}}\tilde{c}_{12}\epsilon'\Delta m^2_{ee},\\
2E(\check{H}''_0)_{33} &= s^2_{\alpha_{23}}\lambda'_2 + c^2_{\alpha_{23}}\lambda'_3.\\
&\quad + 2s_{\alpha_{23}}c_{\alpha_{23}}\,c_{\alpha_{13}}\tilde{c}_{12}\epsilon'\Delta m^2_{ee}
\end{aligned}
\tag{A.4}
$$

and $(\check{H}_0'')_{ij} = (\check{H}_0'')_{ji}$, and

$$\check{H}_1'' = -\frac{\epsilon' \Delta m^2_{ee} \tilde{c}_{12} s_{\alpha_{13}}}{2E} \begin{pmatrix} & c_{\alpha_{23}} & s_{\alpha_{23}} \\ c_{\alpha_{23}} & & \\ s_{\alpha_{23}} & & \end{pmatrix}. \tag{A.5}$$

Now the (2-3) sector must be diagonalized, i.e. α_{23} must satisfy

$$-s_{\alpha_{23}} c_{\alpha_{23}} \Delta\lambda'_{32} - (s^2_{\alpha_{23}} - c^2_{\alpha_{23}}) c_{\alpha_{13}} \tilde{c}_{12} \epsilon' \Delta m^2_{ee} = 0. \tag{A.6}$$

The solution is Eq. 3.5. Since α_{13} is a first order (in ϵ') term, it is evident that $\check{H}_1''$ is in second order.

After the $U_{12}(\alpha_{12})$ rotation, in Eq. 3.7 the Hamiltonian is $\check{H}''' = \check{H}_0''' + \check{H}_1'''$, where

$$\begin{aligned}
2E(\check{H}_0''')_{11} &= c^2_{\alpha_{12}} \lambda_1'' + s^2_{\alpha_{12}} \lambda_2'' \\
&\quad + 2 s_{\alpha_{12}} c_{\alpha_{12}} c_{\alpha_{23}} s_{\alpha_{13}} \tilde{c}_{12} \epsilon' \Delta m^2_{ee}, \\
2E(\check{H}_0''')_{12} &= -s_{\alpha_{12}} c_{\alpha_{12}} \Delta\lambda''_{21} \\
&\quad + (s^2_{\alpha_{12}} - c^2_{\alpha_{12}}) c_{\alpha_{23}} s_{\alpha_{13}} \tilde{c}_{12} \epsilon' \Delta m^2_{ee}, \\
2E(\check{H}_0''')_{13} &= 0, \\
2E(\check{H}_0''')_{22} &= s^2_{\alpha_{12}} \lambda_1'' + c^2_{\alpha_{12}} \lambda_2'' \\
&\quad - 2 s_{\alpha_{12}} c_{\alpha_{12}} c_{\alpha_{23}} s_{\alpha_{13}} \tilde{c}_{12} \epsilon' \Delta m^2_{ee}, \\
2E(\check{H}_0''')_{23} &= 0, \\
2E(\check{H}_0''')_{33} &= \lambda_3'',
\end{aligned} \tag{A.7}$$

and $(\check{H}_0''')_{ij} = (\check{H}_0''')_{ji}$, and

$$\check{H}_1''' = -\frac{\epsilon' \Delta m_{ee}^2 \tilde{c}_{12} s_{\alpha_{13}} s_{\alpha_{23}}}{2E} \begin{pmatrix} & & c_{\alpha_{12}} \\ & & s_{\alpha_{12}} \\ c_{\alpha_{12}} & s_{\alpha_{12}} & \end{pmatrix}. \tag{A.8}$$

It is easy to verify that $\check{H}_1'''$ is already a third order term in ϵ'. And α_{12} must diagonalize the (1-2) sector, i.e.

$$-s_{\alpha_{12}} c_{\alpha_{12}} \Delta\lambda_{21}'' + (s_{\alpha_{12}}^2 - c_{\alpha_{12}}^2) c_{\alpha_{23}} s_{\alpha_{13}} \tilde{c}_{12} \epsilon' \Delta m_{ee}^2 = 0. \tag{A.9}$$

The solution is Eq. 3.8.

The approach for anti-neutrinos is quite similar so we will not provide the detailed procedure. The first additional rotation diagonalizes the (2-3) submatrix with $\theta = \bar{\alpha}_{23}$, and $\lambda_x = \tilde{c}_{12} \epsilon' \Delta m_{ee}^2$; the second additional rotation diagonalizes the (1-3) submatrix with $\theta = \bar{\alpha}_{13}$, and $\lambda_x = -c_{\bar{\alpha}_{23}} \tilde{s}_{12} \epsilon' \Delta m_{ee}^2$; the third additional rotation diagonalizes the (1-2) submatrix with $\theta = \bar{\alpha}_{12}$, and $\lambda_x = c_{\bar{\alpha}_{13}} s_{\bar{\alpha}_{23}} \tilde{s}_{12} \epsilon' \Delta m_{ee}^2$.

For both cases of neutrino and anti-neutrino, the Hamiltonian after each rotation is summarized in Table A.1.

APPENDIX B

LODE VERSUS LORT

In Chapter 2 and Chapter 3, after the vacuum rotation U_{23}, our strategy to determine order of the rotations to produce the zeroth order results is killing the largest (absolute value) off-diagonal elements (LODE) of the Hamiltonian. However, there is another possible strategy that we may choose a 2×2 sector which can be diagonalized by a largest rotation angles (LROT). In most ranges of $Y_e \rho E$, these two strategies give exactly the same procedures and results. We do find some ranges that the two strategies give different orders of rations, for example when a is around Δm^2_{21}, after the vacuum U_{23} rotation, for LROT we need to implement a rotation in the 12 sector rather than the U_{13} rotation for LODE. We built codes to execute both strategies and compare their precision by calculating the largest absolute values of off-diagonal elements (perturbative terms) of the Hamiltonian after the rotations. The results are displayed in Fig. B.1. The vacuum parameters used in the computation are $\sin^2\theta_{12} = 0.31$, $\sin^2\theta_{13} = 0.022$, $\sin^2\theta_{23} = 0.58$, CP-phase is 215°, $\Delta m^2_{21} = 7.5 \times 10^{-5}$eV, $\Delta m^2_{31} = 2.5 \times 10^{-3}$eV [32]. We consider cases with/without the first vacuum U_{23} rotation. In the case of without the vacuum U_{23}, we start implementing the strategies from the flavor basis Hamiltonian. It is evident that whenever LROT and LODE give different results, LODE has better precision (same number of rotations). On the other hand, the two approaches have the same computation complexity, thus we have no reason to adopt LROT in practice.

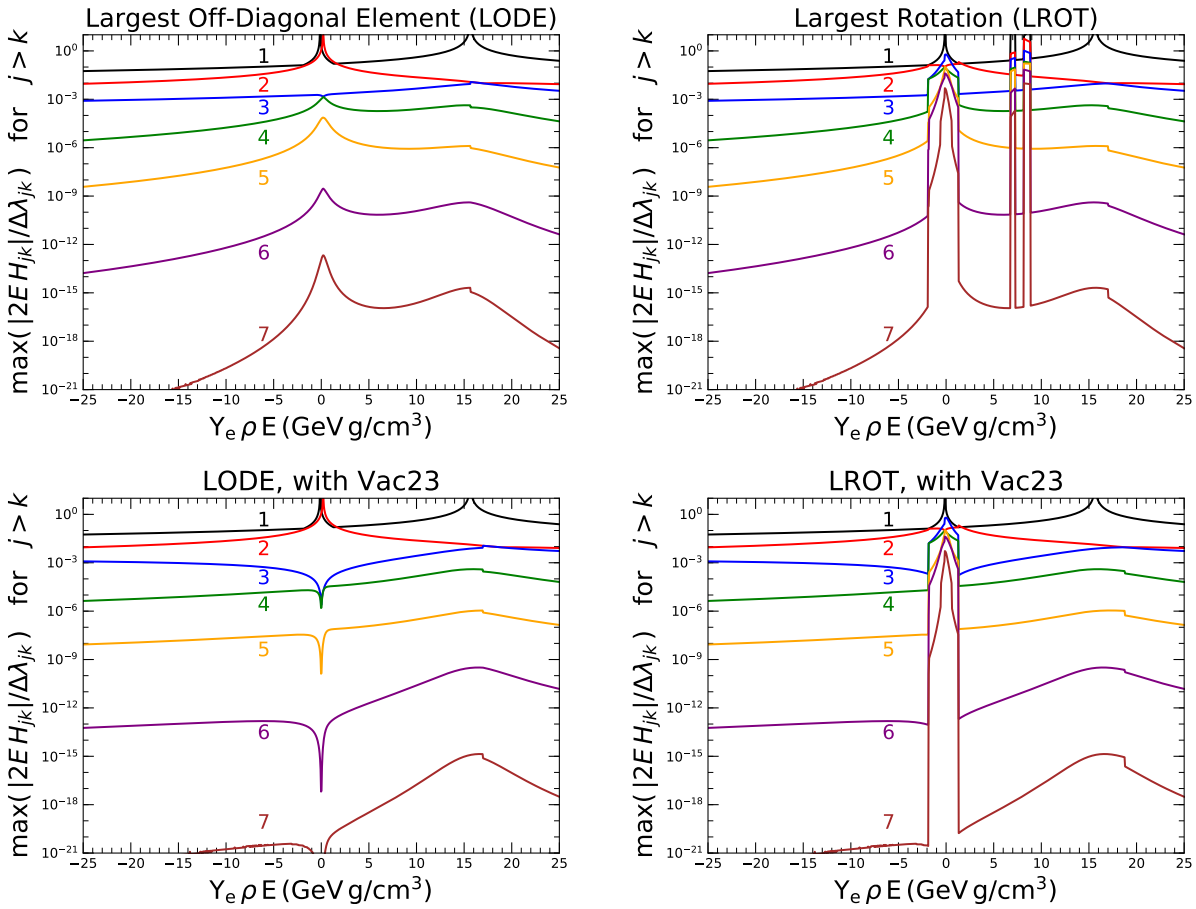

Figure B.1: The size of the corrections to the eigenvectors, $max_{j>k}(2E(H_1)_{ij}/\Delta\tilde{m}^2_{jk})$ after N rotations by the LODE and LROT strategies.

APPENDIX C

THE EXACT EIGENVALUES IN MATTERS FOR 3νSM

In the standard three flavors scheme, if the matter potential term is a defined in Eq. 2.5, the corrected eigenvalues of the Hamiltonian are [62]:

$$\tilde{m}_1^2 = m_1^2 + \frac{A}{3} - \frac{S}{3}\sqrt{A^2 - 3B} - \frac{\sqrt{3}}{3}\sqrt{A^2 - 3B}\sqrt{1 - S^2}, \tag{C.1}$$

$$\tilde{m}_2^2 = m_2^2 + \frac{A}{3} - \frac{S}{3}\sqrt{A^2 - 3B} + \frac{\sqrt{3}}{3}\sqrt{A^2 - 3B}\sqrt{1 - S^2}, \tag{C.2}$$

$$\tilde{m}_3^2 = m_3^2 + \frac{A}{3} + \frac{2S}{3}\sqrt{A^2 - 3B}, \tag{C.3}$$

with

$$A = \Delta m_{21}^2 + \Delta m_{31}^2 + a, \tag{C.4}$$

$$B = \Delta m_{21}^2 \Delta m_{31}^2 + a[\Delta m_{31}^2 c_{13}^2 + \Delta m_{21}^2 (c_{13}^2 c_{12}^2 + s_{13}^2)], \tag{C.5}$$

$$C = a \Delta m_{31}^2 \Delta m_{21}^2 c_{13}^2 c_{12}^2, \tag{C.6}$$

$$S = \cos\frac{1}{3}\arccos\frac{2A^3 - 9AB + 27C}{2\sqrt[3]{A^2 - 3B}}. \tag{C.7}$$

APPENDIX D

EIGENVALUES OF THE 2×2 MINORS

In Eq. 4.9, $\xi_{e,\mu,\tau}$ and $\chi_{e,\mu,\tau}$ haven't been given. It is observed that to calculate $|U_{\alpha\, i}|^2$, we need $\xi_\alpha \chi_\alpha$ and $\xi_\alpha + \chi_\alpha$. To derive these values, we first define $\mathcal{H} \equiv U_{23}^\dagger(\theta_{23}, \delta)\, H_f\, U_{23}(\theta_{23}, \delta)$. H_f can be found in Eq. 2.2. After some calculation we have

$$\mathcal{H} = \frac{1}{2E} \begin{pmatrix} a + \Delta m^2_{ee} s^2_{13} + \Delta m^2_{21} s^2_{12} & c_{13} s_{12} c_{12} \Delta m^2_{21} & s_{13} c_{13} \Delta m^2_{ee} \\ * & \Delta m^2_{21} c^2_{12} & -s_{13} s_{12} c_{12} \Delta m^2_{21} \\ * & * & \Delta m^2_{ee} c^2_{13} + \Delta m^2_{21} s^2_{12} \end{pmatrix}. \quad \text{(D.1)}$$

$\mathcal{H}$ is a symmetric. With $\mathcal{H}$ we can get

$$\begin{aligned} \xi_e + \chi_e =& (2E)(\mathcal{H}_{\mu\mu} + \mathcal{H}_{\tau\tau}) \\ \xi_e \chi_e =& (2E)^2(\mathcal{H}_{\mu\mu}\mathcal{H}_{\tau\tau} - \mathcal{H}^2_{\mu\tau}) \\ \xi_\mu + \chi_\mu =& (2E)(\mathcal{H}_{ee} + c^2_{23}\mathcal{H}_{\tau\tau} + s^2_{23}\mathcal{H}_{\mu\mu} - 2 s_{23} c_{23} \cos\delta \mathcal{H}_{\mu\tau}) \\ \xi_\mu \chi_\mu =& (2E)^2 \big[\mathcal{H}_{ee}(c^2_{23}\mathcal{H}_{\tau\tau} + s^2_{23}\mathcal{H}_{\mu\mu} - 2 s_{23} c_{23} \cos\delta \mathcal{H}_{\mu\tau}) - |c_{23}\mathcal{H}_{e\tau} - s_{23} e^{-i\delta}\mathcal{H}_{e\mu}|^2\big]. \end{aligned} \quad \text{(D.2)}$$

We can get $\xi_\tau \chi_\tau$ and $\xi_\tau + \chi_\tau$ from $\xi_\mu \chi_\mu$ and $\xi_\mu + \chi_\mu$ under the interchange $c^2_{23} \leftrightarrow s^2_{23}$ and $s_{23} c_{23} \leftrightarrow -s_{23} c_{23}$.

APPENDIX E

SOME CALCULATION DETAILS OF CHAPTER 5

E.1 Mixing angles and phases in the new convention of the PMNS matrix

The PMNS matrix in the new and the usual conventions can be expressed as

$$\mathbf{U}_{\rm PMNS}^{3+1} \equiv \begin{cases} \mathbf{U}_{23}(\theta_{23},\delta_{23})\,\mathbf{U}_{34}(\theta_{34},\delta_{34})\,\mathbf{U}_{24}(\theta_{24},\delta_{24})\,\mathbf{U}_{14}(\theta_{14})\,\mathbf{U}_{13}(\theta_{13})\,\mathbf{U}_{12}(\theta_{12}) \\ \mathbf{U}_{34}(\theta'_{34},\delta'_{34})\,\mathbf{U}_{24}(\theta'_{24},\delta'_{24})\,\mathbf{U}_{14}(\theta'_{14})\,\mathbf{U}_{23}(\theta'_{23},\delta'_{23})\,\mathbf{U}_{13}(\theta'_{13})\,\mathbf{U}_{12}(\theta'_{12}) \end{cases} . \tag{E.1}$$

We will express the parameters of the new convention (without the prime) in formulas of the parameters of the usual convention (with the prime). We notice that $\mathbf{U}_{14}\mathbf{U}_{23} = \mathbf{U}_{23}\mathbf{U}_{14}$, and then

$$\theta_{12} = \theta'_{12}, \quad \theta_{13} = \theta'_{13}, \quad \theta_{14} = \theta'_{14}, \tag{E.2}$$

and

$$\begin{aligned} &\mathbf{U}_{23}(\theta_{23},\delta_{23})\,\mathbf{U}_{34}(\theta_{34},\delta_{34})\,\mathbf{U}_{24}(\theta_{24},\delta_{24}) \\ &= e^{i\mathbf{A}}\mathbf{U}(\theta'_{34},\delta'_{34})\,\mathbf{U}_{24}(\theta'_{24},\delta'_{24})\,\mathbf{U}_{23}(\theta'_{23},\delta'_{23}), \end{aligned} \tag{E.3}$$

where $\mathbf{A}$ is a traceless real diagonal matrix. Solving Eq. E.3 we get the following relations:

$$\begin{aligned} s_{34} &= \left|s'_{34}c'_{23} + s'_{23}s'_{24}c'_{34}\,e^{i(\delta'_{23}-\delta'_{24}+\delta'_{34})}\right|, \\ s_{24} &= \sqrt{1-\left(\frac{c'_{24}c'_{34}}{c_{34}}\right)^2}, \\ s_{23} &= \frac{s'_{23}c'_{24}}{c_{34}}, \end{aligned} \tag{E.4}$$

and

$$\begin{aligned}
\delta_{34} &= \mathrm{Arg}\big[s'_{34}c'_{23}\,e^{i\delta'_{34}} + s'_{23}s'_{24}c'_{34}\,e^{i(\delta'_{24}-\delta'_{23})}\big],\\
\delta_{24} &= \mathrm{Arg}\big[s'_{24}c'_{23}c'_{34}\,e^{i\delta'_{24}} - s'_{23}s'_{34}\,e^{i(\delta'_{23}+\delta'_{34})}\big],\\
\delta_{23} &= \delta'_{23} + \mathrm{Arg}\big[c'_{23}c'_{34} - s'_{23}s'_{24}s'_{34}\,e^{i(\delta'_{23}-\delta'_{24}+\delta'_{34})}\big].
\end{aligned} \tag{E.5}$$

The approximated formulas, with $\mathcal{O}(\epsilon)$ corrections, are also listed below:

$$\begin{aligned}
s_{34} &\simeq \Big[c'^2_{23}s'^2_{34} + s'^2_{23}c'^2_{34}\\
&\qquad + 2s'_{23}s'_{24}s'_{34}c'_{23}\cos(\delta'_{23}+\delta'_{34}-\delta'_{24})\Big]^{1/2} + \mathcal{O}(\epsilon),\\
s_{24} &\simeq \Big[c'^2_{23}s'^2_{24} + s'^2_{23}s'^2_{34}\\
&\qquad - 2s'_{23}s'_{24}s'_{34}c'_{23}\cos(\delta'_{23}+\delta'_{34}-\delta'_{24})\Big]^{1/2} + \mathcal{O}(\epsilon),\\
s_{23} &\simeq s'_{23} + \mathcal{O}(\epsilon),\\
\delta_{34} &\simeq \arctan\frac{s'_{23}s'_{24}\sin(\delta'_{24}-\delta'_{23}) + s'_{34}c'_{23}\sin\delta'_{34}}{s'_{23}s'_{24}\cos(\delta'_{24}-\delta'_{23}) + s'_{34}c'_{23}\cos\delta'_{34}}\\
&\qquad + \frac{\pi}{2}\big[1-\mathrm{sign}(s'_{34}c'_{23}+s'_{23}s'_{24}c'_{34})\big] + \mathcal{O}(\epsilon),\\
\delta_{24} &\simeq \arctan\frac{c'_{23}s'_{24}\sin\delta'_{24} - s'_{23}s'_{34}\sin(\delta'_{23}+\delta'_{34})}{c'_{23}s'_{24}\cos\delta'_{24} - s'_{23}s'_{34}\cos(\delta'_{23}+\delta'_{34})}\\
&\qquad + \frac{\pi}{2}\big[1-\mathrm{sign}(s'_{24}c'_{23}c'_{34}-s'_{23}s'_{34})\big] + \mathcal{O}(\epsilon),\\
\delta_{23} &\simeq \delta'_{23} + \mathcal{O}(\epsilon).
\end{aligned} \tag{E.6}$$

E.2 Complex phases convention

In Section 5.1 we chose $\mathbf{U}_{12}$ and $\mathbf{U}_{13}$ to be real; however, now α_{12} and α_{13} are nonzero. To recover the initial convention of the complex phases, we need to implement a phase transformation. Firstly, we multiply the first row by $e^{-i\,\alpha_{12}}$ and the first column by $e^{i\,\alpha_{12}}$; then the

third row is multiplied by $e^{i(\alpha_{13}-\alpha_{12})}$ and the third column is multiplied by $e^{i(-\alpha_{13}+\alpha_{12})}$. Finally, all the complex phases are absorbed into $\mathbf{U}_{23}$, $\mathbf{U}_{24}$, and $\mathbf{U}_{34}$. The zeroth order phases are

$$\begin{aligned}
\tilde{\delta}_{12} &= 0, \\
\tilde{\delta}_{13} &= 0, \\
\tilde{\delta}_{23} &= \delta_{23} - \alpha_{13} + \alpha_{12}, \\
\tilde{\delta}_{24} &= \delta_{24} + \alpha_{12}, \\
\tilde{\delta}_{34} &= \delta_{34} + \alpha_{13}.
\end{aligned} \tag{E.7}$$

E.3 Elements of $\check{\mathbf{H}}_M$

Since the Hamiltonian must be Hermitian, we will just present the fourth column.

$$\begin{aligned}
(\check{\mathbf{H}}_M)_{14} =& \frac{1}{2E}\Big[\tilde{c}_{12}\tilde{c}_{13}s_{14}c_{14}\big(a + b\,c_{24}^2c_{34}^2\big) \\
&- b\,\tilde{s}_{12}s_{24}c_{14}c_{24}c_{34}^2\,e^{i(\delta_{24}+\alpha_{12})} \\
&- b\,\tilde{s}_{13}\tilde{c}_{12}s_{34}c_{14}c_{24}c_{34}\,e^{i(\delta_{34}+\alpha_{13})}\Big], \\
(\check{\mathbf{H}}_M)_{24} =& \frac{1}{2E}\Big[\tilde{s}_{12}\tilde{c}_{13}s_{14}c_{14}\big(a + b\,c_{24}^2c_{34}^2\big) \\
&+ b\,\tilde{c}_{12}s_{24}c_{14}c_{24}c_{34}^2\,e^{i\delta_{24}} \\
&- b\,\tilde{s}_{12}\tilde{s}_{13}s_{34}c_{14}c_{24}c_{34}\,e^{i(\delta_{34}-\alpha_{12}+\alpha_{13})}\Big], \\
(\check{\mathbf{H}}_M)_{34} =& \frac{1}{2E}\Big[\tilde{s}_{13}s_{14}c_{14}\big(a + b\,c_{24}^2c_{34}^2\big)e^{-i\alpha_{13}} \\
&+ b\,\tilde{c}_{13}s_{34}c_{14}c_{24}c_{34}\,e^{i\delta_{34}}\Big].
\end{aligned} \tag{E.8}$$

E.4 Perturbation expansions

E.4.1 First order corrections

Since all diagonal elements have been absorbed into the zeroth order Hamiltonian, by Eq. 5.39, the first order corrections to the eigenvalues, which are the diagonal elements of the perturbative Hamiltonian, are zero, i.e.,

$$\lambda_i^{(1)} = 2E\,(\check{\mathbf{H}}_1)_{ii} = 0. \tag{E.9}$$

As for the eigenvectors, to first order, by Eq. 5.40,

$$\begin{aligned}\mathbf{W}_1 =& \frac{\epsilon' \Delta m^2_{ee}}{2E} \begin{pmatrix} 0 & 0 & -\frac{\tilde{s}_{12}}{\Delta\lambda_{31}} e^{i(\alpha_{12}+\alpha_\epsilon)} & 0 \\ 0 & 0 & \frac{\tilde{c}_{12}}{\Delta\lambda_{32}} e^{i\alpha_\epsilon} & 0 \\ \frac{\tilde{s}_{12}}{\Delta\lambda_{31}} e^{-i(\alpha_{12}+\alpha_\epsilon)} & -\frac{\tilde{c}_{12}}{\Delta\lambda_{32}} e^{-i\alpha_\epsilon} & 0 & 0 \\ 0 & 0 & 0 & 0 \end{pmatrix} \\ &+ (2E) \begin{pmatrix} 0 & 0 & 0 & -\frac{(\check{\mathbf{H}}_M)_{14}}{\lambda_1 - M^2} \\ 0 & 0 & 0 & -\frac{(\check{\mathbf{H}}_M)_{24}}{\lambda_2 - M^2} \\ 0 & 0 & 0 & -\frac{(\check{\mathbf{H}}_M)_{34}}{\lambda_3 - M^2} \\ \frac{(\check{\mathbf{H}}_M)^*_{14}}{\lambda_1 - M^2} & \frac{(\check{\mathbf{H}}_M)^*_{24}}{\lambda_2 - M^2} & \frac{(\check{\mathbf{H}}_M)^*_{34}}{\lambda_3 - M^2} & 0 \end{pmatrix}. \end{aligned} \tag{E.10}$$

E.4.2 Second order corrections

The second order corrections to eigenvalues are

$$\lambda_i^{(2)} = \sum_{i \neq k} \frac{|2E(\check{\mathbf{H}}_1)_{ik}|^2}{\lambda_i - \lambda_k}, \tag{E.11}$$

or explicitly as

$$\begin{aligned}
\lambda_1^{(2)} =& -(\epsilon' \Delta m_{ee}^2)^2 \frac{\tilde{s}_{12}^2}{\Delta\lambda_{31}} + \frac{|2E(\check{\mathbf{H}}_M)_{14}|^2}{\lambda_1 - M^2}, \\
\lambda_2^{(2)} =& -(\epsilon' \Delta m_{ee}^2)^2 \frac{\tilde{c}_{12}^2}{\Delta\lambda_{32}} + \frac{|2E(\check{\mathbf{H}}_M)_{24}|^2}{\lambda_2 - M^2}, \\
\lambda_3^{(2)} =& (\epsilon' \Delta m_{ee}^2)^2 \big(\frac{\tilde{s}_{12}^2}{\Delta\lambda_{31}} + \frac{\tilde{c}_{12}^2}{\Delta\lambda_{32}}\big) + \frac{|2E(\check{\mathbf{H}}_M)_{34}|^2}{\lambda_3 - M^2}, \\
\lambda_4^{(2)} =& -\frac{|2E(\check{\mathbf{H}}_M)_{14}|^2}{\lambda_1 - M^2} - \frac{|2E(\check{\mathbf{H}}_M)_{24}|^2}{\lambda_2 - M^2} - \frac{|2E(\check{\mathbf{H}}_M)_{34}|^2}{\lambda_3 - M^2}.
\end{aligned} \tag{E.12}$$

where $\Delta\lambda_{ij} \equiv \lambda_i - \lambda_j$.

The second order corrections to eigenvectors can be calculated by the corrections to the PMNS matrix:

$$(\mathbf{W}_2)_{ij} = \begin{cases} -\frac{1}{2} \sum\limits_{k\neq i} \frac{|2E(\check{\mathbf{H}}_1)_{ik}|^2}{(\lambda_i - \lambda_k)^2} & i = j \\ \frac{1}{\lambda_i - \lambda_j} \sum\limits_{k\neq i, k\neq j} \frac{2E(\check{\mathbf{H}}_1)_{ik} 2E(\check{\mathbf{H}}_1)_{kj}}{\lambda_k - \lambda_j} & i \neq j \end{cases}. \tag{E.13}$$

We list the elements of $\mathbf{W}_2$ below:

$$\begin{aligned}
(\mathbf{W}_2)_{11} =& -(\epsilon' \Delta m_{ee}^2)^2 \frac{\tilde{s}_{12}^2}{2(\Delta\lambda_{31})^2} - \frac{(2E)^2 |(\check{\mathbf{H}}_M)_{14}|^2}{2(M^2 - \lambda_1)^2}, \\
(\mathbf{W}_2)_{12} =& (\epsilon' \Delta m_{ee}^2)^2 \frac{\tilde{s}_{12}\tilde{c}_{12}\, e^{i\alpha_{12}}}{\Delta\lambda_{32}\Delta\lambda_{21}} \\
& - (2E)^2 \frac{(\check{\mathbf{H}}_M)_{14}(\check{\mathbf{H}}_M)_{24}^*}{(M^2 - \lambda_2)\Delta\lambda_{21}}, \\
(\mathbf{W}_2)_{13} =& -(2E)^2 \frac{(\check{\mathbf{H}}_M)_{14}(\check{\mathbf{H}}_M)_{34}^*}{(M^2 - \lambda_3)\Delta\lambda_{31}}, \\
(\mathbf{W}_2)_{21} =& -(\epsilon' \Delta m_{ee}^2)^2 \frac{\tilde{s}_{12}\tilde{c}_{12}\, e^{-i\alpha_{12}}}{\Delta\lambda_{31}\Delta\lambda_{21}} \\
& + (2E)^2 \frac{(\check{\mathbf{H}}_M)_{24}(\check{\mathbf{H}}_M)_{14}^*}{(M^2 - \lambda_1)\Delta\lambda_{21}}, \\
(\mathbf{W}_2)_{22} =& -(\epsilon' \Delta m_{ee}^2)^2 \frac{\tilde{c}_{12}^2}{2(\Delta\lambda_{32})^2} - (2E)^2 \frac{|(\check{\mathbf{H}}_M)_{24}|^2}{2(M^2 - \lambda_2)^2},
\end{aligned}$$

$$
\begin{aligned}
(\mathbf{W}_2)_{23} &= -(2E)^2 \frac{(\check{\mathbf{H}}_M)_{24}(\check{\mathbf{H}}_M)^*_{34}}{(M^2-\lambda_3)\Delta\lambda_{32}},\\
(\mathbf{W}_2)_{31} &= (2E)^2 \frac{(\check{\mathbf{H}}_M)_{34}(\check{\mathbf{H}}_M)^*_{14}}{(M^2-\lambda_1)\Delta\lambda_{31}},\\
(\mathbf{W}_2)_{32} &= (2E)^2 \frac{(\check{\mathbf{H}}_M)_{34}(\check{\mathbf{H}}_M)^*_{24}}{(M^2-\lambda_2)\Delta\lambda_{32}},\\
(\mathbf{W}_2)_{33} &= -\frac{(\epsilon'\Delta m^2_{ee})^2}{2}\Big[\frac{\tilde{s}^2_{12}}{(\Delta\lambda_{31})^2}+\frac{\tilde{c}^2_{12}}{(\Delta\lambda_{32})^2}\Big]\\
&\qquad -(2E)^2\frac{|(\check{\mathbf{H}}_M)_{34}|^2}{2(M^2-\lambda_3)^2},\\
(\mathbf{W}_2)_{14} &= -\epsilon'\Delta m^2_{ee}\frac{(2E)\tilde{s}_{13}(\check{\mathbf{H}}_M)_{34}e^{i(\alpha_{13}+\alpha_\epsilon)}}{(\lambda_2-M^2)(\lambda_3-M^2)},\\
(\mathbf{W}_2)_{24} &= \epsilon'\Delta m^2_{ee}\frac{(2E)\tilde{c}_{13}(\check{\mathbf{H}}_M)_{34}e^{i\alpha_\epsilon}}{(\lambda_1-M^2)(\lambda_3-M^2)},\\
(\mathbf{W}_2)_{34} &= -\epsilon'\Delta m^2_{ee}(2E)e^{-i\alpha_\epsilon}\Big[\frac{\tilde{s}_{13}(\check{\mathbf{H}}_M)_{14}e^{-i\alpha_{13}}}{(\lambda_3-M^2)(\lambda_1-M^2)}\\
&\qquad +\frac{\tilde{c}_{13}(\check{\mathbf{H}}_M)_{24}}{(\lambda_3-M^2)(\lambda_2-M^2)}\Big],\\
(\mathbf{W}_2)_{41} &= -\epsilon'\Delta m^2_{ee}\frac{(2E)\tilde{s}_{13}(\check{\mathbf{H}}_M)^*_{34}e^{-i(\alpha_{13}+\alpha_\epsilon)}}{(M^2-\lambda_1)\Delta\lambda_{31}},\\
(\mathbf{W}_2)_{42} &= \epsilon'\Delta m^2_{ee}\frac{(2E)\tilde{c}_{13}(\check{\mathbf{H}}_M)^*_{34}e^{-i\alpha_\epsilon}}{(M^2-\lambda_2)\Delta\lambda_{32}},\\
(\mathbf{W}_2)_{43} &= \epsilon'\Delta m^2_{ee}(2E)e^{i\alpha_\epsilon}\Big[\frac{\tilde{s}_{13}(\check{\mathbf{H}}_M)^*_{34}e^{i\alpha_{13}}}{(M^2-\lambda_3)\Delta\lambda_{31}}\\
&\qquad -\frac{\tilde{c}_{13}(\check{\mathbf{H}}_M)^*_{34}}{(M^2-\lambda_3)\Delta\lambda_{32}}\Big],\\
(\mathbf{W}_2)_{44} &= -2E^2\Big[\frac{|(\check{\mathbf{H}}_M)_{14}|^2}{(M^2-\lambda_1)^2}\\
&\qquad +\frac{|(\check{\mathbf{H}}_M)_{24}|^2}{(M^2-\lambda_2)^2}+\frac{|(\check{\mathbf{H}}_M)_{34}|^2}{(M^2-\lambda_3)^2}\Big].
\end{aligned}
\tag{E.14}
$$

REFERENCES

[1] M. G. Aartsen et al. Searches for Sterile Neutrinos with the IceCube Detector. *Phys. Rev. Lett.*, 117(7):071801, 2016.

[2] K. Abe et al. The T2K Experiment. *Nucl. Instrum. Meth.*, A659:106–135, 2011.

[3] K. Abe et al. A Long Baseline Neutrino Oscillation Experiment Using J-PARC Neutrino Beam and Hyper-Kamiokande. 12 2014.

[4] K. Abe et al. Physics potential of a long-baseline neutrino oscillation experiment using a J-PARC neutrino beam and Hyper-Kamiokande. *PTEP*, 2015:053C02, 2015.

[5] K. Abe et al. First measurement of the muon neutrino charged current single pion production cross section on water with the T2K near detector. *Phys. Rev. D*, 95(1):012010, 2017.

[6] K. Abe et al. Physics potentials with the second Hyper-Kamiokande detector in Korea. *PTEP*, 2018(6):063C01, 2018.

[7] R. Acciarri et al. Long-Baseline Neutrino Facility (LBNF) and Deep Underground Neutrino Experiment (DUNE). 2015.

[8] R. Acciarri et al. Long-Baseline Neutrino Facility (LBNF) and Deep Underground Neutrino Experiment (DUNE): Conceptual Design Report, Volume 1: The LBNF and DUNE Projects. 1 2016.

[9] M. A. Acero et al. Measurement of neutrino-induced neutral-current coherent π^0 production in the NOvA near detector. *Phys. Rev. D*, 102(1):012004, 2020.

[10] Sanjib Kumar Agarwalla, Sabya Sachi Chatterjee, Arnab Dasgupta, and Antonio Palazzo. Discovery Potential of T2K and NOvA in the Presence of a Light Sterile Neutrino. *JHEP*, 02:111, 2016.

[11] Sanjib Kumar Agarwalla, Sabya Sachi Chatterjee, and Antonio Palazzo. Physics Reach of DUNE with a Light Sterile Neutrino. *JHEP*, 09:016, 2016.

[12] V. M. Aquino, J. Bellandi, and M. M. Guzzo. On mixing angles and resonances in three neutrino oscillations in matter. *Braz. J. Phys.*, 27:384–391, 1997.

[13] Katsuhiro Asano and Hisakazu Minakata. Large-Theta(13) Perturbation Theory of Neutrino Oscillation for Long-Baseline Experiments. *JHEP*, 06:022, 2011.

[14] D. S. Ayres et al. NOvA: Proposal to Build a 30 Kiloton Off-Axis Detector to Study $\nu_\mu \to \nu_e$ Oscillations in the NuMI Beamline. 3 2004.

[15] Michael Baird. Summary of the Latest 3-Flavor Neutrino Oscillation Results from the NOvA Experiment. In *40th International Conference on High Energy Physics (Prague)*, 7 2020.

[16] Gabriela Barenboim, Peter B Denton, Stephen J Parke, and Christoph Andreas Ternes. Neutrino Oscillation Probabilities through the Looking Glass. *Phys. Lett. B*, 791:351–360, 2019.

[17] Vernon D. Barger, K. Whisnant, S. Pakvasa, and R. J. N. Phillips. Matter Effects on Three-Neutrino Oscillations. *Phys. Rev.*, D22:2718, 1980. [,300(1980)].

[18] Mattias Blennow, Enrique Fernandez-Martinez, Julia Gehrlein, Josu Hernandez-Garcia, and Jordi Salvado. IceCube bounds on sterile neutrinos above 10 eV. *Eur. Phys. J. C*, 78(10):807, 2018.

[19] Mattias Blennow and Alexei Yu. Smirnov. Neutrino propagation in matter. *Adv. High Energy Phys.*, 2013:972485, 2013.

[20] A. Cervera, A. Donini, M. B. Gavela, J. J. Gomez Cadenas, P. Hernandez, Olga Mena, and S. Rigolin. Golden measurements at a neutrino factory. *Nucl. Phys.*, B579:17–55, 2000. [Erratum: Nucl. Phys.B593,731(2001)].

[21] Glen Crawford. HEP Research Program Status. In *DOE HEPAP Meeting*, 11 2019.

[22] André de Gouvêa and Andrew Kobach. Global Constraints on a Heavy Neutrino. *Phys. Rev. D*, 93(3):033005, 2016.

[23] Mona Dentler, Álvaro Hernández-Cabezudo, Joachim Kopp, Pedro A. N. Machado, Michele Maltoni, Ivan Martinez-Soler, and Thomas Schwetz. Updated Global Analysis of Neutrino Oscillations in the Presence of eV-Scale Sterile Neutrinos. *JHEP*, 08:010, 2018.

[24] Peter Denton. Recent Results in Neutrino Oscillation Theory. In *UMass Amherst Seminar (Amherst)*, 11 2019.

[25] Peter B. Denton, Hisakazu Minakata, and Stephen J. Parke. Compact Perturbative Expressions For Neutrino Oscillations in Matter. *JHEP*, 06:051, 2016.

[26] Peter B Denton, Stephen J Parke, Terence Tao, and Xining Zhang. Eigenvectors from Eigenvalues: a survey of a basic identity in linear algebra. *Bull. Amer. Math. Soc.*, 2 2021.

[27] Peter B. Denton, Stephen J. Parke, and Xining Zhang. Rotations Versus Perturbative Expansions for Calculating Neutrino Oscillation Probabilities in Matter. *Phys. Rev. D*, 98(3):033001, 2018.

[28] Peter B Denton, Stephen J Parke, and Xining Zhang. Fibonacci Fast Convergence for Neutrino Oscillations in Matter. *Phys. Lett. B*, 807:135592, 2020.

[29] Peter B Denton, Stephen J Parke, and Xining Zhang. Neutrino oscillations in matter via eigenvalues. *Phys. Rev. D*, 101(9):093001, 2020.

[30] S. Dev, Desh Raj, Radha Raman Gautam, and Lal Singh. New mixing schemes for (3+1) neutrinos. *Nucl. Phys. B*, 941:401–424, 2019.

[31] Alejandro Diaz. Status of Sterile Neutrino fits with Global Data. In *Meeting of the APS Division of Particles and Fields*, 10 2017.

[32] Ivan Esteban, M. C. Gonzalez-Garcia, Alvaro Hernandez-Cabezudo, Michele Maltoni, and Thomas Schwetz. Global analysis of three-flavour neutrino oscillations: synergies and tensions in the determination of θ_{23}, δ_{CP}, and the mass ordering. *JHEP*, 01:106, 2019.

[33] Enrique Fernandez-Martinez, Josu Hernandez-Garcia, and Jacobo Lopez-Pavon. Global constraints on heavy neutrino mixing. *JHEP*, 08:033, 2016.

[34] Gian Luigi Fogli, E. Lisi, and A. Palazzo. Quasi energy independent solar neutrino transitions. *Phys. Rev. D*, 65:073019, 2002.

[35] Chee Sheng Fong, Hisakazu Minakata, and Hiroshi Nunokawa. A framework for testing leptonic unitarity by neutrino oscillation experiments. *JHEP*, 02:114, 2017.

[36] Chee Sheng Fong, Hisakazu Minakata, and Hiroshi Nunokawa. Non-unitary evolution of neutrinos in matter and the leptonic unitarity test. *JHEP*, 02:015, 2019.

[37] Sébastien Galais, James Kneller, and Cristina Volpe. The neutrino-neutrino interaction effects in supernovae: the point of view from the matter basis. *J. Phys. G*, 39:035201, 2012.

[38] M. C. Gonzalez-Garcia and Michele Maltoni. Phenomenology with Massive Neutrinos. *Phys. Rept.*, 460:1–129, 2008.

[39] P. F. Harrison and W. G. Scott. CP and T violation in neutrino oscillations and invariance of Jarlskog's determinant to matter effects. *Phys. Lett.*, B476:349–355, 2000.

[40] T. Ishida. The JHF-Kamioka neutrino project. 11 2002.

[41] C. Jarlskog. Commutator of the Quark Mass Matrices in the Standard Electroweak Model and a Measure of Maximal CP Violation. *Phys. Rev. Lett.*, 55:1039, 1985.

[42] Kevin J. Kelly and Stephen J. Parke. Matter Density Profile Shape Effects at DUNE. 2018.

[43] Keiichi Kimura, Akira Takamura, and Hidekazu Yokomakura. Exact formulas and simple CP dependence of neutrino oscillation probabilities in matter with constant density. *Phys. Rev.*, D66:073005, 2002.

[44] N. Klop and A. Palazzo. Imprints of CP violation induced by sterile neutrinos in T2K data. *Phys. Rev. D*, 91(7):073017, 2015.

[45] Joachim Kopp, Pedro A. N. Machado, Michele Maltoni, and Thomas Schwetz. Sterile Neutrino Oscillations: The Global Picture. *JHEP*, 05:050, 2013.

[46] Wei Li, Jiajie Ling, Fanrong Xu, and Baobiao Yue. Matter Effect of Light Sterile Neutrino: An Exact Analytical Approach. *JHEP*, 10:021, 2018.

[47] Ziro Maki, Masami Nakagawa, and Shoichi Sakata. Remarks on the unified model of elementary particles. *Prog. Theor. Phys.*, 28:870–880, 1962. [,34(1962)].

[48] Hisakazu Minakata. Large-Theta(13) Perturbation Theory of Neutrino Oscillation. *Acta Phys. Polon.*, B40:3023–3031, 2009.

[49] Hisakazu Minakata and Stephen J Parke. Simple and Compact Expressions for Neutrino Oscillation Probabilities in Matter. *JHEP*, 01:180, 2016.

[50] Vadim A. Naumov. Three neutrino oscillations in matter, CP violation and topological phases. *Int. J. Mod. Phys.*, D1:379–399, 1992.

[51] Tommy Ohlsson and Hakan Snellman. Neutrino oscillations with three flavors in matter: Applications to neutrinos traversing the Earth. *Phys. Lett. B*, 474:153–162, 2000. [Erratum: Phys.Lett.B 480, 419–419 (2000)].

[52] Vaia Papadimitriou et al. Design Status of the LBNF/DUNE Beamline. In *9th International Particle Accelerator Conference*, 4 2018.

[53] Stephen J. Parke, Peter B. Denton, and Hisakazu Minakata. Analytic Neutrino Oscillation Probabilities in Matter: Revisited. In *2017 International Workshop on Neutrinos from Accelerators (NuFact17) Uppsala University Main Building, Uppsala, Sweden, September 25-30, 2017*, 2018.

[54] Stephen J Parke and Xining Zhang. Compact Perturbative Expressions for Oscillations with Sterile Neutrinos in Matter. *Phys. Rev. D*, 101(5):056005, 2020.

[55] R. B. Patterson. The NOvA Experiment: Status and Outlook. 2012. [Nucl. Phys. Proc. Suppl.235-236,151(2013)].

[56] B. Pontecorvo. Neutrino Experiments and the Problem of Conservation of Leptonic Charge. *Sov. Phys. JETP*, 26:984–988, 1968. [Zh. Eksp. Teor. Fiz.53,1717(1967)].

[57] Marcia Teckenbrock. Fermilab computing experts bolster NOvA evidence, 1 million cores consumed. *Fermilab News*, 7 2018.

[58] S. Toshev. On T violation in matter neutrino oscillations. *Mod. Phys. Lett.*, A6:455–460, 1991.

[59] Natalie Wolchover. Neutrinos Lead to Unexpected Discovery in Basic Math. *Quanta Magazine*, 11 2019.

[60] L. Wolfenstein. Neutrino Oscillations in Matter. *Phys. Rev.*, D17:2369–2374, 1978. [,294(1977)].

[61] H. Yokomakura, K. Kimura, and A. Takamura. Matter enhancement of T violation in neutrino oscillation. *Phys. Lett. B*, 496:175–184, 2000.

[62] H. W. Zaglauer and K. H. Schwarzer. The Mixing Angles in Matter for Three Generations of Neutrinos and the Msw Mechanism. *Z. Phys.*, C40:273, 1988.